MANUFACTURABILITY IMPROVEMENT OF HIGH FREQUENCY TRANSFORMERS

by

BAREND JACQUES SWART

submitted in fulfilment of the requirements of the degree

MASTER IN ENGINEERING

in

ELECTRICAL AND ELECTRONIC ENGINEERING

in the

FACULTY OF ENGINEERING

of the

RAND AFRIKAANS UNIVERSITY

SUPERVISOR: PROF J.A. FERREIRA
CO-SUPERVISOR: PROF J.D. VAN WYK

JANUARY 1995

Summary

In order to improve the industrialisation of modern power converters, its physical size must be reduced, material must be utilised more efficiently and its manufacturability improved. Consequently, many converters are operated in the ultrasonic frequency range, where the size of its constituent components are considerably reduced. Even at high frequencies of operation, however, magnetic components are still the largest and heaviest components in converters, and do not utilise materials to their maximum benefit. The aim of this work is to investigate the possibility of improving the industrialisation of power electronic converters by making use of a novel, multiple core magnetic component structure, called the distributed transformer

Existing magnetic component structures are evaluated from a materials point of view and the concept of distributed magnetic components introduced. A generalised transformer model is developed for the distributed transformer and pertinent design considerations discussed.

A 1.5 kw battery charger industrialised by Spoornet is based on the Cuk DC-DC converter and is used as a case study. A conventional monolithic isolation transformer is used in its construction after a complete mathematical analysis of the converter topology, and compared with the equivalent distributed transformer configuration.

The distributed transformer is then compared with the conventional monolithic transformer and evaluated in terms of its physical and electrical performance, design and ease of manufacture.

Opsomming

Om die industrialisasie van moderne elektroniese omsetters te verbeter, moet die fisiese grootte verminder word, materiale moet beter benut word en die vevaardigbaarheid daarvan moet verbeter. Meeste drywingsmutators word dus by hoë frekwensies bedryf, waar die grootte van die komponente wesenlik kleiner is, maar by hoë frekwensies is magnetiese komponente nog steeds die grootste en swaarste komponente in 'n omsetter, en benut nie materiale ten volle nie. Die doel van die werk is om die moontlike verbetering in die industrialisasie van drywings eleketroniese omsetters te ondersoek deur gebruik te maak van 'n nuwe magnetiese struktuur wat bekend staan as die verspreide transformator.

Konvensionele magnetiese komponente word geëvalueer vanuit die oogpunt van materiaalbenutting, en die konsep van die verspreide magnetiese komponent word bekend gestel. 'n Algemene transformatormodel word vir die verspreide transformator voorgestel en die nodige ontwerpsbeginsels is bespreek.

'n 1.5 kW batterylaaier wat deur Spoornet geïndustrialiseer is, is gebasseer op die Cuk GS-GS omsetter en is as 'n gevalle studie beskou. 'n Konvensionele monolitiese isolasietransformator is gebruik in sy samestelling na 'n volledige wiskundige analise van die topologie, en is vergelyk met die ekwivalente verspreide transformatorkonfigurasie.

Die verspreide transformator is dan vergelyk met die konvensionele monolitiese transformator en geëvalueer in terme van fisiese en elektriese werkverrigting, ontwerp en vervaardigbaarheid

Acknowledgements

To my heavenly father who provides meaning to this work

To my parents for their patience, understanding and support

To professor J.A Ferreira and J.D van Wyk for their guidance and support

Table of contents

1. Introduction

2. The development of the distributed magnetic component

3. Distributed transformers - analysis and design

4. The isolated Cuk converter - Transformer design

5. Case study - Experimental Results

6. Conclusion

Appendixes

1. Introduction

1. INTRODUCTION

1.1. MAGNETIC COMPONENTS - AN INTEGRAL PART OF POWER CONVERSION

In principle the lossless transfer and transformation of power can be accomplished by an ideal device, illustrated in Figure.1-1, called the power processor. The power processor accepts power from an available source, and then through dynamic and controlled manipulation, transforms it into an alternative form so that it is useful for some predetermined purpose [1].

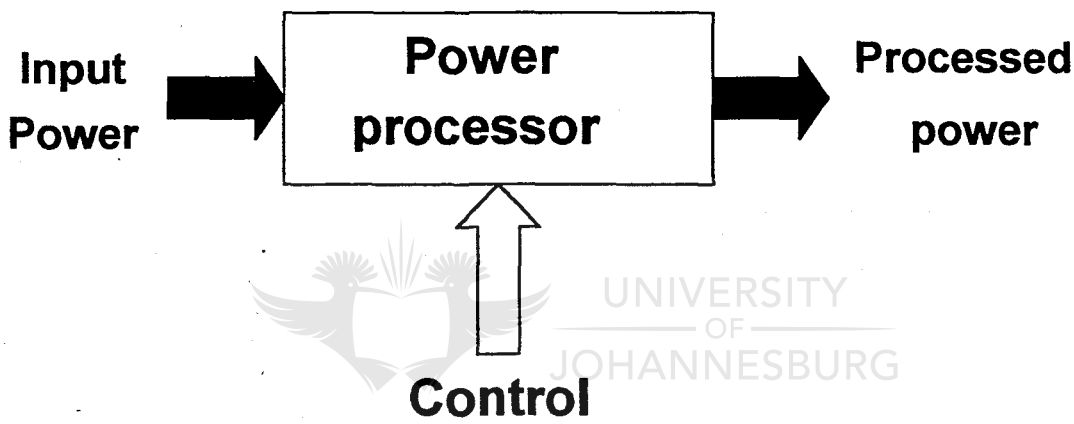

Figure.1-1. The ideal power processor

The switched mode power converter is an electronic device that is designed to emulate the power processing function, so that electrical power from available power supplies may be effectively managed and put to good use. In general, the practising engineer is faced with the challenge of combining principles and techniques from three fields of expertise to develop a practical power converter, namely (1) power conversion methods, (2) magnetic circuit design and (3) control system strategies [1,2].

(1) Power conversion methods

Power conversion methods concentrate on the various ways in which components can be interconnected and controlled, to transfer and transform energy from the input of the power converter to its output, with minimal loss. The breakdown of components available for use in power circuit topologies is described in [2] , and is illustrated in Figure.1-2.

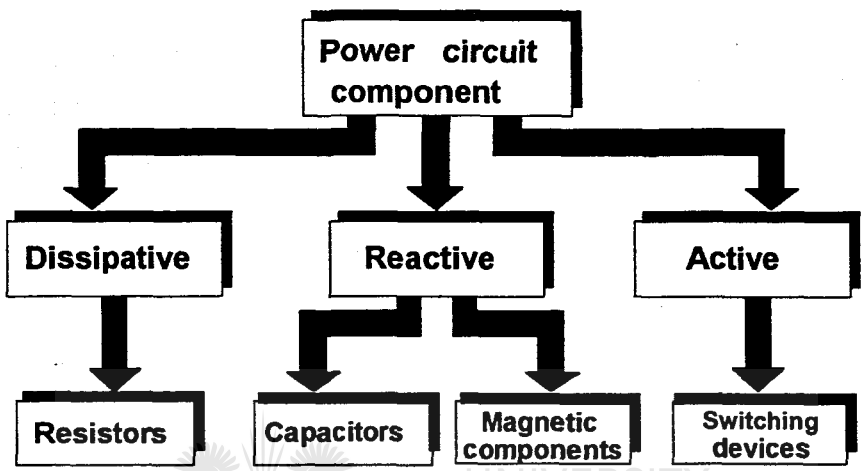

Figure.1-2. Breakdown of components used in power electronic converters

Active components: The power converter always consists of at least one semiconductor device, placed between the power source and load. These devices are usually used as switches, i.e. they are driven to operate between a state of conduction and non-conduction, hence the term "switched mode power converters". By controlling the time interval of the conducting state relative to the time interval of the non-conducting state, the flow of power from the input of the converter to its output can be efficiently controlled. The semiconductor switch, has losses induced within its infrastructure due to the switching action, but the power dissipation by semiconductor devices operating in the switching mode of operation, is far less than that of semiconductor devices operating in the linear mode of operation [1,2].

Reactive components: Due to the switching action, the pulsating characteristics of voltage and current, often need to be smoothed out. Ideally, non-dissipative storage components such as capacitors and inductors are an obvious choice, but in reality they are lossy in nature and introduce losses into the system, reducing the overall efficiency of the power converter. Reducing the lossy nature of dielectric materials in capacitors is a task for the materials scientist, but minimising the losses in transformers, inductors and chokes is a task for the engineer.

Dissipative Components: Dissipative components are generally undesirable, since they do not contribute directly to the power processing function, and intentionally introduce losses into the system. They are still included in Figure.1-2, however, because their use is sometimes unavoidable, e.g. where damping is required.

(2) Magnetic circuit design

The magnetics in a power converter are an integral part of the power conversion process and serve a multitude of purposes such as energy storage, filtering, galvanic isolation and AC power conversion. Transformers and a number of more complex magnetically coupled structures must be exploited to achieve efficient power processing with minimal loss effects.

(3) Control system strategies

Control system strategies concentrate on the various ways in which the semiconductor switches can be switched, so that its mutual interaction with the rest of the circuitry correctly manages the flow of power, from the input of the power converter to its output, or vise-verse if necessary.

The effective combination of the aforementioned fields of expertise have made power electronic converters the backbone for industrial applications such as induction heating for the heat treatment of steel, arc welding, motor drives, Ups (Uninterruptable Power Supplies), and harmonic compensation in power grids.

1.2. CURRENT TRENDS OBSERVED IN THE INDUSTRIALISATION OF POWER ELECTRONIC CONVERTERS

Over the past few years, power electronics has found its rightful place in industry and like any business organisation is subject to the fundamental principle of economics, defined as follows [3],

" In the case of a business organisation, therefore, the economic principle is defined as the endeavour to earn the highest possible income on the market at the lowest possible cost, with profit as the favourable difference between the two."

While reliability and efficiency still maintain precedence, it is found that many of the current trends observed in the industrialisation of power converters, have cost reduction as one of the underlying root causes. Consequently, norms which have progressively cut deep inroads into the development of power converters can be grouped into the three major areas of concern illustrated in Figure.1-3.

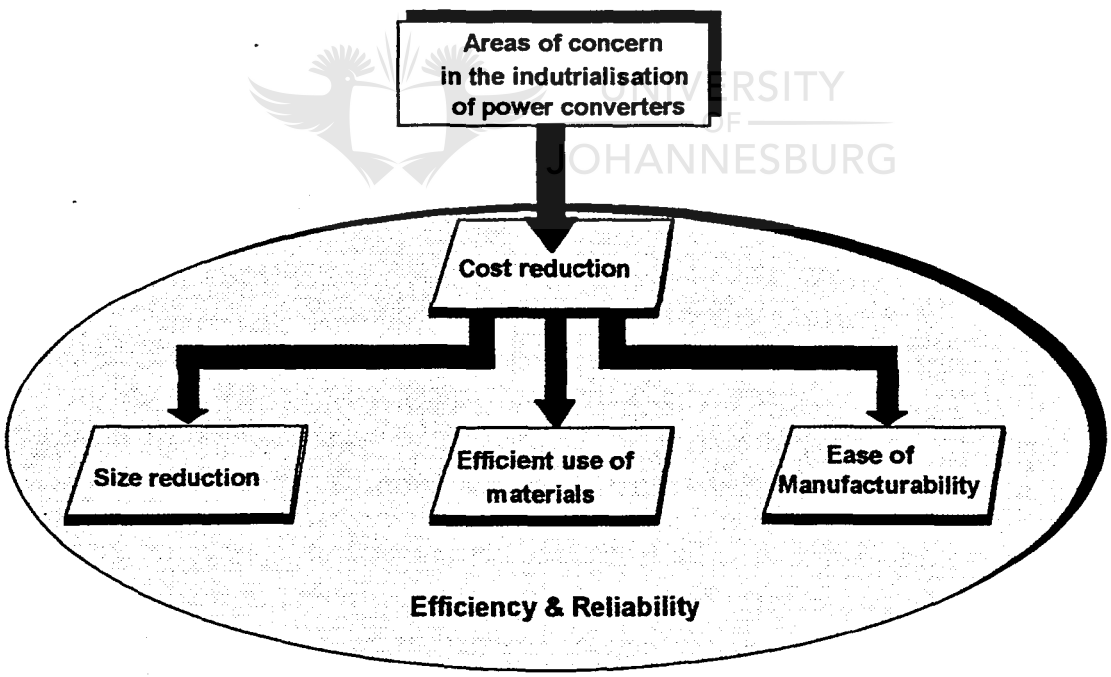

Figure.1-3. Current trends in the development of modern power converters

1.2.1. Size reduction

There have been an increasing number of applications where the space permitted for the positioning of a converter is limited, consequently the demand for compact converters with high power densities has escalated. As a result, many of the components used in converters, are operated at higher frequencies since it is the simplest way in which to accomplish a reduction in size, coupled with an increase in power density.

1.1.2. Materials utilisation

The space limitation introduced previously, not only imposes a restriction on size but also on the quantity of material used in the converter. The word "material", used in this context, refers to all substances which contribute to the functionality of the converter, aswell as to those substances which serve an auxiliary purpose - consider Figure.1-4 for a more detailed breakdown.

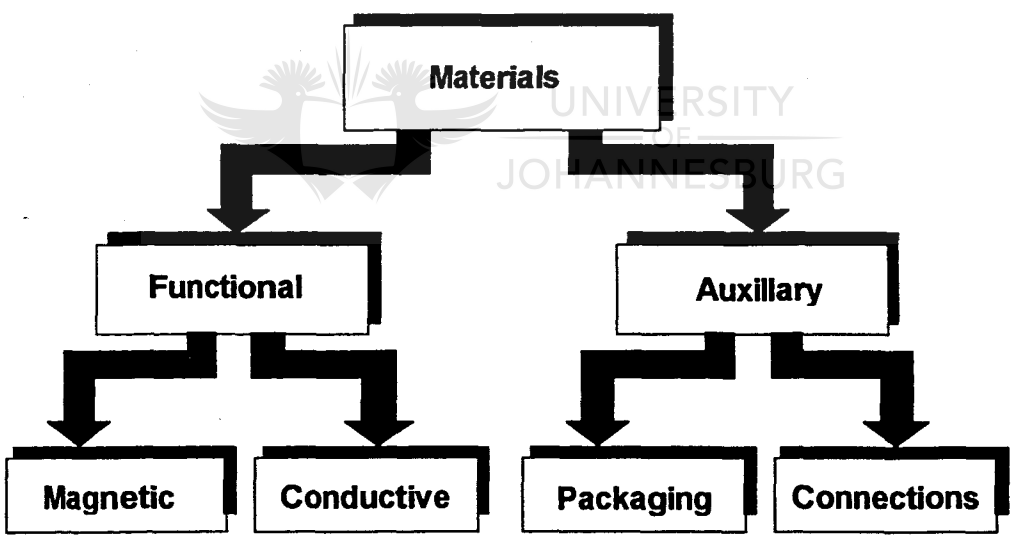

Figure. 1-4 Breakdown of materials used in power converters

Functional materials include magnetic materials which concentrate and direct the path of magnetic flux, and conductive materials which concentrate and direct the path of current flow. Auxiliary materials, on the other hand, include aluminium based alloys for cooling and other metals or polymers for brackets, fixtures, interconnections and packaging.

To accommodate the materials limitation in smaller, high frequency, switched mode converters, methods to gain maximum benefit from materials with minimal wastage has received renewed interest.

1.1.3. Ease of manufacturability

Finally, the space limitation introduced previously usually carries with it, a constraint on the form of the converter. As a result, the structure and orientation of the circuitry requires considerable attention, not only to accommodate the space limitation and efficient materials usage, but also to assist in overcoming the thermal problems associated with high frequency switching. Although existing manufacturing techniques for components are deeply ingrained within the design operandi of the practising engineer, they are quickly becoming difficult to implement in power converters with inherent size and structural constraints. As a result, the manufacturability of power converters is receiving renewed attention.

1.3. EVALUATING THE INDUSTRIALISATION OF MODERN POWER CONVERTERS

1.3.1. Drawbacks common to power electronic converters

The signal electronics industry has been revolutionised by the development of large scale integration techniques which include monolithic IC's, surface mounting, thick film and thin film technology. Some efforts have been made to duplicate the results in the power electronics industry [4,5,6,7], but their application has unfortunately been limited to lower power levels (<100W). The industrialisation of power equipment operating in the higher power range (> 500W) , therefore, has changed very little over the years, and still involves the typical interconnection of sub-assemblies such as power circuitry, house-keeping circuitry, control circuitry and magnetic components.

Consequently, all power equipment which falls within the genre of modern switching mode power converters, is seen to suffer from a number of common drawbacks when evaluated within the framework illustrated in Figure.1-3, and are listed as follows,

(1) Reliability: Failure due to mechanical interconnections are common in power equipment, therefore an interconnecting wire harness is a liability when considered from a reliability point of view.

(2) Size reduction: The overall size and weight distribution of any converter, is dependent on the size and placement of the magnetic components, since they are in general the largest and heaviest components in the converter, even at relatively high frequencies of operation. Furthermore, due to the switching nature of power converters, a fair amount of house keeping circuitry such as snubbers and dissipative damping is required, which naturally contributes to the size and weight of the converter.

(3) Materials utilisation: Due to high frequency excitations, excessive materials are used in the magnetic components to compensate for the heat induced within their infrastructure. Furthermore, excessive materials are required for packaging purposes to compensate for over sized components and poor layout of circuitry.

(4) Ease of manufacture: Due to the number of sub-assemblies that must be interconnected, labour intensive manufacturing processes are unavoidable. The complexity of the interconnections contribute to the time required for manufacture and hence to the cost of the final product.

It is evident from the observations listed above, that the industrialisation of power converters can be improved, i.e. further size reduction, improved materials utilisation and an alternative manufacturing technique is possible.

1.3.2. The need for alternative magnetic structures

From the evaluation presented in the previous section, it is seen that magnetic components are responsible for a large portion of the physical drawbacks observed in the industrialisation of power converters.

Much literature has been dedicated to the optimisation of magnetic components currently used in industrial power converters [8,9,10,11], however, so very little can be done to improve their materials utilisation, size reduction and manufacture any further. If the industrialisation of power converters is to be improved, alternative structures for magnetic components must be introduced, which can embrace the following characteristics when compared with conventional magnetic components designed to operate at the same power level and frequency,

(1) Smaller physical dimensions.

(2) Improved materials utilisation.

(3) Improved weight distribution.

(4) Improved temperature stability and efficiency.

(5) Improved manufacturability.

1.3.3. High frequency transformers - the common denominator

There has been an increasing demand for galvanic isolation in all industrial power equipment, consequently, isolation transformers have become the common denominator in converter switching topologies. As a first step, therefore, it follows that the industrialisation of converters can only be improved, if the design, structure and manufacture of the high frequency transformers used for galvanic isolation can be improved, and made to comply with the requirements listed in section 1.3.2.

1.4. Aim of this work

The aim of this work is,

(1) to develop an alternative structure for high frequency transformers used in hard switched DC-DC converters, with the characteristics listed in section 1.3.2.

(2) to investigate and compare the alternative transformer assembly with conventional high frequency transformers.

Since the operating conditions for the isolation transformer in DC-DC converters are generic, the 1.5 kW battery charger illustrated in the photograph of Figure.1-5, is used as a case study (the operation of the battery charger is based on the Cuk DC-DC converter topology).

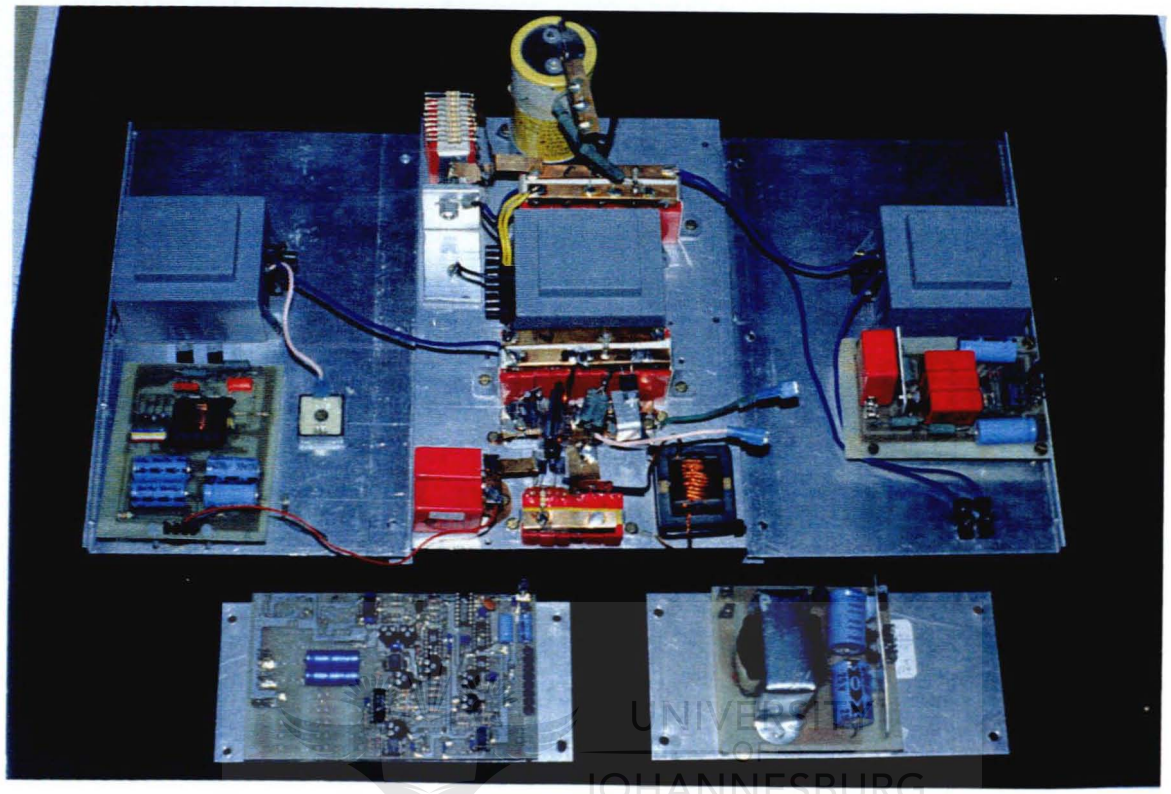

Figure.1-5 The prototype of a 1.5 kW battery charger

The operation of the converter is analysed mathematically to determine the operating conditions for the isolation transformer. The conventional barrel wound, isolation transformer used in the construction of the battery charger, is then replaced by the alternative transformer assembly, and the two evaluated from a performance as well as a manufacturing point of view.

2. The development of the distributed magnetic component

2. THE DEVELOPMENT OF THE DISTRIBUTED MAGNETIC COMPONENT

2.1. INTRODUCTION

In an attempt to develop a new magnetic component it is imperative to evaluate existing magnetic structures within the framework established in section 1.2, to ascertain their advantages and disadvantages. Magnetic component topologies that have found wide spread use in power electronic engineering of today, can be grouped in accordance to their structural assembly as illustrated in the block diagram of Figure.2-1.

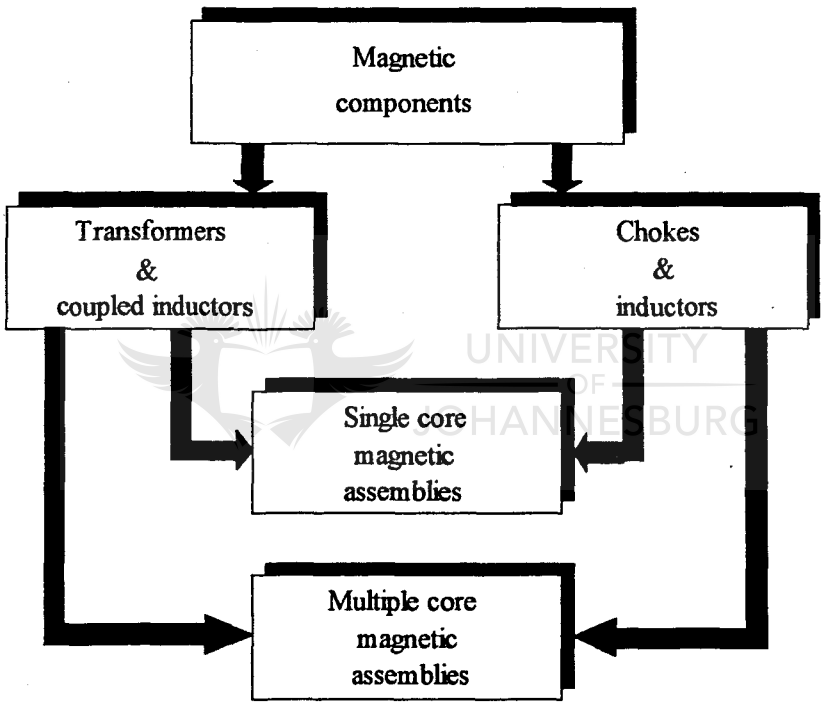

Figure. 2-1 Grouping of magnetic components in accordance to structural assembly

The single core or monolithic magnetic component is obtained by the assembly of a core around a multiple of previously wound coils, or by the winding of multiple coils on a previously manufactured core [1]. A multiple core magnetic component on the other hand, is obtained by the appropriate interconnection of a multitude of single core magnetic structures.

Although the two basic structures will be treated as distinctly different, each of the two structures can be derived from the other. Consider, for example, the E-core of a monolithic magnetic component, stripped of its windings and separated into n smaller cores as illustrated in Figure.2-2. By fitting each of the smaller cores with the necessary windings and interconnecting them in an appropriate fashion, a multiple core magnetic component consisting of n single core structures, which will henceforth be referred to as elements, is obtained.

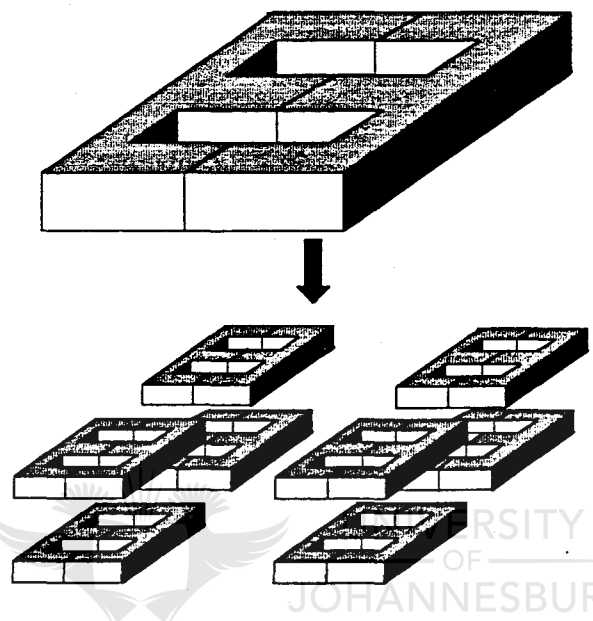

Figure. 2-2 Subdivision of an E-core into smaller element cores

If the elements of a multiple core magnetic assembly had to be reduced to n=1, a monolithic magnetic component would be obtained, i.e. the single core magnetic structure is a special case within the family of multiple core magnetic components.

Single core magnetic components are prominent in modern power electronic designs, and although some attempts have been made at developing useful multiple core magnetic components [2], their application is limited and their advantages are to a large extent still unknown. Since a new magnetic component would ultimately form part of one of these structural groups, an analysis into the characteristics of single core and multiple core assemblies is essential to serve as a springboard into the development of a novel magnetic structure that complies with the constraints identified in chapter.1.

2.2. MATERIALS UTILISATION AND SPACE VOLUME CONSUMPTION OF TYPICAL MAGNETIC COMPONENTS - A COMPARISON

Three basic types of materials are prevalent in the manufacture of magnetic components, and can be classified in accordance to their general function [3], as illustrated by the diagram in Figure.2-3.

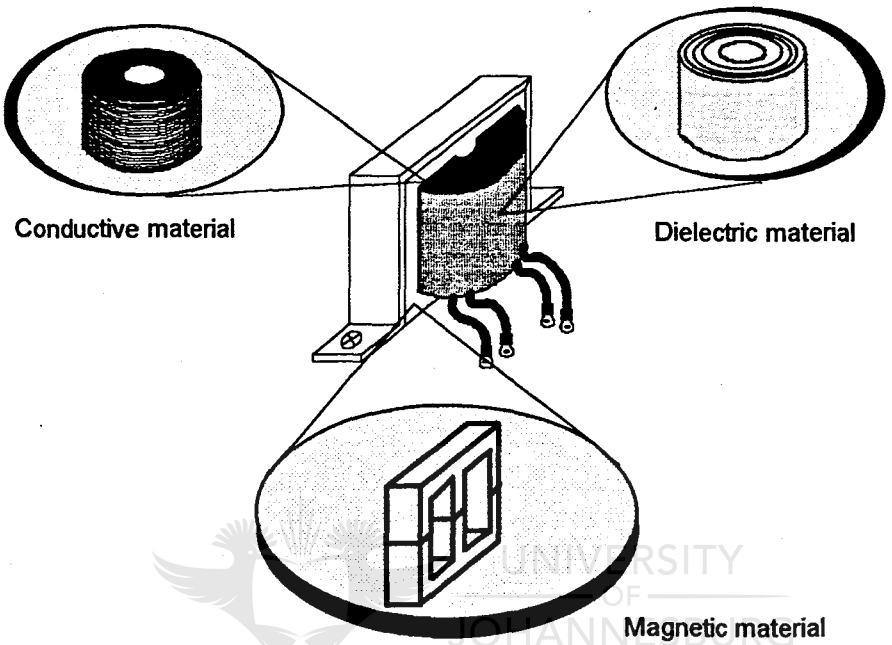

Figure. 2-3 Grouping of materials in magnetic components according to their general function

The analysis that follows is concerned primarily with the optimisation of the magnetic and conductive materials, dielectric materials are included by implication.

2.2.1. Geometrical considerations

To simplify the analysis a basic structure for single core magnetic assemblies, and consequently for the elements of a multiple core assembly, is assumed as illustrated in Figure.2-4.

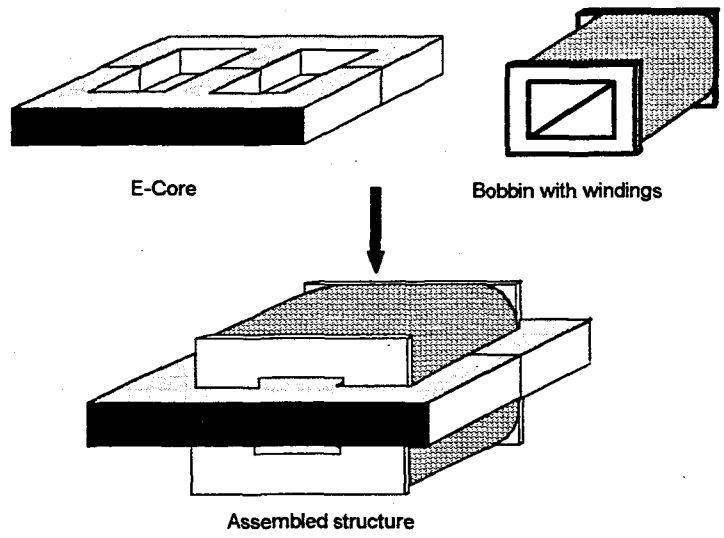

Figure. 2-4 Basic geometry of single core magnetic component used in analysis

The magnetic core consists of two E-core halves moulded from Mg-Zn ferrite material. A bobbin supporting the necessary windings, is fitted over the centre leg of the core.

Note: The assumption of a basic structure only facilitates in the simplification of the analysis that follows, and should in no way be seen as a restriction. The concepts and findings can be extrapolated to magnetic components with any other basic geometrical configuration.

2.2.2. Single core magnetic assemblies

2.2.2.1. Factors limiting the efficient use of magnetic materials in single core magnetic assemblies

It has been well established that magnetic components operating below ultrasonic frequencies are large and costly when implemented in applications where power levels are in excess of 1 kVA. In keeping with current trends towards compact high power converters, the volume of magnetic material in such components have been reduced by their operation at frequencies well above the ultrasonic range. The power levels and frequencies in question necessitate the use of ferrimagnetic materials such as ferrite.

The use of ferrimagnetic materials, however is not without its problems, for, at ultrasonic frequencies the losses and consequent heat dissipation of a magnetic core is a prominent design criterion for magnetic components in equipment where high power efficiency or temperature stability is required, or where its contribution to the ambient temperature is critical. In such applications, where magnetic components are referred to as core loss limited [4,5], it is desirable to constrain the rise in temperature of the core to an acceptable value (below the curie temperature) by constraining the maximum permissible flux density excursion to a value in the lower linear region of the magnetisation curve. The quantity of magnetic material required for a magnetic component has a near inverse proportion to the product of flux density and frequency, consequently, the reduction in magnetic material volume obtained by an increase in frequency of operation, is partly negated by an increase in magnetic material volume due to the reduction in total flux density.

This derating effect and its influence on materials utilisation can be examined analytically, but the mechanisms responsible for heat generation in ferrites must first be examined.

The heat energy generated in ferrimagnetic materials subject to cyclic magnetising forces, is attributed to a combination of three principle loss mechanisms, namely, (1) hysteresis loss, (2) eddy current loss and (3) residual loss.

(1) Hysteresis loss

Magnetic materials have a tendency to oppose changes in its magnetic state. This effect, called magnetic hysteresis, is physically caused by the impediment of domain wall motion at structural inhomogeneities within the material and is responsible for the characteristic area of the B-H loop.

The area enclosed by this B-H magnetisation curve represents energy converted into heat over every cycle, as a result of work done on the material when it responds to magnetisation.

The power lost per unit volume during the cyclic magnetisation of material, is referred to as hysteresis loss, and by integration over the B-H loop is given by [5] as follows;

$$P_h = \eta f \left(\hat{B}\right)^a \qquad (2.1)$$

P_h ≡Hysteresis loss per unit volume
η ≡Materials constant
f ≡Frequency of excitation
$\hat{B}$ ≡Maximum flux density excursion
a ≡Steinmetz constant

(2) Eddy current loss

Circulating currents will be induced in any medium of finite conductivity, permeated by time changing magnetic fields, creating losses in the material.

The power loss per unit volume for such a medium is given as;

$$P_e = \frac{J^2}{2\sigma} \qquad (2.2)$$

Pe ≡Eddy current losses per unit volume
J ≡Magnitude of current density in the medium
σ ≡Conductivity of conducting medium

The above equation may be applied to ferrites provided an average conductivity can be defined that takes the polycrystalline structure of ferrites into account [6].

(3) Residual loss

Residual loss is loosely defined as that portion of the total magnetic loss that cannot be attributed to hysteresis or eddy current phenomena. These losses are attributed, by Soohoo [7], to domain wall relaxation and domain rotation resonance.

The largest core loss component in ferrites for significant magnitudes of flux density is attributed to hysteres and is proportional to the peak flux density, $\hat{B}$, and frequency of excitation, f, in the following manner [5];

$$Core\ Loss\ \alpha\ \left(\hat{B}^{(a)}\right)f \qquad 1.9 \le a \le 2.9 \qquad (2.3)$$

Under steady state operating conditions, thermal equilibrium is reached when the internally generated heat of the core is equal to the heat lost due to dissipation. From basic principles of heat transfer, it is seen that the temperature rise in the core material is directly proportional to the internally generated power loss, consequently, for a given operating temperature $\hat{B}\alpha\left(\frac{1}{f}\right)^{-a}$. In order to maintain a required core temperature in core loss limited applications, thereforee, flux density excursions slightly less in magnitude than the saturation flux density are permissible at low frequencies, but at higher frequencies the maximum permissible flux density excursion must be reduced considerably.

From Faraday's law, the size of the core required for a transformer at a specific power level, is inversely proportional to the product of the peak flux density and frequency of excitation [8,9];

$$A_c A_{Win} = \frac{S}{kk_u \hat{B} J f} \qquad (2.4)$$

A_c ≡Core cross-sectional area
A_{win} ≡Window area of core
S ≡ VA rating of the transformer
k ≡form factor describing the nature of the voltage waveform
k_u ≡Packing factor of windings
$\hat{B}$ ≡Peak flux density
J ≡Current density
f ≡Frequency

Similarly the size of the core required for an inductor of specific value, subject to a particular level of excitation is inversely proportional to the peak flux density and frequency of excitation[9];

$$A_c A_{Win} = \frac{L\hat{I}_p I_{rms}}{ck_u \hat{B} J} = \frac{X_L \hat{I}_p I_{rms}}{2\pi c k_u \hat{B} J f} \qquad (2.5)$$

L ≡ Inductance

$X_L = 2\pi f L$ ≡ Inductive reactance

$\hat{I}_p$ ≡ Peak current

$Irms$ ≡ Effective current in windings

c ≡ Constant dependent on number of turns

From equations (2.3), (2.4) and (2.5), it follows that for a specific power loss, the reduction in magnetic material achieved by an increase in frequency of operation is partly negated by the increase in material due to the decrease in flux density.

2.2.2.2. Factors limiting the efficient use of conductive materials in single core magnetic assemblies

An increase in frequency of operation leads not only to a reduction in magnetic material volume but also to a reduction in conductive material volume. At ultrasonic frequencies, however, the current density must be constrained to an acceptably low value to prevent excessive heating and consequent failure of dielectric insulation. In a manner analogous to magnetic materials, the reduction in conductive material volume obtained by an increase in frequency, is partially counteracted by the limitations placed on the current density.

This derating effect and its influence on materials utilisation can be examined analytically, but the mechanisms responsible for heat generation in the windings must first be examined.

The heat generated in the windings of magnetic component is directly attributed to the Joule effect and is proportional to the square of the current density, J, and resistivity, ρ, of the conductor material, as given in equation (2.2) and repeated in equation (2.6) for convenience;

$$P_e = \frac{J^2}{2\sigma} \tag{2.6}$$

In general, the current distribution is non-uniform within the windings due to skin and proximity effects, so that the relationship given in equation (2.6) becomes a complex function of the winding geometry and frequency of excitation [4,5,10]. The effective resistance of windings increases with increasing frequency, causing an increase in the joule losses, which from equation (2.6) can be associated with an increase in the magnitude of the current density. The current density cannot be allowed to increase indefinitely, however, because the associated increase in losses would reach a point where the dielectric material would fail resulting in breakthrough and ultimately, failure of the magnetic component. It is desirable, therefore, to constrain the rise in temperature of the windings to an acceptable value.

From Faraday's law, the total copper cross-sectional area required for a transformer at a given power level and magnitude of magnetic induction, is inversely proportional to the product of frequency and current density in the following manner;

$$A_{cu} = k_u A_{Win} = \frac{S}{k \hat{\phi} J f} \tag{2.7}$$

$\hat{\phi}$ ≡Peak flux in magnetic core

Similarly the total copper cross-sectional area required for an inductor of specific value, subject to a particular level of excitation is inversely proportional to the maximum current density;

$$A_{cu} = k_u A_{Win} = \frac{L\hat{I}_p I_{rms}}{c\hat{\phi} J} = \frac{X_L \hat{I}_p I_{rms}}{2\pi c \hat{\phi} J f} \tag{2.8}$$

From equation (2.6), (2.7) and (2.8), it follows that for given winding losses, the reduction in conductive material obtained by an increase in frequency is partly negated by the increase in material due to the decrease in current density.

2.2.3 Multiple core magnetic assemblies

From the previous section it is seen that heat generation in the core and windings of a monolithic magnetic component has a prominent influence on the efficient use of conductive and magnetic materials. To ascertain the influence of heat generation in multiple core assemblies, the effect of geometrical structure on heat dissipation must first be considered.

2.2.3.1. Thermal aspects related to magnetic components and their structure

The heat that is generated in magnetic cores and in their windings in response to cyclic excitations can be dissipated in three ways, namely, (1) heat transfer by conduction, (2) heat transfer by convection and (3) heat transfer by radiation [11,12].

(1) Heat transfer by conduction

When a temperature gradient exists within a body it is found that heat flow exists in the direction of decreasing temperature. Under steady state conditions the rate of heat flow is related to the geometry and material properties of the body in the following manner;

$$Q_{conduction} = \frac{k\ A_{conductoion}\ \Delta T}{L_{conduction}} \qquad (2.9)$$

$\frac{\Delta T}{L_{conduction}}$ ≡ Temperature gradient

$Q_{conduction}$ ≡ Rate of heat transfer by conduction

$A_{conduction}$ ≡ Cross-sectional area perpendicular to heat flow

$L_{conduction}$ ≡ Distance of heat flow

k ≡ Conduction heat transfer coefficient

Similarly, when two bodies with different temperatures are brought into physical contact with each other, heat energy is transferred at the junction from the warmer body to the cooler body. The resultant heat flow rate in each body is numerically equal in value to the total rate of heat transfer between the two.

(2) Heat transfer by convection

Consider a thermally excited body immersed in a viscous medium. Heat is transferred by means of conduction to a thin layer of the medium directly in contact with the body, causing a change in its density due to thermal expansion. The heated layer is forced into motion away from the body, due to the resultant density gradient and replaced by another cooler layer of the medium. As the process is repeated time and time again, heat is transferred from the body and allowed to disperse in the bulk of the medium. The heat transfer depends on the shape and orientation of the body , the properties of the medium and the nature of the medium's flow. A general approximation used in engineering applications for the heat transfer by convection is given as;

$$Q_{convection} = \bar{h} A_{convection} (T_s - T_\infty) \qquad (2.10)$$

$Q_{convection}$ ≡ Rate of heat transfer by convection
$A_{convection}$ ≡ Surface area in contact with viscous medium
$\bar{h}$ ≡ Convection heat transfer coefficient
T_s ≡ Surface temperature
T_∞ ≡ Temperature of the viscous medium

(3) Heat transfer by radiation

Every body at a finite temperature emits electromagnetic radiation with an associated energy called radiant energy. The rate at which heat is transferred to the environment, is related to the geometry and material properties of the body as follows;

$$Q_{radiation} = A_{radiation}\ e\ \sigma_R \left(T_s^4 - T_\infty^4\right) \qquad (2.11)$$

$Q_{radiation}$ ≡ Rate of heat transfer by radiation
$A_{radiation}$ ≡ Surface area of radiating body
e ≡ Emissivity of radiant body
σ_R ≡ Stefan - Boltzman constant (5.669×10^{-8})

2.2.3.2. Improved heat dissipation of magnetic components by core subdivision

From equations (2.9),(2.10) and (2.11) it is seen that the heat transfer rate of a thermally excited body, is a function of the available surface area per volume and the surface temperature. Consequently, for a given power loss, an increase in the surface area of a geometrical solid would result in a decrease in its surface temperature. It is mathematically supported that the surface area per volume ratio of any geometric solid can be increased by its subdivision into smaller elements of the same shape and size. Consider, for example, the subdivision of a cube into smaller element cubes, as illustrated in Figure.2-5.

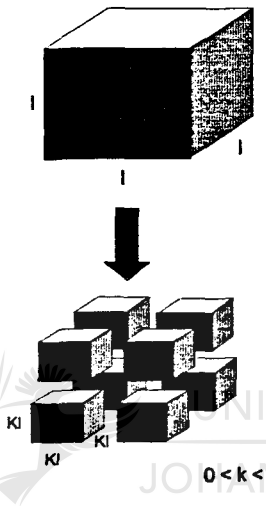

Figure. 2-5 Subdivision of a cube into smaller unit cubes

The total surface area to volume ratio of the original cube is given by;

$$\frac{Surface\ Area}{Volume} = \frac{1}{\ell} \qquad (2.12)$$

The increased surface area to volume ratio achieved by the cube's subdivision into smaller elements is given by[†];

$$\left(\frac{Surface\ Area}{Volume}\right)_{total} = \frac{\Sigma(Surface\ Area)_{unit}}{\Sigma(Volume)_{unit}} = \frac{1}{k\ell} \qquad (2.13)$$

[†]The surface area to volume ratio for a single unit cube is also described by equation (2.10).

Similarly, the surface area to volume ratio of a magnetic core and its windings can be increased by its subdivision into smaller element cores of the same shape and size, as is the case with multiple core magnetic assemblies. The rise in temperature of the magnetic core and its windings will, therefore, be lower for the elements of a multiple core assembly than for a single core assembly operating at the same power level and frequency.

2.2.3.2. Influence of multiple core structures on the derating effect for conductive material

To illustrate the effect that the subdivision of a magnetic component, into appropriately interconnected elements, has on conductive material, consider the winding geometry of Figure.2-6.

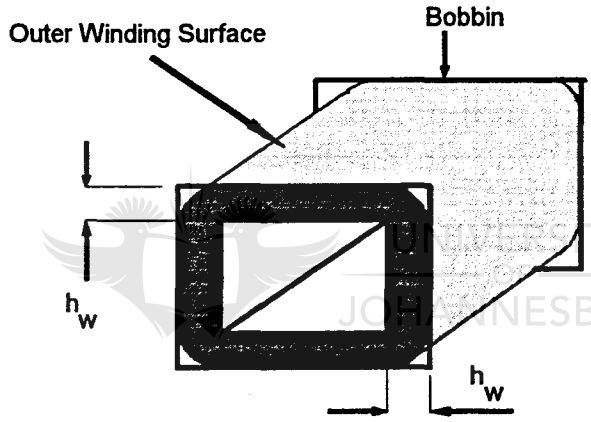

Figure. 2-6 Schematic view of windings on bobbin

An exact mathematical description of the variation in current density with core size is complicated by high frequency loss mechanisms such as the skin and proximity effects. These effects can be neglected, however, and a reasonable approximation obtained by assuming perfect litz wire windings. The current distribution over the conductor cross-section would be then be uniform, and the only opposition to current flow would be the DC resistance of the winding conductors.

If it is assumed that the heat dissipation is limited to the surface areas indicated by the light shade of grey in Figure.2-6, it can be shown from loss considerations, described in Appendix.A, that the relationship between current density, J, and winding height, h_w, for naturally cooled magnetic components is a constant as given by;

$$J = \frac{k'}{\sqrt{h_w}} \qquad (2.14\text{-a})$$

where

$$k' = \sqrt{\frac{\bar{h}\,\Delta T}{\sigma}} \qquad (2.14\text{-b})$$

$\bar{h}$ ≡ Convection heat transfer coefficient
ΔT ≡ Temperature difference between winding surface and environment
σ ≡ Conductivity of windings

If it is assumed that the windings of a magnetic component make maximum use of the available window area of the core, then h_w has a value approximately equal to the window height. Then, from equation (2.14), it follows that the maximum permissible current density in the windings of a magnetic component increases with a decrease in core size. The maximum permissible current density may be increased in the elements of a multiple core assembly therefore, and the derating effect in conductive material is reduced in multiple core assemblies.

2.2.3.3. Influence of multiple core structures on the derating effect for magnetic material

In core loss limited magnetic components, an explicit relationship exists between the core size, core surface area, core surface temperature, flux density and frequency of excitation but due to the complexity of the thermal aspects involved, a closed form analytical expression is difficult to derive. Consequently, the relationship had to be determined empirically from a range of carefully co-ordinated temperature experiments described in detail in Appendix B.

The measured results, showing the relationship between rise in surface temperature, flux density and frequency are given in Figures (C-6..C-10) of Appendix C, for five E-type cores of grade 3C80 ferrite material subjected to natural convection cooling. A typical set of results is illustrated in Figure.2-7.

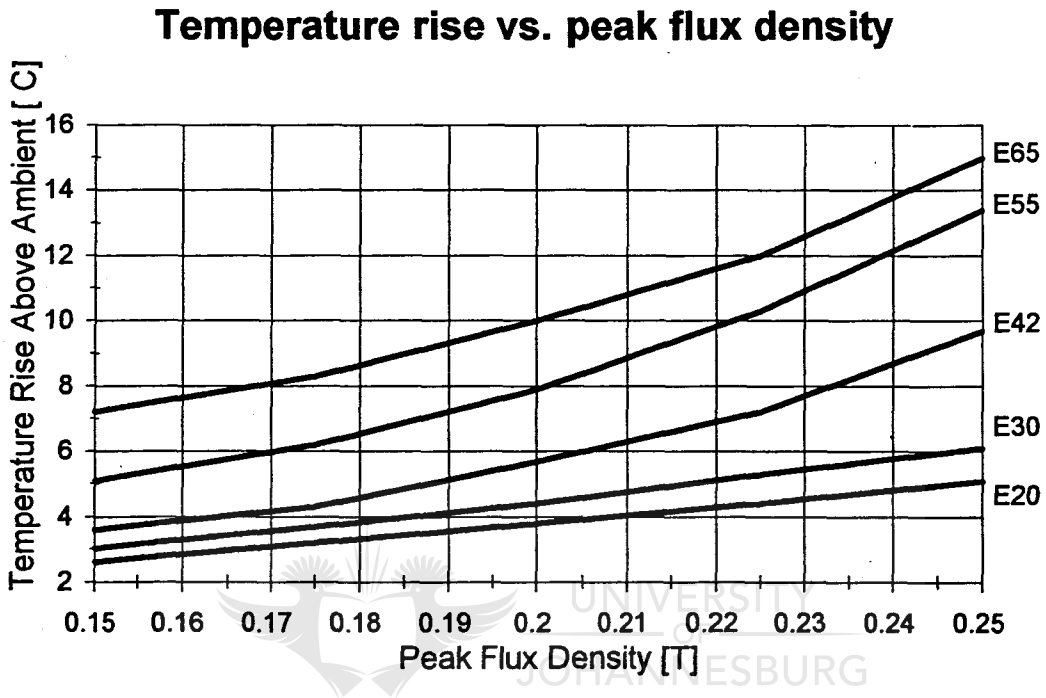

Figure. 2-7 Surface temperature comparisons for various size E-cores at 10 kHz

From the graphical results given in figures (C-6 .. C-10), it is seen that, E-cores of smaller physical dimension experience a smaller temperature rise than their larger counterparts at the same frequency and flux density excursion. This is attributed to the larger surface area to volume ratio in the smaller cores. Consequently, it is seen that the smaller cores of a multiple core assembly may be driven at higher flux density excursions than their larger counterparts and experience lower surface temperature distributions and improved temperature stability. The derating effect is thereforee reduced in the elements of a multiple core magnetic assembly, and consequently for the entire multiple core configuration.

2.2.4. Evaluation of single core and multiple core magnetic assemblies.

It is now of primary concern to evaluate the utilisation of magnetic material volume, conductive material volume and space volume in naturally cooled, single core and multiple core magnetic components. This section, is dedicated to (1) the development of mathematical expressions that may be used to observe the influence of derating effects on materials utilisation, and space volume consumption in magnetic components, and to (2) the comparison of magnetic components from a materials point of view.

2.2.4.1. Magnetic material volume

The defining equation that explicitly includes information pertaining to the size of the core required for a transformer is given by equation (2.4), and repeated in equation (2.15) for convenience;

$$S = k\, k_u\, \hat{B}\, J\, f\, A_c\, A_{Win} \qquad (2.15)$$

by defining a constant, Λ, as follows

$$\Lambda \equiv \frac{S}{f} \qquad (2.16)$$

equation (2.15) can be expressed as follows

$$A_c\, A_{Win}\, \hat{B}\, J = \frac{\Lambda}{k\, k_u} = \lambda \qquad (2.17)$$

where λ is defined as a constant given that the form factor, k, and the packing factor k_u, remain constant.

Similarly, the defining equation that explicitly includes information pertaining to the size of the core required for an inductor is given by equation (2.5) and is repeated in equation (2.18) for convenience;

$$L\hat{I}_p I_{rms} = c k_u \hat{B} J A_c A_{Win} \tag{2.18}$$

By defining a constant, Γ, as follows;

$$\Gamma \equiv L\hat{I}_p I_{rms} \tag{2.19}$$

equation (2.23) can be expressed as follows;

$$\hat{B} J A_c A_{Win} = \frac{\Gamma}{c k_u} = \beta \tag{2.20}$$

where β is defined as a constant given that the turns constant, c, and the packing factor k_u, remain constant.

From equations (2.17) and (2.20), it is seen that the defining equation used to select the core size of any single core magnetic component subject to specific operating conditions, has the following general form,

$$\hat{B} J A_c A_{Win} = \xi_1 \tag{2.21}$$

where the constant ξ_1 can adopt any positive real value.

If ξ_1 is kept invariable with frequency, equation (2.21) can be used as follows to observe the deleterious influences of derating effects on magnetic material utilisation in single core magnetic components,

> As the frequency of operation increases the flux density and current density is reduced due to derating effects. The additional increase in magnetic material volume warranted by the decrease in the density product ($\hat{B}J$), is indicative of the quantity of magnetic material which is not used to its full extent. The derating effect in monolithic magnetic components, therefore, can be observed by the growth in magnetic material volume with increasing frequency.

An expression similar to equation (2.21) can be derived for a multiple core magnetic assembly with n identical elements, and is given as follows,

$$n\left(\hat{B}\,J\,A_c\,A_{Win}\right)=\xi_n \qquad (2.22)$$

where the constant ξ_n can adopt any positive real value.

If ξ_n is kept invariable with frequency, equation (2.22) can be used as follows to observe the deleterious influences of derating effects on magnetic material utilisation in multiple core magnetic components,

> As the frequency of operation increases the flux density and current density is reduced due to derating effects. If the core size of the elements are kept constant, then the reduction in density product ($\hat{B}J$) is counteracted by an increase in the total number of elements, n. The additional increase in magnetic material volume warranted by the decrease in the density product, is indicative of the quantity of magnetic material which is not used to its full extent. The derating effect in multiple core magnetic components, therefore, can be observed by the growth in the total magnetic material volume with increasing frequency.

Equations (2.22) and (2.23) can be used to compare the magnetic materials utilisation of single core and multiple core magnetic components as follows,

If a single core magnetic component is to be replaced by a multiple core magnetic assembly with n identical elements, then $\xi_1 = \xi_n$, i.e.

$$n\left(\hat{B}\,J\,A_c\,A_{Win}\right)_{element} = \left(\hat{B}\,J\,A_c\,A_{Win}\right)_{monolithic} \qquad (2.23)$$

The variability of the current density can be included in equation (2.23) by substitution of equation (2.14). The condition for equivalence between multiple core assemblies and single core assemblies is then given by,

$$n\left(\frac{\hat{B}A_cA_{Win}}{\sqrt{h_w}}\right)_{element} = \left(\frac{\hat{B}A_cA_{Win}}{\sqrt{h_w}}\right)_{monolithic} \qquad (2.24)$$

The variability of the peak flux density can be included in equation (2.24) by rewriting it in the following form,

$$n\left(\frac{\hat{B}(f)A_cA_{Win}}{\sqrt{h_w}}\right)_{element} = \left(\frac{\hat{B}(f)A_cA_{Win}}{\sqrt{h_w}}\right)_{monolithic} = \xi \qquad (2.25)$$

where the value of $\hat{B}(f)$ can be accounted for by reference to the results given in figures (C-6 .. C-10).

Equation (2.25) can now be used to evaluate and compare the change in magnetic material volume, of the single core and multiple core magnetic assembly as a function of frequency. Where the magnetic material volume of the monolithic assembly, and for each of the elements in the multiple core assembly can be obtained with reference to data books.

2.2.4.2. Conductive material volume

The defining equation that explicitly includes information pertaining to the quantity of conductive material required for a monolithic transformer with a given core size, can be derived from equation (2.17) and is given as follows,

$$k_u A_{Win} = \frac{\Lambda}{k A_C \hat{B} J} \tag{2.26}$$

where $k_u A_{Win}$ is indicative of the cross-sectional area of conductive material required for the given operating conditions.

By defining a constant, τ, as follows,

$$\tau = \frac{\Lambda}{k} \tag{2.27}$$

equation (2.26) can be expressed as follows,

$$k_u \hat{B} J A_C A_{Win} = \tau \tag{2.28}$$

Similarly, the defining equation that explicitly includes information pertaining to the quantity of conductive material required for a monolithic inductor with a given core size, can be derived from equation (2.20) and is given as follows;

$$k_u A_{Win} = \frac{\Gamma}{c A_C \hat{B} J} \tag{2.29}$$

By defining a constant, ψ, as follows,

$$\psi = \frac{\Gamma}{c} \tag{2.30}$$

equation (2.29) can be expressed as follows,

$$k_u \hat{B} J A_C A_{Win} = \psi \tag{2.31}$$

Hence the defining equation that contains information pertaining to the quantity of conductive material for any monolithic magnetic component subject to specific operating conditions, is given as follows,

$$k_u \hat{B} J A_C A_{win} = K_1 \tag{2.32}$$

where the constant, K_1 , can adopt any positive real value.

By keeping K_1 invariable with frequency, equation (2.32) can be used as follows to observe the deleterious influences of derating effects on conductive material utilisation in single core magnetic components,

> As the frequency of operation increases the flux density and current density is reduced due to derating effects. If K_1 is to remain invariable with frequency, the reduction in the density product ($\hat{B}J$) must be counteracted by an increase in the area product ($A_c\ A_{win}$). Consequently the product $k_u\ A_{Win}$, is seen to increase, if the packing factor k_u is kept constant. The additional increase in conductive material volume warranted by the decrease in the density product, is indicative of the quantity of conductive material which is not used to its full extent.

The derating effect in monolithic magnetic components, therefore, can be observed by the growth in conductive material volume with increasing frequency, where the volume of conductive material with reference to Figure.2-4 is defined as,

$$V_{cu} \equiv k_u A_{Win}(MLT) \tag{2.33}$$

V_{cu} ≡ Volume of copper used in windings
(MLT) ≡ Mean length of turn for windings

An expression similar to equation (2.32) can be derived for a multiple core magnetic assembly with n identical elements, and is given as follows,

$$n\left(k_u \hat{B} J A_C A_{win}\right)_{element} = K_n \tag{2.34}$$

By keeping K_n invariable with frequency, equation (2.34) can be used as follows to observe the deleterious influences of derating effects on conductive material utilisation in multiple core magnetic components,

As the frequency of operation increases the flux density and current density is reduced due to derating effects. If the core size of the elements are kept constant, then the reduction in density product ($\hat{B}J$) is counteracted by an increase in the total number of elements, n. Consequently, the product $n(k_u A_{Win})_{element}$ is seen to increase if the packing factor k_u is kept constant. The additional increase in conductive material volume warranted by the decrease in the density product, is indicative of the quantity of conductive material which is not used to its full extent.

The derating effect in multiple core magnetic components, therefore, can be observed by the growth in the total conductive material volume with increasing frequency, where, the volume of conductive material, with reference to Figure.2-4, is defined as[‡],

$$V_{cu} \equiv n\left(k_u A_{Win}\left(MLT\right)\right)_{element} \qquad (2.35)$$

The conductive materials utilisation for single core and multiple core magnetic components must be evaluated in conjunction with equation (2.25). Once the equivalence of equation (2.25) has been established, equations (2.33) and (2.35) can be used to evaluate and compare the change in conductive material volume as a function of frequency.

2.2.4.3. Space volume

A magnetic component incorporating an E-core, requires a finite volume of space, called the space volume. The space volume required for packaging purposes and allows for the dissipation of heat. The general space volume dimensions are graphically illustrated in Figure 2.8.

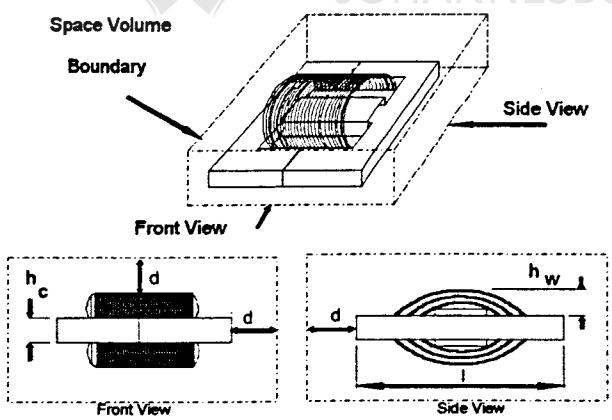

Figure. 2-8 Top and side views of magnetic component using an E-core, showing the relative dimensions of the space volume

[‡]Equation (2.34) is a reasonable estimate for the conductive material volume in multiple core assemblies, since only a small percentage of the total copper volume required by a multiple core assembly with n elements is used for interconnection purposes.

With reference to Figure 2.8, the space volume for the component can be expressed as;

$$Space\,Volume = \left[2(h_w + d) + h_c\right]\left[2d + l\right] \qquad (2.36)$$

$hw \equiv$ Winding height
$hc \equiv$ Core height
$l \equiv$ Magnetic core length
$d \equiv$ Length of extreme core dimensions to sides of space volume boundary

Since the space volume of a monolithic magnetic components is dependent on the dimensions of the core and windings, it follow that its value will increase with increasing frequency.

If it is assumed that the elements of a multiple core assembly can be packed next to each other and on top of each other in such a manner that the adjacent sides of their space volumes touch, then the summed space volume required for a multiple core assembly with n elements is given as;

$$Space\,Volume = n\left[2(h_w + d) + h_c\right]\left[2d + l\right]_{element} \qquad (2.37)$$

Since the space volume of a multiple core magnetic component is dependent on the dimensions of the core and windings of the elements, it follow that its value will increase with increasing frequency

The space volume consumption for single core and multiple core magnetic components must be evaluated in conjunction with equation (2.25). Once the equivalence of equation (2.25) has been established, equations (2.33) and (2.35) can be used to evaluate and compare the change in space volume as a function of frequency.

The summed space volume for a multiple core magnetic component will be invariable, even though its geometry may change. Consider, for example, the two space volume geometry's illustrated in Figure.2-9 and Figure.2-10.

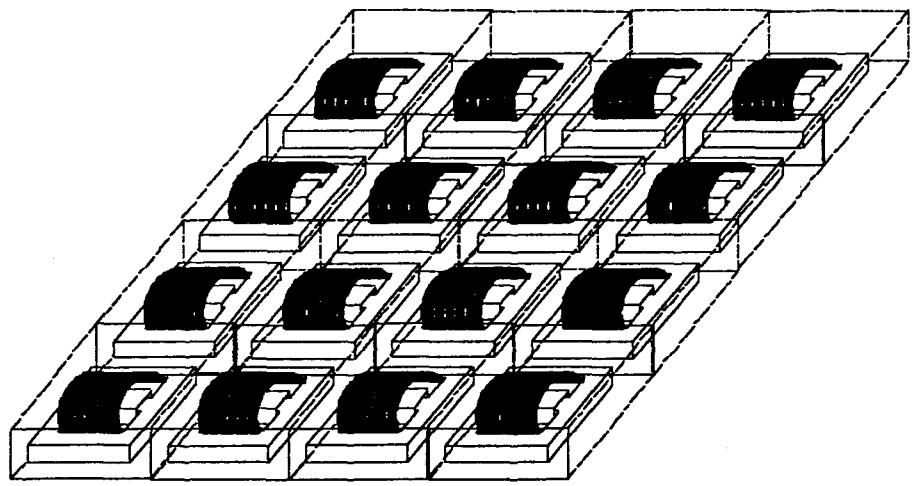

Figure. 2-9 Single layer packing of elements in a multiple core assembly

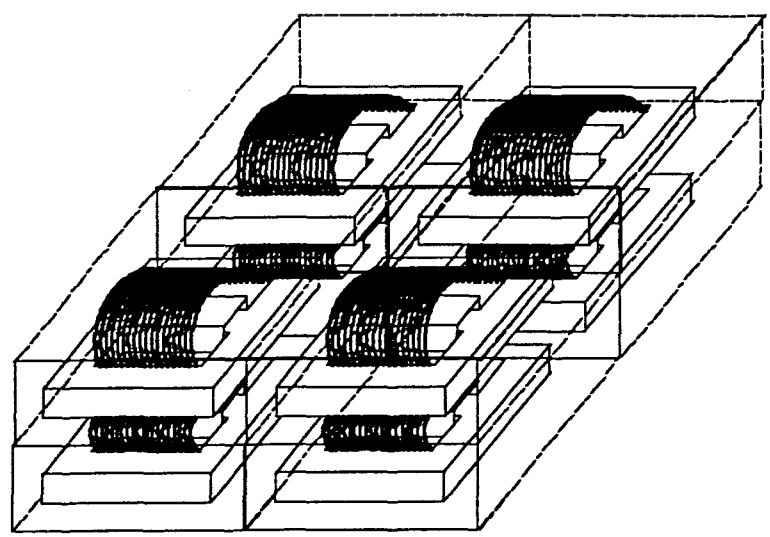

Figure. 2-10 Double layer packing of elements in a multiple core assembly

2.2.4.4. Comparison of magnetic assemblies from a materials point of view

The mathematical formulation developed in sections 2.2.4.1-2.2.4.3, can now be implemented to gain insight into the materials usage and space volume consumption of naturally cooled single core and multiple core magnetic assemblies as a function of frequency and temperature rise in the magnetic and conductive materials.

The investigation will be conducted as follows,

- The maximum permissible temperature rise in the magnetic material and windings will not be allowed to exceed the assumed ambient temperature by more than 30 °C - a condition inherent to natural convection cooled magnetic components. This investigation is therefore, conducted at three temperatures within this range, namely at (1) 10 °C, (2) 20 °C and (3) 30 °C above an ambient temperature of 25 °C.

- The investigation assumes an E-type core geometry for the monolithic assembly and for the elements in the multiple core assembly. Five different E-core sizes as specified by Phillips are considered in the investigation, namely (1) E65 core, (2) the E55 core, (3) the E42 core, (4) the E30 core and (5) the E20 core.

- The first step of the investigation is concerned with definition of a reference value for ξ ,so that the equations of the previous section may be used. For purposes of this investigation, the reference value will be assigned to a monolithic magnetic component with an E65 core, operating at a frequency of 10 kHz - (the lowest operating frequency considered in this investigation). The total number of elements required for an equivalent multiple core assembly is then calculated from equation (2.25) for each of the four remaining core sizes listed above.

- The next step of the investigation is concerned with the growth in conductive material volume, magnetic material volume and space volume of each of the magnetic assemblies, with increasing frequency.

- This is accomplished by stepping up the frequency from (1) 10 kHz to (2) 30 kHz and then to (3) 50 kHz, and calculating in each case the total conductive material volume, magnetic material volume and space volume that is required by each magnetic assembly to maintain a value for ξ, constant and equal to the reference value.

(1) Materials comparison with a maximum rise in core and winding temperature of 10 ℃ above ambient

From the results given in Figures (C-6 .. C-10), it is seen that a maximum flux density of 200 mT is permissible in the magnetic material of the E65 core at 10 kHz, so that the reference value for ξ is given as follows,

$$\xi_{E65}(10\,kHz) = \frac{\hat{B}(10\,kHz)\,A_c\,A_{Win}}{\sqrt{h_w}} = 16\,433\,mm^3T \qquad (2.38)$$

Calculating the actual value of ξ for each of the five core sizes at frequencies of 10 kHz, 30 kHz and 50 kHz produces the results given in Table.2-1.

	10 kHz		30 kHz		50 kHz	
	B [mT]	ξ [mm^{3}T]	B [mT]	ξ [mm^{3}T]	B [mT]	ξ [mm^{3}T]
E65	**200**	**16 433**	**150**	**12 324**	-	-
E55	**220**	**9 180**	**160**	**6 676**	**175**	**7 032**
E42	**250**	**3 961**	**175**	**2 772**	**185**	**2 931**
E30	**250**	**721**	**215**	**620**	**220**	**635**
E20	**250**	**191**	**230**	**176**	**250**	**191**

Table.2-1 Change in ξ for each core size as a function of frequency

The total number of elements, n, required for an equivalent multiple core assembly is evaluated for each core size by making use of equation (2.25) and using ξ_{65} (10kHz) as a reference. The results are given in Table.2-2 over the frequency range of interest.

Core Size	n at 10 kHz	n at 30 kHz	n at 50 kHz
E65	**1**	**2**	-
E55	**2**	**3**	**3**
E42	**5**	**6**	**7**
E30	**23**	**26**	**36**
E20	**86**	**93**	**126**

Table.2-2 The total number of elements required by each multiple core assembly

The total magnetic material volume can now be calculated for each case with reference to data books, the total conductive material volume can be calculated from equation (2.33) and (2.35), and the space volume can be calculated from equations (2.36) and (2.37). The results are illustrated graphically in figures (2-11 .. 2-13).

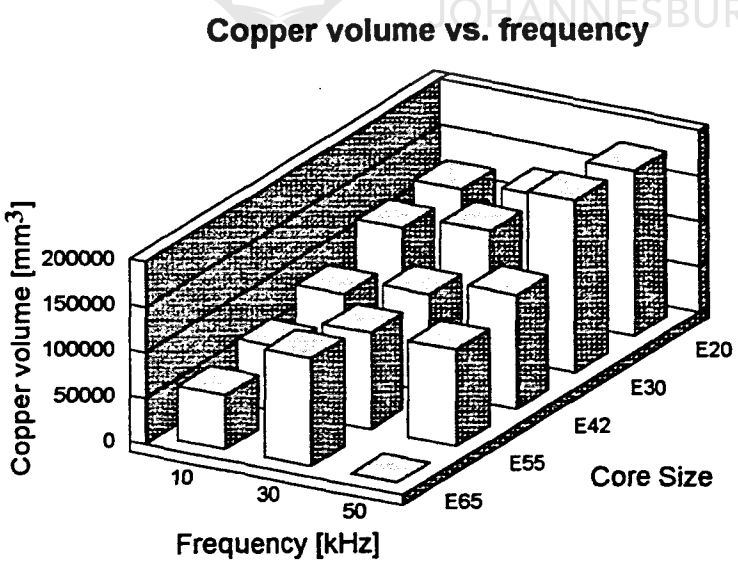

Figure. 2-11 Comparison of the total conductive material volume for a single core assembly and four equivalent multiple core assemblies with different elements

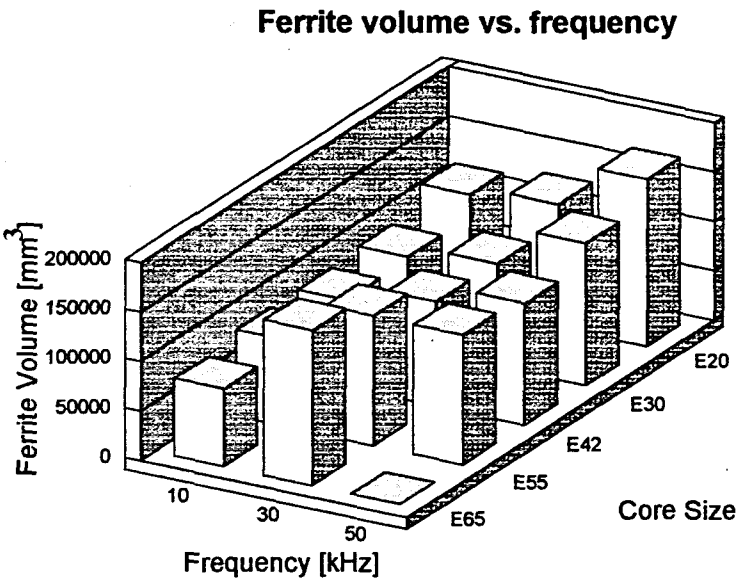

Figure. 2-12 Comparison of the total magnetic material volume for a single core assembly and four equivalent multiple core assemblies with different elements

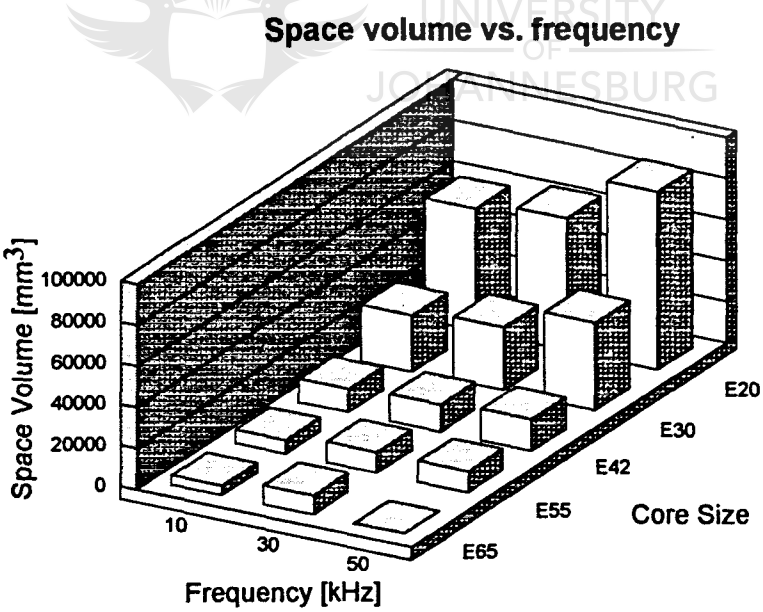

Figure. 2-13 Comparison of the space volume for a single core assembly and four equivalent multiple core assemblies with different elements, d=5mm

(2) Materials comparison with a maximum rise in core and winding temperature of 20℃ above ambient

From the results given in Figures (C-6 .. C-10), it is seen that a maximum flux density of 250 mT is permissible in the magnetic material of the E65 core at 10 kHz, so that the reference value for ξ is given as follows,

$$\xi_{E65}(10\,kHz) = \frac{\hat{B}(10\,kHz)\,A_c\,A_{Win}}{\sqrt{h_w}} = 20\,541 mm^3 T \qquad (2.39)$$

Calculating the actual value of ξ for each of the five core sizes at frequencies of 10 kHz, 30 kHz and 50 kHz produces the results given in Table.2-3.

	10 kHz		30 kHz		50 kHz	
	B [mT]	ξ [mm^{3}T]	B [mT]	ξ [mm^{3}T]	B [mT]	ξ [mm^{3}T]
E65	**250**	**20 541**	**175**	**14 378**	-	-
E55	**250**	**10 432**	**200**	**8 345**	**175**	**7 032**
E42	**250**	**3 961**	**225**	**3 564**	**185**	**2 931**
E30	**250**	**721**	**250**	**721**	**220**	**635**
E20	**250**	**191**	**250**	**191**	**250**	**191**

Table.2-3 Change in ξ for each core size as a function of frequency

The total number of elements, n, required for an equivalent multiple core assembly is evaluated for each core size by making use of equation (2.25) and using ξ_{65} (10kHz) as a reference. The results are given in Table.2-4 over the frequency range of interest.

Core Size	n at 10 kHz	n at 30 kHz	n at 50 kHz
E65	**1**	**2**	-
E55	**2**	**3**	**3**
E42	**6**	**6**	**7**
E30	**29**	**29**	**31**
E20	**107**	**107**	**107**

Table.2-4 Total number of elements required for each multiple core assembly.

The total magnetic material volume can now be calculated for each case with reference to data books, the total conductive material volume can be calculated from equation (2.33) and (2.35), and the space volume can be calculated from equations (2.36) and (2.37). The results are illustrated graphically in figures (2-14 .. 2-16).

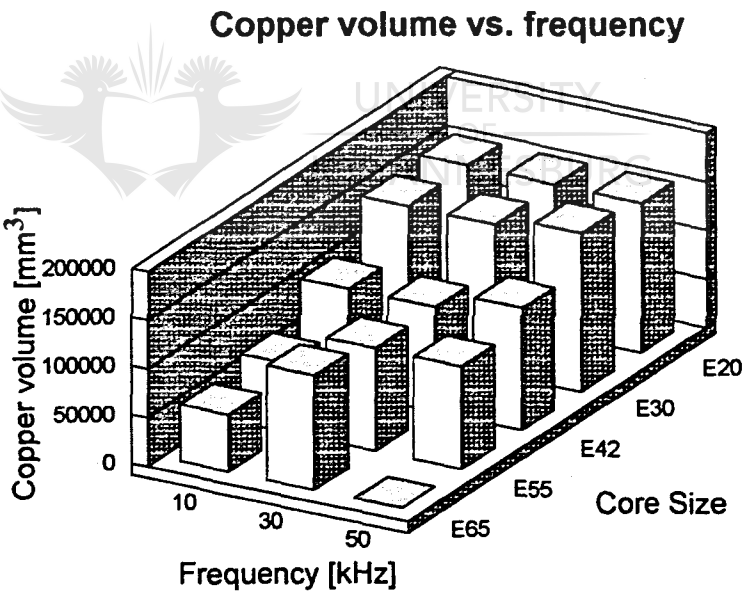

Figure. 2-14 Comparison of the total copper volume for a single core assembly and four equivalent multiple core assemblies with different elements

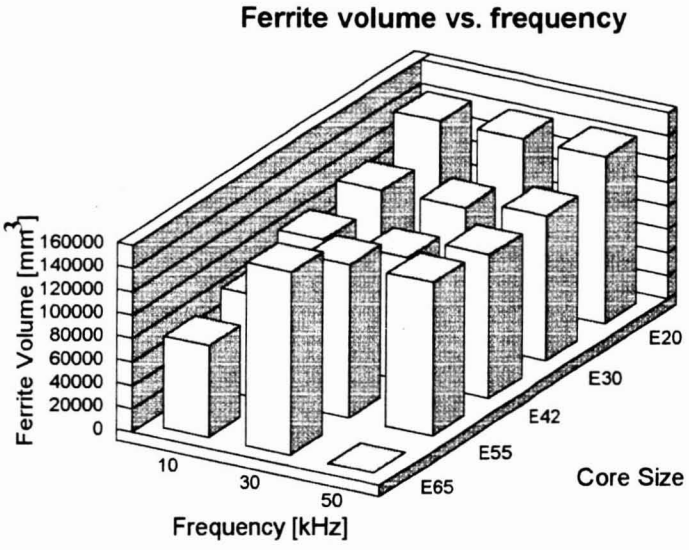

Figure. 2-15 Comparison of the total ferrite volume for a single core assembly and four equivalent multiple core assemblies with different elements

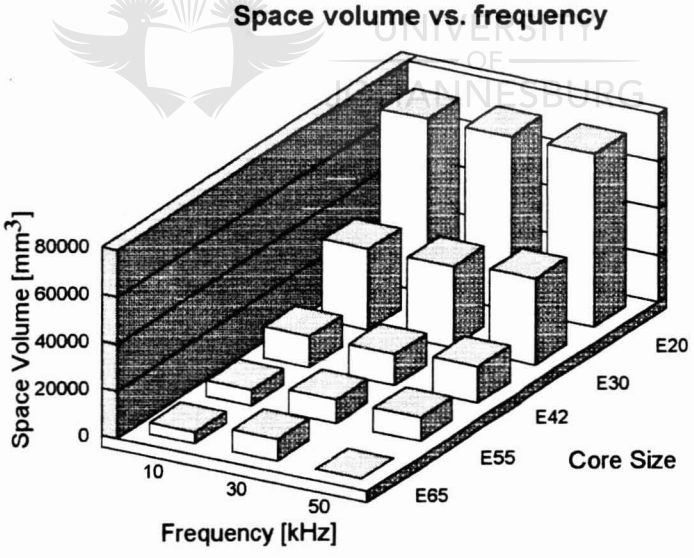

Figure. 2-16 Comparison of space volume for a single core assembly and four equivalent multiple core assemblies with different elements, d=5mm

(3) Materials comparison with a maximum rise in core and winding temperature of 30 °C above ambient

From the results given in Figures (C-6 .. C-10), it is seen that a maximum flux density of 250 mT is permissible in the magnetic material of the E65 core at 10 kHz, so that the reference value for ξ is given as follows,

$$\xi_{E65}(10\,kHz) = \frac{\hat{B}(10\,kHz)\,A_c\,A_{Win}}{\sqrt{h_w}} = 20\,541 mm^3 T \qquad (2.40)$$

Calculating the actual value of ξ for each of the five core sizes at frequencies of 10 kHz, 30 kHz and 50 kHz produces the results given in Table.2-5.

	10 kHz		30 kHz		50 kHz	
	B [mT]	ξ [mm^{3}T]	B [mT]	ξ [mm^{3}T]	B [mT]	ξ [mm^{3}T]
E65	**250**	**20 541**	**175**	**14 378**	-	-
E55	**250**	**10 432**	**200**	**8 345**	**175**	**7 032**
E42	**250**	**3 961**	**225**	**3 564**	**185**	**2 931**
E30	**250**	**721**	**250**	**721**	**220**	**635**
E20	**250**	**191**	**250**	**191**	**250**	**191**

Table.2-5 Change in ξ for each core size as a function of frequency

The total number of elements, n, required for an equivalent multiple core assembly is evaluated for each core size by making use of equation (2.25) and using ξ_{65} (10kHz) as a reference. The results are given in Table.2-6 over the frequency range of interest.

Core Size	n at 10 kHz	n at 30 kHz	n at 50 kHz
E65	**1**	**2**	-
E55	**2**	**3**	**3**
E42	**6**	**6**	**7**
E30	**29**	**29**	**31**
E20	**107**	**107**	**107**

Table.2-6 Total number of elements required for each multiple core assembly.

The total magnetic material volume can now be calculated for each case with reference to data books, the total conductive material volume can be calculated from equation (2.33) and (2.35), and the space volume can be calculated from equations (2.36) and (2.37). The results are illustrated graphically in figures (2-17 .. 2-19).

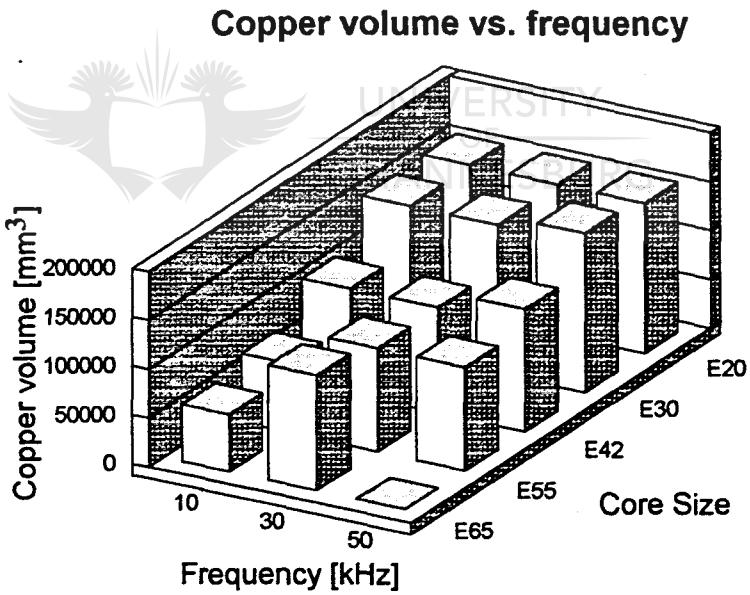

Figure. 2-17 Comparison of the total copper volume for a single core assembly and four equivalent multiple core assemblies with different elements

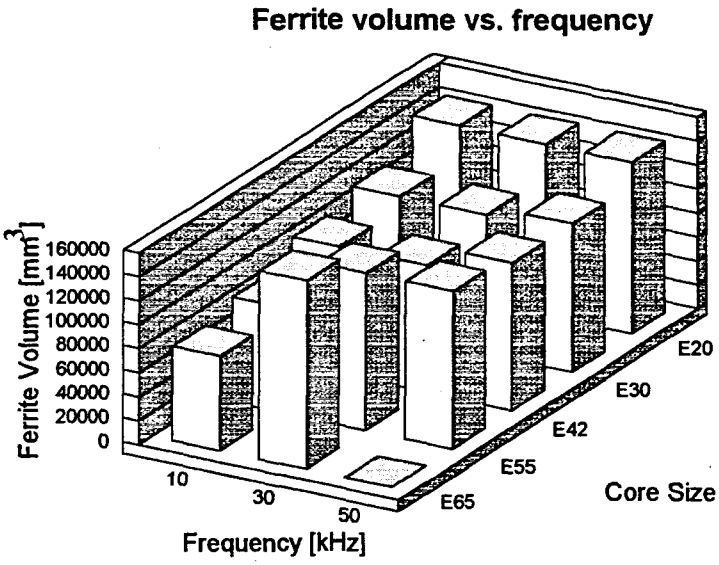

Figure. 2-18 Comparison of the total ferrite volume for a single core assembly and four equivalent multiple core assemblies with different elements

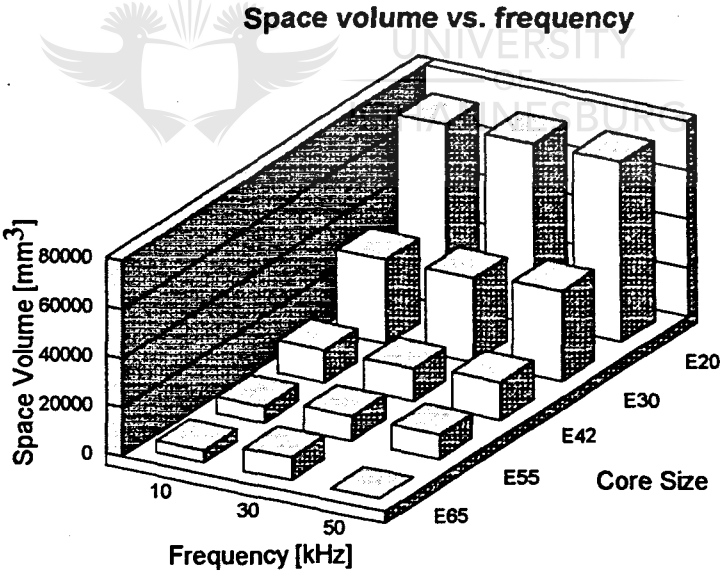

Figure. 2-19 Comparison of space volume for a single core assembly and four equivalent multiple core assemblies with different elements, d=5mm

2.2.4.5. Observations regarding single core and multiple core magnetic components

The following observations can then be made with regards to the results presented in Figures (2-11 .. 2-19),

1. For each case, the single core magnetic assembly required less materials volume and space volume at 10 kHz than any of the other multiple core assemblies. At higher frequencies(30 khz and 50 kHz), the single core magnetic component started utilising materials rather poorly.

2. At higher frequencies (30 kHz and 50 kHz), there is always at least one multiple core assembly that requires less materials volume than any of the other magnetic assemblies, with a reasonable space volume consumption. The single core assembly, however, still has the best space volume consumption of all the magnetic structures.

3. At higher frequencies (30 kHz and 50 kHz), there is always at least one multiple core magnetic assembly which requires more materials volume and space volume than any of the other magnetic assemblies. This is always associated with multiple core magnetic assemblies using the smaller core sizes for their elements.

From the previously listed observations, two types of single core and multiple core assemblies can be identified;

Type 1: Single core and multiple core assemblies which utilise materials and space volumes extremely well.

Type 2: Single core and multiple core assemblies which utilise materials and space volumes very poorly.

The grouping for magnetic components according to structural assembly can now be revised as illustrated in Figure.2-20.

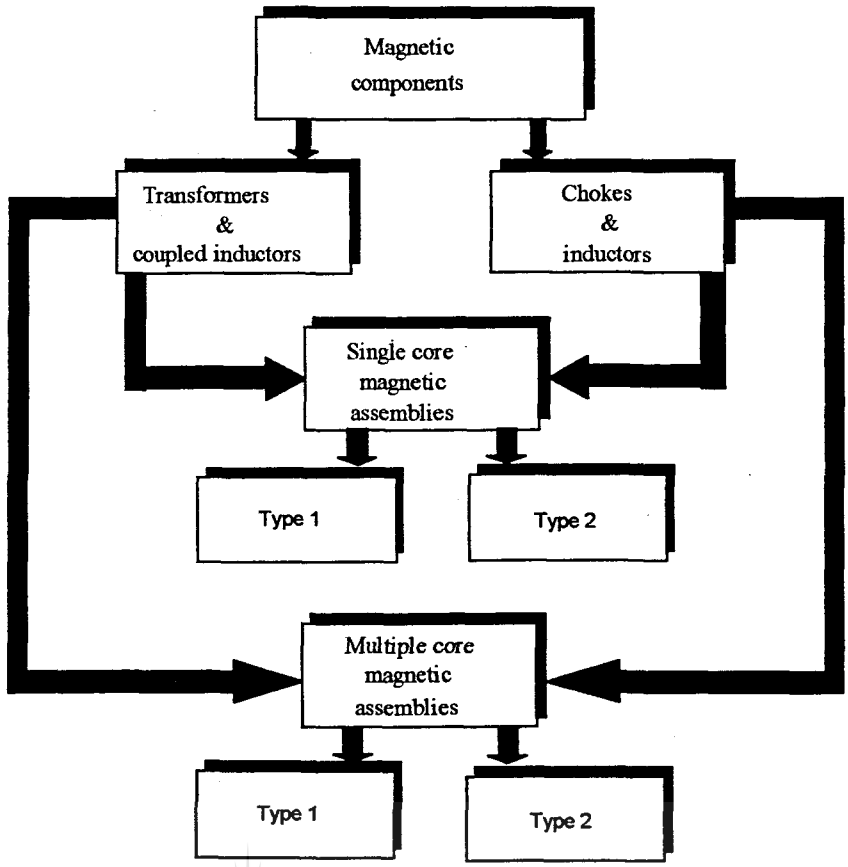

Figure. 2-20 Revised grouping of magnetic components according to structural assembly

2.3. INTRODUCING THE DISTRIBUTED MAGNETIC COMPONENT

It is of interest to take note that monolithic magnetic assemblies have become deeply entrenched in medium to high power switching mode applications. Multiple core assemblies have only found limited application, usually at lower power levels. With this in mind, the distributed magnetic component is introduced.

At every power level and frequency there exists a unique, type two multiple core magnetic assembly, that utilises an optimum core size for its elements, so that the overall configuration requires less materials and space volume than any other magnetic assembly. This unique magnetic assembly has been called "the distributed magnetic component".

2.4. CONCLUSION

An evaluation, illuminating some of the most important characteristics of existing magnetic components was considered. As a result a magnetic structure with unique characteristics was identified, leading to the novel concept of distributed magnetic components

3. Distributed transformers - analysis and design

3. DISTRIBUTED TRANSFORMERS - ANALYSIS AND DESIGN

3.1 INTRODUCTION

" At every power level and frequency there exists a unique, type two multiple core magnetic assembly, that utilises an optimum core size for its elements, so that the overall configuration requires less materials and space volume than any other magnetic assembly. This unique magnetic assembly has been called the distributed magnetic component"

The distributed magnetic component is a viable option for most high frequency switching mode applications with a flexibility of design and ease of manufacture comparable to existing single core magnetic structures. This chapter is therefore, dedicated to the development of the generalised distributed transformer configuration and the fundamental design principles that must be implemented to realise the assertion stated in bold type above.

3.2. THE GENERALISED DISTRIBUTED TRANSFORMER

3.2.1 The basic element

In general, the elements of a distributed transformer are considered to be identical in every respect, where the basic element implemented in a conventional distributed transformer assembly, can be described as a typical, multi-winding, single core, magnetic assembly with m turns in the primary winding and n turns in the secondary windings (where m and n can assume any appropriate positive integer value). The element is, therefore, subject to all fundamental principles of design and manufacture applicable to high frequency single core transformer assemblies.

The symbol adopted for its graphic representation is illustrated in Figure.3-1.

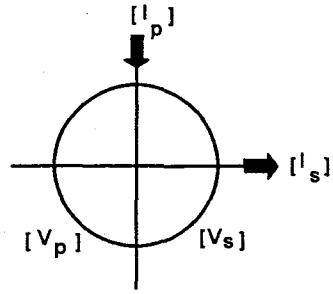

[V_p] :Primary voltage [V_s] :Secondary voltage

[I_p] :Primary current [I_s] :Secondary current

Figure.3-1. Symbol for an element in distributed transformers

The impedance and electrical parameters of an element will always be enclosed within square braces as illustrated in figure.3-1.

3.2.1.1. Electrical characteristics of the basic element

The basic element, as a generic two winding transformer, can be modelled by the two port network illustrated in Figure.3-2 [1], and will be adopted for further discussions in this dissertation.

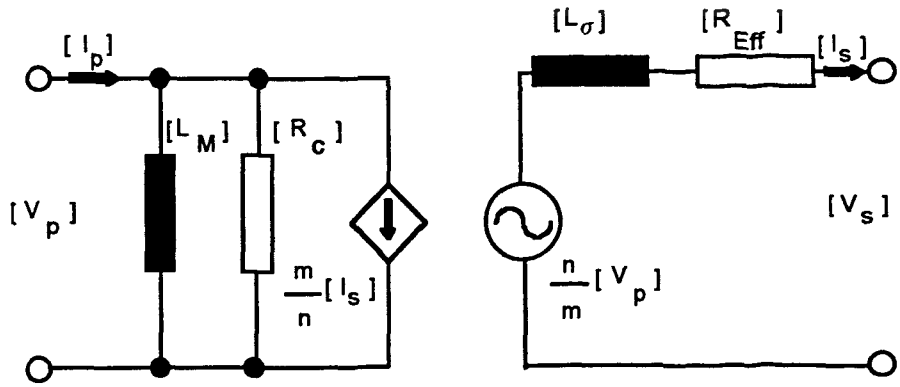

Figure.3-2. Equivalent model of an element

The physical significance of each of the parameters included in the two port of Figure.3-2, is described as follows;

3.2.1.2. Core loss resistance

The two port equivalent of the transformer, attributes core loss to a dissipative parameter referred to as the core loss resistance and is defined as follows;

$$[R_c] = \frac{[V_p]^2}{[P_c]} \tag{3.1}$$

R_c ≡Core loss resistance
V_p ≡Rated primary voltage
P_c ≡Core loss

As established in chapter 2, the power loss generated in ferrites in response to high frequency excitations is strongly dependent on the maximum permissible flux density excursion and frequency of excitation as given by equation (2.1). Furthermore, under steady state operating conditions, thermal equilibrium occurs where the power loss is equal to the total heat dissipated and is thereforee found to be a function of the core geometry and magnetic material properties as given by equations (2.9), (2.10) and (2.11).

Consequently, the value of R_c is a function of the maximum permissible flux density excursion, frequency of excitation, nature of excitation, method of cooling, core geometry and magnetic material properties. A mathematical description for R_c , therefore, is only meaningful once a definitive structure for the element is established.

3.2.1.3. The magnetising inductance

The magnetising inductance of the two winding element transformer is defined as the total self inductance of the primary winding, or alternatively, as the inductive component of the open circuit impedance of the two port network in Figure.3-2. The definition of a constant inductive parameter, however, is complicated by the variable nature of the permeability of the magnetic core.

This problem can be overcome by defining a constant average permeability as follows;

$$\mu_{ave} \triangleq \frac{B_s}{H_s} \tag{3.2}$$

μ_{ave} ≡ Average Permeability of Magnetic Material
B_s ≡ Saturation Flux Density of Magnetic Material[1]
Hs ≡ Magnetic Field Intensity at Saturation[1]

A reasonable approximation for the magnetising inductance is then given as;

$$[L_M] = \frac{\mu_{ave}\, m^2 A_{Eff}}{l_{Eff}} \tag{3.3}$$

$[L_M]$ ≡ Magnetising Inductance of an Element Transformer
m ≡ Number of Primary Turns
A_{Eff} ≡ Effective Cross sectional Area of Magnetic Path
l_{Eff} ≡ Effective Magnetic Path Length

The magnetising inductance, therefore, unlike any of the other two port parameters, may be considered as having a constant value for a given transformer structure.

3.2.1.4. The leakage inductance

In the two winding element transformer, the leakage inductance is defined as the energy storage element accountable for that portion of flux which does not successfully couple both windings, or alternatively, it may be defined as the inductive component of the short circuit impedance of the two port network in Figure 3.2.

It can be shown that the leakage flux in a two winding transformer is a function of frequency, core geometry, conductor cross-section and winding geometry [2]. A suitable mathematical description, therefore, can only be meaningful once a definitive structure for the element has been developed. Furthermore, no exact analytical expression for leakage inductance has been formulated because of the difficulty involved in determining the quantity of leakage flux and its magnetic path length. General techniques, however, have been suggested for the derivation of a conservative estimate [2].

[1] defined at knee of saturation on BH curve.

3.2.1.5. The effective AC resistance

At high frequencies each turn in a winding is immersed in time changing magnetic fields generated by the current in neighbouring turns. The eddy currents induced in each turn due to the resultant magnetic field distribution over the entire winding section, causes the natural flow of current to skew, creating a complex non-linear distribution of current over the cross section of the winding's conductors. Effectively, the opposition to current flow is higher under such conditions than it would be for an equivalent uniformly distributed dc current, and would increase with a further increase in frequency. In short, the resistance and, consequently, the conduction losses of a winding is found to increase with an increase in frequency. Furthermore, since the eddy currents responsible for the non-linear distribution in current density can be attributed to skin and proximity effects, it can be shown that the effective resistance is a function of conductor cross-section and winding geometry[3].

The effective AC resistance, therefore, refers to that dissipative parameter responsible for the heating effect in the windings, or alternatively, may be defined as the dissipative parameter of the short circuit impedance of the two port network in Figure 3.2. A mathematical description for the effective resistance can only be derived once a definitive selection for conductor cross-section and winding geometry is made.

3.2.1.6. Performance characteristics of the basic element

For power applications, the performance of an element is measured by its (1) power efficiency and (2) output voltage regulation, defined as follows;

(1) Power efficiency : The power efficiency is a measure of the total input power that is retrieved at the output terminals of the element transformer [1], and is defined as follows;

$$Efficiency = \frac{Power\ output}{Power\ input} = \frac{Power\ output}{Power\ output + (Core\ losses + Winding\ losses)}$$

$$\Rightarrow \quad [\eta] = \frac{[V_s][I_s][Cos\theta]}{[V_s][I_s][Cos\theta] + \left(\frac{[V_p]^2}{[R_c]} + [I_s]^2[R_{Eff}]\right)} \qquad (3.4)$$

$[\eta]$ ≡ Efficiency of an element

$[Cos\ \theta]$ ≡ Power factor of an element as governed by the load

The power efficiency of any transformer is usually expressed as a percentage where an efficiency of 100 % is ideal, i.e. where leakage inductance, winding resistance and core losses are absent.

(2) Output voltage regulation : The output voltage regulation is a measure of the change in output voltage under varying load conditions [1], and is defined as follows;

$$Regulation = \frac{No\ load\ voltage - Full\ load\ voltage}{Full\ load\ voltage} = \frac{Voltage\ drop\ over\ \{[R_{Eff}]\ \&\ [L_\sigma]\}}{Rated\ voltage}$$

$$\Rightarrow \quad [Regulation] = \frac{[I_s]^2\ [R_{Eff}] + j[wL_\sigma]}{[V_s]} \qquad (3.5)$$

Usually the voltage regulation is expressed as a percentage, where a regulation of 0 % is ideal, i.e. where leakage inductance and winding resistance is absent.

As can be seen from equations (3.4) and (3.5), the performance of an element is dependent on its impedance parameters. The leakage inductance, winding resistance and core loss is therefore, a major topic of concern in the design procedure.

3.2.2. Design considerations for the basic element

The impedance parameters of an element transformer are largely dependent on design and it is considered appropriate therefore, to discuss some general design considerations and their influence on an element. Since most of these considerations are encountered in conventional high frequency transformer designs, they are only briefly discussed - detailed explanations can be obtained from the pertinent references. There are some significant deviations in design from standard techniques, however, and these are emphasised strongly.

The design of a basic element can be sub-divided into two main parts, that of (1) magnetic core design and (2) winding design.

3.2.2.1. Magnetic core design

(a) Core geometry : The magnetic core used for the elements in a general distributed transformer assembly, is usually selected to best satisfy a number of functional and economic trade-offs since it can be of any shape, size and grade of material. The magnetic core can be pre-manufactured and bought off the shelf from local suppliers, or it can be custom manufactured to the design engineers specifications. In either case, consideration would be given to the following [4,5];

Personal preference: A given type of core could be selected purely because the design engineer is familiar with its use from prior experience or because it exhibits favourable physical characteristics such as a low profile structure for example.

Ease of Manufacture: Because the method of manufacture is a matter of preference, with fully automated assembly lines on one end of the scale and labour intensive assembly lines on the other, the complexity, time and cost required to manufacture a given magnetic component is very often determined by the geometry of the core.

Design specifications: The application in which the magnetic component is to be used, introduces design constraints which would bias the selection process to favour some core geometries over others. The use of a ring core, for example, is favourable for use in the forward and push-pull converter topologies but is unfavourable for use in the flyback converter topology, due to the leakage reactance requirements.

Regulations: Additional standards impose further operational and practical constraints on transformers such as EMI specifications, creepage distances, insulation specifications and shielding specifications. Low EMI specifications, for example, would restrict the selection of a magnetic core to geometries conducive to good coupling and magnetic screening.

(b) Core size and magnitude of excitation : The superior materials utilisation and space volume consumption associated with distributed transformers is dependent on three mutually inclusive considerations, the magnetic core size of the elements, the maximum flux density excursion permissible in the core material and the interconnection of the elements. Since this combination is unique to the distributed transformer, it stands to reason that the techniques ordinarily employed for the selection of core size in conventional transformer design [5,6,7], are not applicable. Considerations such as core losses, winding losses, maximum power dissipation density, type of cooling used and placement, are still included in the selection process but the method of selection is unique to the distributed transformer and is described in section 3.3 of this chapter.

3.2.2.2. Winding design

(a) Conductor cross-section and winding geometry : The winding geometry and type of conductor used in the windings of an element transformer is usually selected to best satisfy a number of functional and economic trade-offs[4,8]. Consideration would be given to the following factors in the selection process;

Ease of manufacture : The conductor cross-section and winding geometry influences the manufacturing technique required to form the windings, with labour intensive techniques on one end of the scale and machine automation on the other. Windings with multiple winding sections made from rectangular cross-section (foil windings), for example, must be wound by hand since the interconnections between winding sections are difficult to realise, whereas round wire windings with two winding sections may be wound with machines. The complexity, time and cost of a magnetic component is thereforee influenced by the conductor cross-section and geometry of the windings.

Design constraints : The application in which the magnetic component is to be used, introduces design constraints which would bias the selection process to favour some conductor cross-sections and winding geometries over others. The predominant design consideration would be its influence on magnetic coupling and total winding loss.

Since the non-linear current distribution in the conductors of a winding is attributed to skin and proximity effects, it can be shown that the effective resistance is dependent on the winding configuration and type of conductor used in the windings. The engineer is, therefore, afforded the freedom to minimise the effective resistance during the design procedure as described in [4,8]. Furthermore, since it can be shown that the leakage flux in a two winding transformer is a function of frequency, core geometry, conductor cross-section and winding geometry it follows that the engineer can minimise the leakage inductance during the design procedure as described in [2].

3.2.3. The basic interconnection of elements

A concept referred to as matrix interconnection has become a popular novelty for interconnecting the elements in multiple core assemblies, as can be seen from the number of publications dedicated to its use [9,10,11,]. Despite its popularity, matrix transformers have found limited application in switching mode converters operating in the medium to high power range (power levels in excess of 1 kVA). The reasons for its limited applications may be attributed to the philosophy in design of its elements.

According to [9], the elements in a conventional matrix transformer are designed to support a minimum number of turns per winding (usually no more than four), while maximum possible utilisation of the available winding area is maintained. This notable design feature results in excellent magnetic coupling within the windings and ultimately in lower leakage inductance, a characteristic common to the matrix transformer. It is also this one design feature in the elements that is responsible for the major differences in matrix transformers and distributed transformers.

The preference for a minimum number of turns per winding implies the use of a large number of relatively small cores, a characteristic common to type-1 multiple core assemblies. Consequently, the matrix transformer is found to have poor materials efficiency and excessive space volume characteristics. The matrix interconnection is not reliant on the geometry or construction of the elements, however, and can therefore be used as a convenient means of interconnection for the elements in a distributed transformer.

Note: The conventional matrix transformer is fundamentally different in design to the distributed transformer, because it is purposely not designed for maximum utilisation of materials and space volume efficiencies.

3.2.3.1 The generalised matrix interconnection

The distributed transformer with a generic two dimensional M:N matrix interconnection, resembles the tabular format associated with mathematical matrices, where the numerical values of M and N respectively describe the number of rows and columns in the configuration. The general matrix interconnection is realised by connecting the primary windings of every element in a column in series and then each column in parallel [9]. Similarly, the secondary winding of every element in a row is connected in series and each row is connected in parallel. Consider, for example, the matrix interconnection of a 2:3 distributed transformer as illustrated in Figure.3-3.

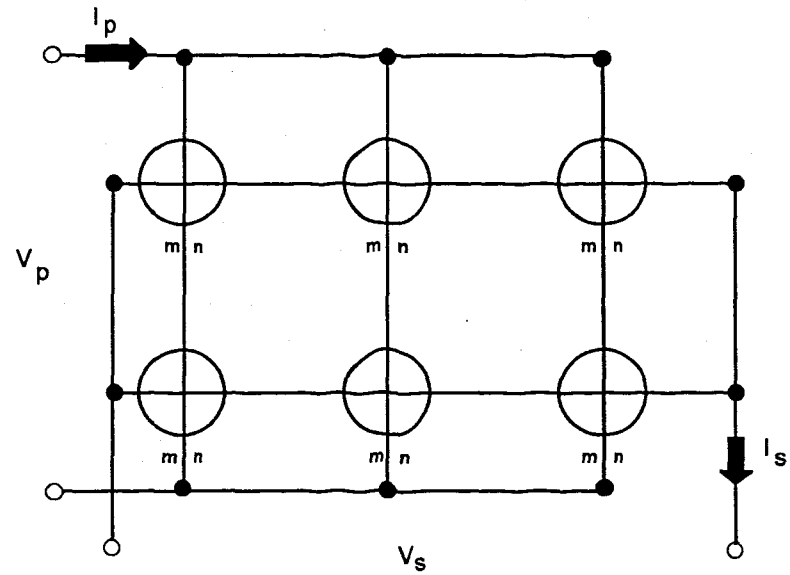

Figure.3-3. Example of a 2:3 matrix interconnection

The following convention will henceforth be adopted: Reference to any one particular element, or any of its electrical parameters will be accompanied by a set of subscripts denoting its position in the matrix. The electrical parameter [A] of the element in the first row and second column will, for example, be denoted as $[A_{12}]$.

3.2.3.2. Fundamental operation of the distributed transformer

The operation of the 2:3 distributed transformer is subject to four constraints governing the validity of the matrix interconnection [9], two are laws derived from fundamental electromagnetic principles, while the other two are rules derived from basic circuit analysis. These are given as follows;

1. **Law 1:** By Lenz's law the net ampere-turns in an element must be equal to zero,

i.e. $$m\left[I_p\right]_{ij} = n\left[I_s\right]_{ij} \qquad i = 1..M, j = 1..N$$

The exciting current is considered to be very small in comparison with the primary current, and is therefore omitted in the above formulation.

2. **Law 2:** By Faraday's law the volts per turn in each winding of an element must be equal,

i.e. $$\frac{[V_p]_{ij}}{m} = \frac{[V_s]_{ij}}{n} \qquad i = 1..M, j = 1..N$$

3. **Rule 1:** By Ohm's law the current in every part of a series interconnection must be equal.

4. **Rule 2:** By Ohm's law, the voltage over ever parallel interconnection must be equal.

Consider the distribution of current in the 2:3 distributed transformer as illustrated in Figure.3-4.

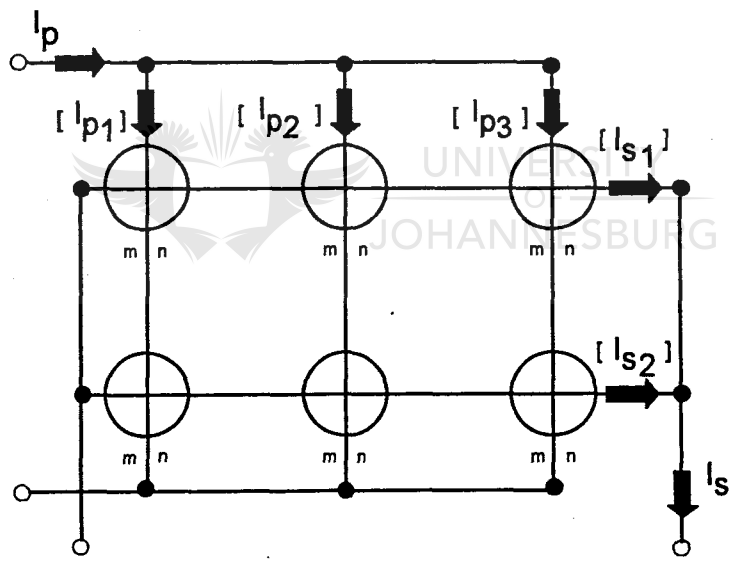

Figure.3-4. Current distributions in a distributed transformer with a 2:3 matrix interconnection

The current [I_{p1}] flowing in the primary windings of each of the elements in the first column, couples with the currents [I_{s1}] and [I_{s2}] flowing in the secondary windings of each of the elements in the first and second rows respectively.

By Lenz's law the currents are related as follows;

$$\left[I_{p1}\right] = \frac{n}{m}\left[I_{s1}\right] = \frac{n}{m}\left[I_{s2}\right] \tag{3.6}$$

Similarly, the current I_{s1} flowing in the secondary windings of each element in the first row couples with the currents, I_{p1}, I_{p2} and I_{p3} flowing in the primary windings of each of the elements in the first, second and third columns respectively .

By Lenz's law the currents are related as follows;

$$\left[I_{s1}\right] = \frac{m}{n}\left[I_{p1}\right] = \frac{m}{n}\left[I_{p2}\right] = \frac{m}{n}\left[I_{p3}\right] \tag{3.7}$$

and the following equalities can be derived from Ohm's law;

$$\left[I_{p1}\right] = \left[I_{p2}\right] = \left[I_{p3}\right] = \frac{I_p}{3} \tag{3.8a}$$

$$\left[I_{s1}\right] = \left[I_{s2}\right] = \frac{I_s}{2} \tag{3.8b}$$

By combining equations (3.6), (3.7) and (3.8), the following equality is obtained;

$$\frac{I_p}{I_s} = \left(\frac{3}{2}\right)\left(\frac{n}{m}\right) \tag{3.9}$$

The relationship given in equation (3.9) is the current transformation ratio for the 2:3 distributed transformer.

Consider the distribution of voltages in the 2:3 distributed transformer as illustrated in Figure.3-5.

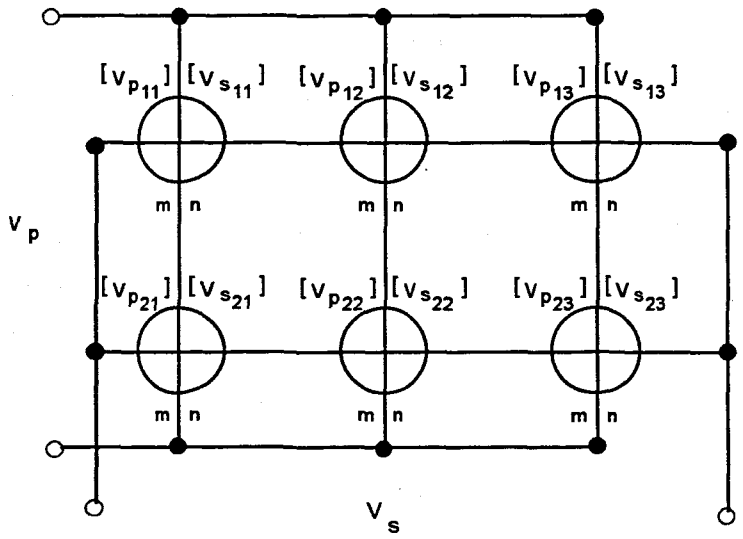

Figure.3-5. Voltage distributions in a distributed transformer with a 2:3 matrix interconnection

The voltage relationship for the first element in the configuration is given by Faraday's law as follows;

$$\left[V_{p11}\right] = \left(\frac{m}{n}\right)\left[V_{s11}\right] \tag{3.10}$$

From Ohm's law, the following equalities can be derived.

$$\left[V_{p11}\right] = \left[V_{p21}\right] = \left[V_{p12}\right] = \left[V_{p22}\right] = \left[V_{p13}\right] = \left[V_{p23}\right] = \frac{V_p}{2} \tag{3.11a}$$

$$\left[V_{s11}\right] = \left[V_{s21}\right] = \left[V_{s12}\right] = \left[V_{s22}\right] = \left[V_{s13}\right] = \left[V_{s23}\right] = \frac{V_s}{2} \tag{3.11b}$$

By combining equations (3.10) and (3.11), the following equality is obtained;

$$\frac{V_p}{V_s} = \left(\frac{2}{3}\right)\left(\frac{m}{n}\right) \tag{3.12}$$

The voltage relationship given in equation (3.12) is the voltage transformation ratio for the 2:3 distributed transformer which, as it should be, is the inverse of the current transformation ratio given by equation (3.9).

A similar argument for the general case of an M:N distributed transformer, leads to the following voltage and current relationships;

$$\left[V_p\right] = \frac{V_p}{M} \qquad \& \qquad \left[V_s\right] = \frac{V_s}{N} \tag{3.13a}$$

$$\left[I_p\right] = \frac{I_p}{N} \qquad \& \qquad \left[I_s\right] = \frac{I_s}{M} \tag{3.13b}$$

Consequently, the voltage and current transformation ratios of an M:N distributed transformer containing elements with an m:n turns ratio, is given as follows;

$$\frac{V_p}{V_s} = \left(\frac{M}{N}\right)\left(\frac{m}{n}\right) \qquad \& \qquad \frac{I_p}{I_s} = \left(\frac{N}{M}\right)\left(\frac{n}{m}\right) \tag{3.14}$$

The effect of matrix interconnection on transformer operation is clearly reflected by the expressions given in equations (3.13) and (3.14).

3.2.3.3. Electrical characteristics of the distributed transformer

The equivalent two port model of the generalised M:N distributed transformer is given as follows;

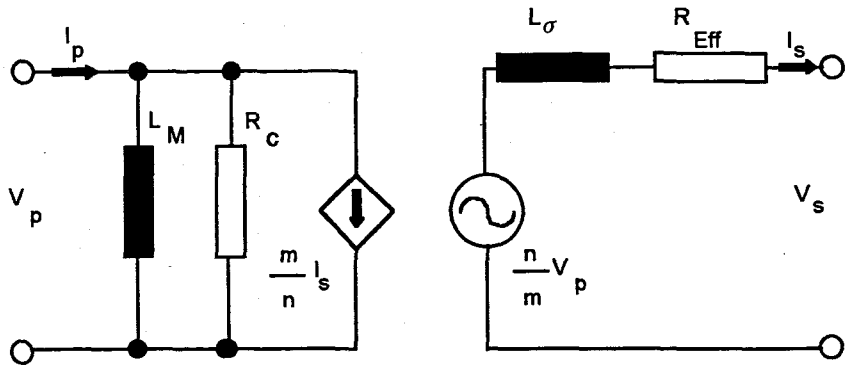

Figure.3-6 Equivalent two port model of the generalised M:N distributed transformer

The parameters of an M:N distributed transformer with elements each having a core loss resistance of [R_c], a magnetising inductance [L_M], a leakage inductance of [L_σ,] and an effective resistance of [R_{eff}] can be determined from simple network analysis, and is given as;

$$R_c = \frac{M}{N}[R_c] \tag{3.15}$$

$$L_M = \frac{M}{N}[L_M] \tag{3.16}$$

$$L_\sigma = \frac{N}{M}[L_\sigma] \tag{3.17}$$

$$R_{Eff} = \frac{N}{M}[R_{Eff}] \tag{3.18}$$

where R_c is the core loss resistance of the distributed transformer, L_M is its magnetising inductance, $L_,$ is its leakage inductance and R_{EFF} is its effective copper resistance.

By substituting equations (3.13 - 3.18) into the two port model illustrated in Figure.3-6, the equivalent two port model of a distributed transformer can be redefined in terms of the parameters of a single element as illustrated in Figure.3-7.

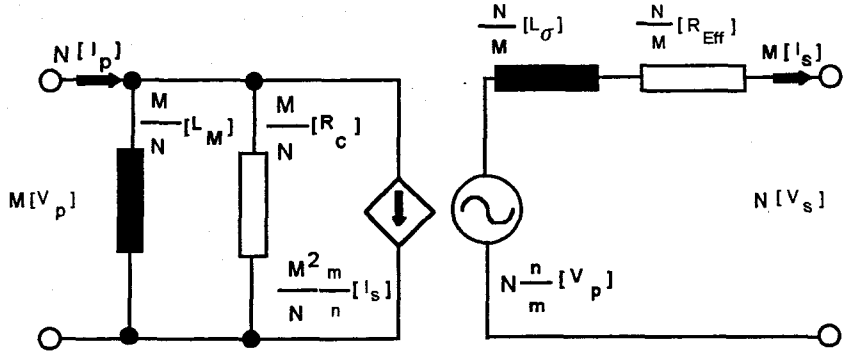

Figure.3-7 Two port model of a distributed transformer in terms of its element parameters

The parameters of a single element is, to a larger or lesser extent, reflected to the overall distributed transformer configuration in a manner dependent on the dimensions of the matrix interconnection, consider the following three possibilities;

The Case for M > N: The magnetising inductance of the distributed transformer is larger than the magnetising inductance of a single element, but the leakage inductance and effective copper resistance is smaller.

The Case for M < N: The magnetising inductance of the distributed transformer is smaller than the magnetising inductance of a single element, but the leakage inductance and effective copper resistance is larger.

The Case for M=N: The electrical characteristics of the distributed transformer is identical to that of a single element.

3.2.3.4. Performance characteristics of the generalised distributed transformer

(1) Power efficiency : The power efficiency of the distributed transformer is defined as follows;

$$Efficiency = \frac{Power\ output}{Power\ input} = \frac{Power\ output}{Power\ output + (Core\ losses + Winding\ losses)}$$

$$\eta = \frac{V_s I_s \cos\theta}{V_s I_s \cos\theta + \left(\frac{V_p^2}{R_c} + I_s^2 R_{Eff}\right)} \qquad (3.19)$$

By substituting equations (3.13 - 3.18) into equation (3.19), the power efficiency of the distributed transformer can be rewritten in terms of the parameters of a single element as follows;

$$\eta = \frac{M[V_s]N[I_s][\cos\theta]}{M[V_s]N[I_s][\cos\theta] + \left(\frac{M^2[V_p]^2}{\frac{M}{N}[R_c]} + M^2[I_s]^2\frac{N}{M}[R_{Eff}]\right)} \qquad (3.20)$$

which simplifies to the following;

$$\eta = \frac{[V_s][I_s][\cos\theta]}{[V_s][I_s][\cos\theta] + \left(\frac{[V_p]^2}{[R_c]} + [I_s]^2[R_{Eff}]\right)} = [\eta] \qquad (3.21)$$

It is seen from equation (3.21) that the total power efficiency of the generalised distributed transformer, is equivalent to the power efficiency of a single element.

(2) Output voltage regulation : The output voltage regulation of the distributed transformer is defined as follows;

$$Regulation = \frac{No\ load\ voltage - Full\ load\ voltage}{Full\ load\ voltage} = \frac{Voltage\ drop\ over\ \{[R_{Eff}]\&[L_{\sigma}]\}}{Rated\ voltage}$$

$$Regulation = \frac{I_s^2 \left| R_{Eff} + jwL_{\sigma} \right|}{V_s} \qquad (3.21)$$

By substituting equations (3.13 - 3.18) into equation (3.21), the output voltage regulation of the distributed transformer can be rewritten in terms of the parameters of a single element as follows;

$$Regulation = \frac{M[I_s]^2 \frac{N}{M} \left| [R_{Eff}] + jw[L_{\sigma}] \right|}{N[V_s]} \qquad (3.22)$$

which simplifies to the following;

$$Regulation = \frac{[I_s]^2 \left\| [R_{Eff}] + j[wL_{\sigma}] \right\|}{[V_s]} = [Regulation] \qquad (3.23)$$

It is seen from equation (3.23) that the output voltage regulation of the generalised distributed transformer, is equivalent to the output voltage regulation of a single element.

3.2.3.5. Modularity of the generalised distributed transformer

Since the characteristics of the element is entirely reflected in those of the overall configuration, the design of the distributed transformer is simply reduced to the problem of designing a single element. The specification of a single element in a distributed transformer configuration, is analogous to specifying a base value in per unit calculations used in network analysis, because all of the information required to describe the distributed transformer is contained within the description of a single element.

3.2.4. Practical design considerations for the basic interconnection of elements

3.2.4.1. Unequal impedance parameters of elements

So far it has been assumed that the elements of a distributed transformer are identical in every respect, but in practise this is not necessarily the case due to the number of design parameters that could change. In the event where every element is different, equations (3.15 - 3.18) describing the impedance parameters of the generalised M:N distributed transformer can be rewritten as follows;

$$L_M = \left\{ \sum_{i=1}^{N} \left(\frac{1}{\sum_{j=1}^{M} [L_M]_{ij}} \right) \right\}^{-1} \tag{3.24}$$

$$R_c = \left\{ \sum_{i=1}^{N} \left(\frac{1}{\sum_{j=1}^{M} [R_c]_{ij}} \right) \right\}^{-1} \tag{3.25}$$

$$L_{\sigma} = \left\{ \sum_{i=1}^{M} \left(\frac{1}{\sum_{j=1}^{N} [L_{\sigma}]_{ij}} \right) \right\}^{-1} \tag{3.26}$$

$$R_{Eff} = \left\{ \sum_{i=1}^{M} \left(\frac{1}{\sum_{j=1}^{N} [R_{eff}]_{ij}} \right) \right\}^{-1} \tag{3.27}$$

In most cases the differences in the impedance parameters of the elements can be ignored and equations (3.15 - 3.18) used with marginal error.

3.2.4.3. Parasitic impedances of interconnection leads

It is true that excessively long interconnection leads between the elements can introduce additional losses due to their inductance and resistance. Since these parasitic impedances are situated in series with the elements, they can be modelled as part of the equivalent two port model of each element as illustrated in Figure.3-8.

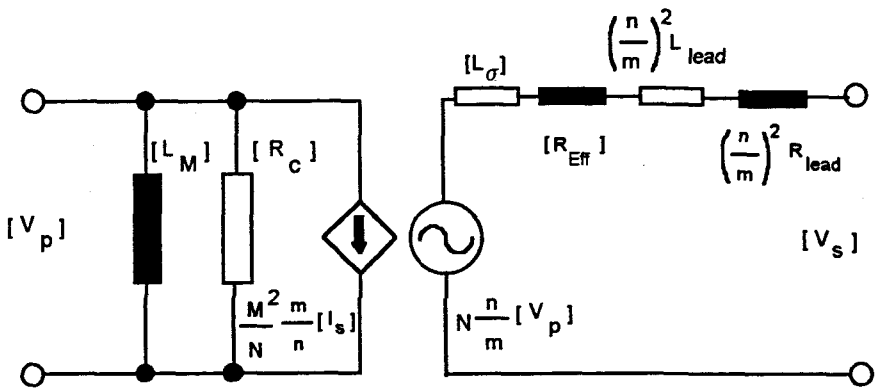

Figure.3-8 Two port model of an element including lead impedances

Assuming identical elements, the impedance parameters of the equivalent two port model for the distributed transformer can then be expressed as follows;

$$R_c = \frac{M}{N}[R_c] \tag{3.28}$$

$$L_M = \frac{M}{N}[L_M] \tag{3.29}$$

$$L_\sigma = \frac{N}{M}\left[L_\sigma + \left(\frac{n}{m}\right)^2 L_{lead} \right] \tag{3.30}$$

$$R_{Eff} = \frac{N}{M}\left[R_{Eff} + \left(\frac{n}{m}\right)^2 R_{Lead} \right] \tag{3.31}$$

From equations (3.28 - 3.31) it is seen that the core loss resistance and magnetising inductance of each element remains unchanged, whereas the leakage inductance and effective resistance are each weighted with an additional term. The above expressions assume identical interconnection leads, which result in equivalent lead impedances, but this is not necessarily the case.

A more general description for the parameters of a distributed transformer including the effect of unequal lead impedances and unequal element impedances is given as follows;

$$L_M = \left\{ \sum_{i=1}^{N} \left(\frac{1}{\sum_{j=1}^{M} [L_M]_{ij}} \right) \right\}^{-1} \tag{3.32}$$

$$R_c = \left\{ \sum_{i=1}^{N} \left(\frac{1}{\sum_{j=1}^{M} [R_c]_{ij}} \right) \right\}^{-1} \tag{3.33}$$

$$L_{\sigma} = \left\{ \sum_{i=1}^{M} \left(\frac{1}{\sum_{j=1}^{N} \left(\left[L_{\sigma} \right]_{ij} + \left(\frac{n}{m} \right)^2 L_{lead\,ij} \right)} \right) \right\}^{-1} \tag{3.34}$$

$$R_{Eff} = \left\{ \sum_{i=1}^{M} \left(\frac{1}{\sum_{j=1}^{N} \left(\left[R_{Eff} \right]_{ij} + \left(\frac{n}{m} \right)^2 R_{lead\,ij} \right)} \right) \right\}^{-1} \tag{3.35}$$

In most cases the elements can be arranged in such a manner that the length of the interconnection leads can be kept to an absolute minimum, so that equations (3.15 - 3.18) can be used with marginal error if parasitic impedances are neglected.

3.3. DESIGN PROCEDURE FOR THE GENERALISED M:N DISTRIBUTED TRANSFORMER

As is evident from the analysis presented in the previous section, it may be possible to design a number of matrix interconnected, multiple core transformer configurations that are suitable for a given application from an operational point of view, but only one of these configurations will have the superior materials efficiency and space volume consumption associated with type 2 distributed magnetic components. The distributed transformer, thereforee, maintains a delicate balance between optimum materials efficiency and space volume consumption, the design of its elements and their interconnection.

The following step by step design procedure is formulated to guarantee this balance for any given application.

The design procedure relies on the following basic input parameters which are assumed given, either directly or by implication;

1) The total rated input voltage
2) The total rated output voltage
3) The total rated input current
4) The total rated output current
5) The maximum permissible temperature rise in the core material
6) The frequency of operation

Step 1: Based on the considerations discussed in sections 3.2.2.1 and 3.2.2.2, select a core geometry and material grade that best suits the needs of the application.

Step 2: Establish a data base for every core size made available by the manufacturers with the selected core geometry. The data base should include the following information;

1. Grade of ferrite material.
2. Detailed dimensions of the core
3. Measured results showing the relationship between the core size, grade of material, temperature rise in the core, maximum flux density excursion, frequency of excitation and method of cooling.

Step 3: Determine the optimum core size and associated matrix dimensions suitable for the application as follows.

(a) Firstly, for each core size, determine the number of elements that would be required for the proposed distributed transformer. This is accomplished by repeating the following procedure for each core size, using the information contained in the data base together with the design specifications;

From Faraday's Law, the maximum positive deviation in the volt-time integral of the primary and secondary voltages of an element are given respectively as;

$$\left|\int [V_p]\, dt\right|_{\max} = 2\, m \hat{B} A_c \qquad (3.36\text{-a})$$

$$\left|\int [V_s]\, dt\right|_{\max} = 2\, n \hat{B} A_c \qquad (3.37\text{-b})$$

therefore, the total positive deviation in the volt-time integral of the primary and secondary voltages for the proposed distributed configuration can be obtained in terms of the matrix dimensions as follows;

$$\left|\int V_p\, dt\right|_{\max} = 2\, mM \hat{B} A_c \qquad (3.38\text{-a})$$

$$\left|\int V_s\, dt\right|_{\max} = 2\, nN \hat{B} A_c \qquad (3.38\text{-b})$$

A constant γ, defined as the product of equations (3.38-a) and (3.38-b), is given as follows;

$$\gamma = mMnN = \frac{\left|\int V_p\, dt\right|_{\max} \left|\int V_s\, dt\right|_{\max}}{\left(2 \hat{B} A_c\right)^2} \qquad (3.39)$$

If it is assumed that the maximum permissible current density is the same in both windings of an element, then the maximum number of turns that can be allowed in the primary and secondary windings for a given core size is given as follows;

$$m_{max} = N \frac{K_u A_{Win} J}{2 I_p} \qquad (3.40\text{-a})$$

$$n_{max} = M \frac{k_u A_{win} J}{2 I_s} \qquad (3.40\text{-b})$$

The above two equations can be rewritten in the following convenient form;

$$m_{max} = F_1 N \qquad where \qquad F_1 = \frac{k_u A_{Win} J}{2 I_p} \qquad (3.41a)$$

$$n_{max} = F_2 M \qquad where \qquad F_2 = \frac{k_u A_{Win} J}{2 I_s} \qquad (3.41b)$$

By substituting equations (3.41a) and (3.41b) into equation (3.39) and simplifying, results in an expression for the minimum number of elements required for the proposed distributed transformer configuration;

$$MN = \sqrt{\frac{\gamma}{F_1 F_2}} \qquad (3.42)$$

(b) Using the values of MN obtained for each core size, calculate the total ferrite volume required in each case for the proposed distributed transformer configuration. The optimum core size is then chosen from the configuration with the least ferrite volume.

Step 4: Because the factors of MN will always provide the dimensions for a valid matrix interconnection, it is seen that more than one matrix interconnection is possible to realise a viable distributed transformer. Once the dimensions best suited for the application is selected from the factors of MN, equations (3.41-a) and (3.41-b) can be used to select the number of turns in the primary and secondary windings of each element, and the winding design can be completed by selecting the conductor cross-section and winding geometry based on the considerations discussed in section 3.2.2.2.

3.4. CONCLUSION

The original concept of a multiple core magnetic assembly with superior materials utilisation and space volume consumption has been expanded into a well defined and extremely flexible magnetic structure. The basic characteristics of its elements and the means by which they are interconnected has been developed together with an all encompassing design procedure that can easily be implemented in any application.

4. The isolated Cuk converter - Transformer design

4. THE ISOLATED CUK CONVERTER - TRANSFORMER DESIGN

4.1. INTRODUCTION

This chapter is dedicated primarily to design of a distributed transformer for the battery charger under investigation, based on the generalised model presented in chapter.3. Firstly, the design constraints and conditions under which the transformer must operate, are identified in an analysis describing the basic principles of operation of the isolated Cuk converter. Then based on the analysis and additional regulations, a definitive structure for the monolithic and equivalent distributed transformer is described.

4.2 OPERATION OF THE ISOLATED CUK CONVERTER WITH AN UNFILTERED INPUT VOLTAGE

The isolated Cuk DC-DC converter topology is illustrated in Figure.4-1.

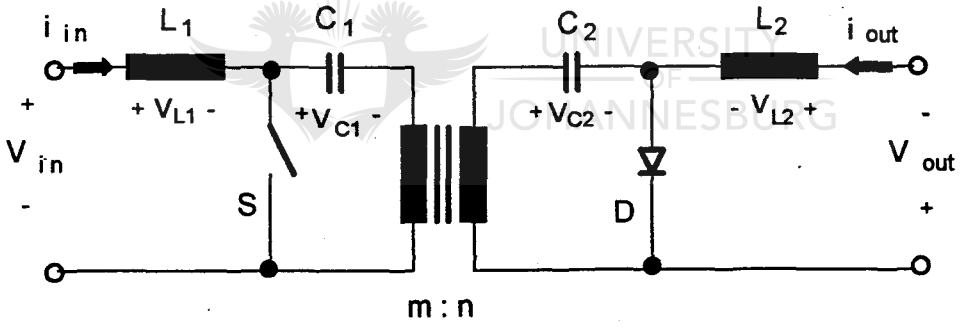

Figure. 4-1 The isolated Cuk DC-DC converter

It is possible to draw sinusoidal currents from the mains supply with a near unity power factor, if the voltage is rectified and used in its unfiltered form as input to the Cuk converter as in the case of the battery charger[†].

[†]A detailed description of the isolated Cuk converter with a filtered DC input voltage, is given in apendix.D.

The unfiltered input voltage can be described as follows;

$$v_{in} = \hat{V}_{in} \left| Sin\left(2\,\pi\,f_m\,t\right)\right| \qquad (4.1)$$

and the input current can be described as follows;

$$i_{in} = \hat{I}_{in} \left| SIN\left(2\pi\,f_m\,t\right)\right| \qquad (4.2)$$

If the switching frequency, f_s , of the converter is chosen to be much higher than the slow varying frequency, f_m , of the input voltage, then the instantaneous input voltage over one switching period can be assumed to remain constant. Consequently, the equations derived in Appendix.D can be applied over each period of the switching frequency, to evaluate the change in the operating conditions of each component over each period of the supply frequency.

4.2.1. Steady state operating conditions for the input and output chokes

The voltages and currents for the two chokes, L_1 and L_2, can be deduced from equations (D.1 - D.4), and are illustrated in Figure. 4-2.

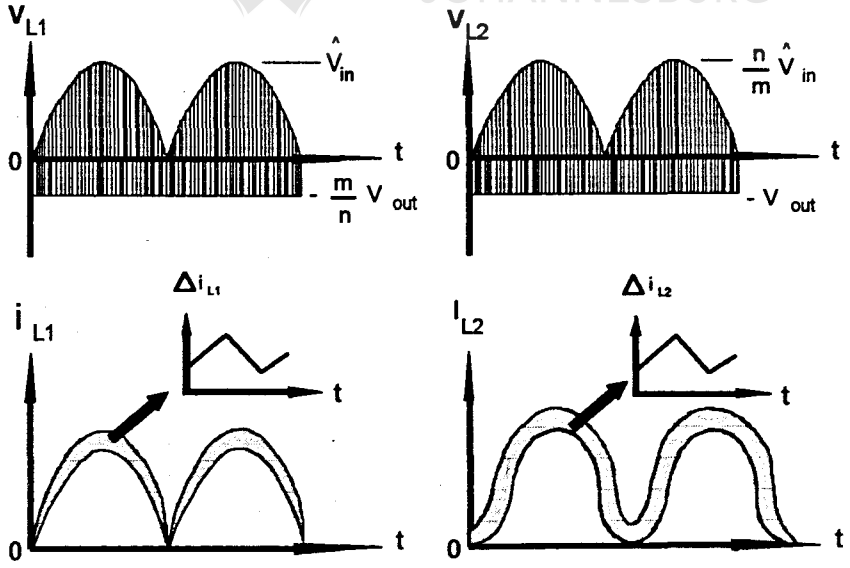

Figure. 4-2 Current and voltage for L_1 and L_2

It is seen in Figure. 4-2, that a significant current ripple is superimposed over the input and output currents of the converter, where their peak to peak magnitudes are described by equations (D.8) and (D.11).

4.2.2 Steady state operating conditions for the energy transfer capacitors

The voltage over each of the capacitors can be deduced from equations (D.13) and (D.14), and are illustrated in Figure.4-3.

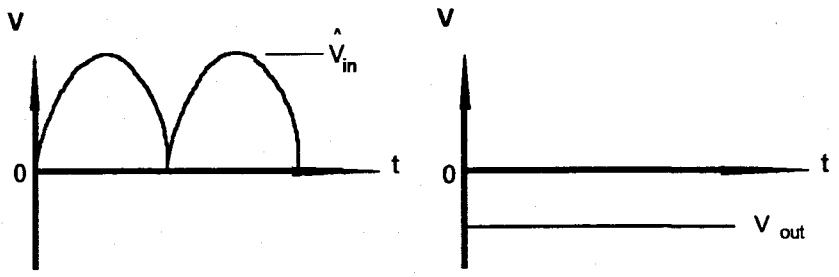

Figure. 4-3 Voltage over capacitors C_1 and C_2

In this case the voltage over capacitor C_1 , is seen to change with input voltage while the voltage over capacitor C_2 , remains constant and equal to the output voltage.

4.2.3. Steady state operating conditions for the isolation transformer

The voltage impressed over the primary windings of the transformer can be deduced from equations (D.15) and (D.16) and is illustrated in Figure. 4-4.

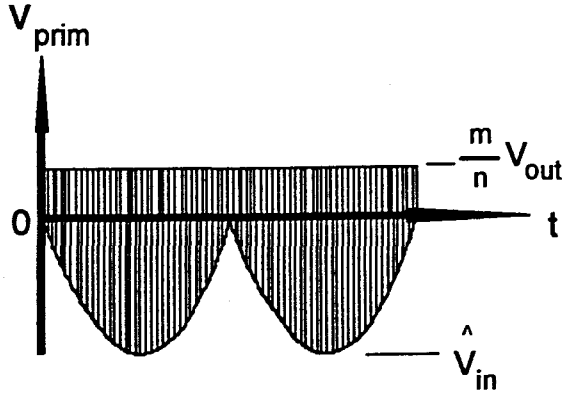

Figure. 4-4 Voltage over the primary windings of the isolation transformer

From equation (D.8-a), the time interval of switch conduction is defined as follows;

$$DT = \frac{L_1 \Delta i_{in}}{v_{in}} \qquad (4.3\text{-a})$$

From equation (D.8-b), the time interval of non-conduction is defined as follows;

$$(1-D)T = \frac{L_1 \Delta i_{in}}{v_{out}} \qquad (4.3\text{-b})$$

From equation (4.3-a) it is seen that the time interval of switch conduction varies with the input voltage if the converter is controlled for a constant input current ripple, whereas the time interval of non-conduction stays constant. Consequently it is seen from equation (D.6), that the switching frequency of the converter does not remain constant, but changes proportionally with the input voltage. The switching frequency reaches its minimum value when the input voltage is a maximum, thereforee the maximum positive deviation in the volt-time integral of the primary windings is given as follows;

$$\left| \int v_{prim}\, dt \right|_{max} = \frac{\hat{V}_{in}\, V_{out}}{(f_s)_{min} \left(\hat{V}_{in} + V_{out} \right)} \qquad (4.4)$$

The current flowing in the primary windings of the isolation transformer can be deduced from equation (D.19) and (D.20) and is illustrated in Figure.4.5.

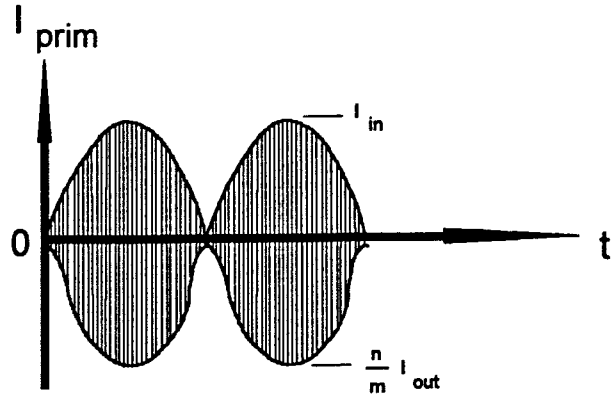

Figure. 4-5 Primary current of the isolation transformer

4.3. THE DESIGN OF AN ISOLATION TRANSFORMER FOR THE 1.5 KW BATTERY CHARGER

The analysis presented in section 4.2 can now be implemented to establish the specific operating conditions for the isolation transformer, used in the 1.5 kW battery charger under investigation. The design and manufacture of the original transformer used in the prototype is given first, followed by the design and manufacture of an equivalent distributed transformer which can be used as its replacement.

4.3.1. Design specifications

The following information with regards to the 1.5 kW Cuk converter is given [1];

- $v_{in} = 311 \left|SIN\, wt\right| \; V$
- $i_{in} = 15 \left|SIN\, wt\right| \; V$
- $V_{out} = 120 \; V$
- $i_{out} = 25 \; SIN^2 wt \; V$

The converter is controlled for a constant peak to peak input ripple current of 2A, consequently the minimum switching frequency is determined from equations (D.6) and (4.3), and is given as follows;

- $(f_s)_{min} = 20 \; KHz$

The maximum volt-time integral for the primary winding of the transformer, is determined by applying equation (4.4), consequently

- $\left|v_{prim}\, dt\right|_{max} = 4.3 \;\; mVs$

The isolation transformer is subject to the following design specifications and regulations;

- A unity turns ratio is required.
- Natural convection cooling is preferred.
- The maximum environment temperature must not exceed 50 °C, therefore, a maximum rise in core and winding temperature of 10 °C - 15 °C above a nominal temperature of 25 °C is permitted.

4.3.2. The design of the 1.5 kW monolithic transformer

The magnetic core design, and winding design of the monolithic transformer is given as follows;

4.3.2.1. Core geometry

The twin E-core geometry, as manufactured by Phillips, is considered suitable for the application for the following reasons;

1. The core type is easily obtainable.
2. The proposed transformer can be assembled with ease, due to the square cross-section and simple shape of the core.
3. The core has a relatively large ferrite area, which is beneficial for heat dissipation.

4.3.2.2. Material grade specification

Grade 3C80 ferrite material was selected because it is recommended by Phillips[2], as suitable for use in power applications, particularly at the frequencies of operation in question.

4.3.2.3. Core data base

Five different core sizes are made available in the E-core range and are listed in Table.4-1, together with pertinent information that will be required to make a selection of core size;

Core Size	Ac [mm^2]	A_{win} [mm^2]	B [T]	J [A / mm^2]
E20	**31**	**27**	**0.220**	**8.0**
E30	**60**	**80**	**0.210**	**7.5**
E42	**182**	**178**	**0.175**	**6.5**
E55	**354**	**250**	**0.160**	**6.0**
E65	**532**	**394**	**0.150**	**4.0**

Table. 4-1 Data base for E-core range

$\hat{B}$ ≡ The maximum permissible flux density excursion which does not lead to an increase in the core temperature of more than 10 °C, above a nominal room temperature of 25 °C. These values can be obtained from the measured data in Appendix.C.

J ≡ The maximum current density permitted in the windings of the transformer as a function of the core size. These values can be obtained from the graph in [3].

4.3.2.4. Core size

The transformer must be designed to cope with a maximum volt-time integral of 4.3 mVs over its primary windings when the input voltage to the converter reaches its peak value, and the switching frequency is at its minimum. The following iterative procedure, therefore, is used to determine the correct core size;

Step 1: The minimum number of turns required to realise a maximum volt-time integral of 4.3 mVs, is determined for each core size listed in table.2-4, by making use of the following equation;

$$N_{required} = \frac{\left|\int v_{prim}\, dt\right|_{max}}{2\hat{B}A_c}$$

Step 2: The total number of turns which can possibly fit into the available winding area is then evaluated for each core size by making use of the following equation[‡];

$$N_{permissable} = \frac{k_u\, A_{Win}\, J}{I_{in}}$$

Step 3: The two values are compared for each core size, and the smallest core where $N_{permissable} \geq N_{Required}$, is then selected.

[‡] This equation is true for a transformer with a unity turns ratio, because the input and output currents of the transformer are equal. If the transformer was to be designed for a given turns ratio, then the packing factor, current and current density for each of the windings would have to be included.

The results of such a comparison are illustrated in Table.4-2.

Core size	$N_{Required}$	$N_{permissable}$	Suitable
E20	**317**	**7**	**No**
E30	**172**	**17**	**No**
E42	**68**	**25**	**No**
E55	**38**	**36**	**No**
E65	**32**	**44**	**Yes**

Table. 4-2 Comparative selection of core size

From Table.4-2, it is seen that the E65 core is the only practical core size which can be used in a transformer assembly to realise a maximum volt-time integral of 4.3 mVs.

4.3.2.5. Winding design

The current flowing in the windings of the transformer during each period of the supply frequency, has a large number of high frequency Fourier components, which contribute to the overall winding loss. From a Fourier analysis of the input current [1], however, it is seen that most of the winding losses can be attributed to the 20 kHz harmonic which has an amplitude of 15A. The winding design will be evaluated using this current component.

The windings of the transformer can be formed with a number of possible conductor cross-sections and winding geometries. The choice of conductor cross-section and winding geometry are mutually inclusive, however, since both have an effect on the total effective resistance and leakage inductance of the transformer. Since the optimum selection of conductor cross-section and winding geometry has enjoyed much attention in literature and has filled many a page with its intricacies, it will not be discussed in detail here. Instead, a software program based on these principles [4], was used to evaluate some of the numerous possibilities to make an optimum selection.

Step 1: Selecting the conductor cross-section

There are three types of windings which are commonly used in modern transformer design, namely (1) foil windings, (2) Litz wire windings and (3) single round wire windings.

(1) Foil windings : The foil type windings are difficult to wind, end connections are difficult to realise and their use is limited to applications where only a few windings are required.

(2) Litz wire windings : True Litz wire presents difficulties in manufacture, and is costly if purchased, but its improved resistance characteristics at high frequencies may be of sufficient significance to justify its use. Furthermore, the use of Litz wire is unavoidable at high frequencies, particularly when large currents are to be conducted.

(3) Single round wire windings : A single round wire is easy to wind, is readily available and low in cost. The convenient use of round wire windings, however, don't necessarily result in the optimum winding configuration of a transformer since its losses at higher frequencies are higher than that of Litz wire.

Based on the above considerations, foil type windings were not considered.

Step 2: Selecting the winding geometry

A number of winding geometries could be implemented, but not all winding geometries are practical from a manufacturing point of view. Consequently, only two winding geometries which are still practically realisable were considered for the design, and are illustrated in Figure.4-6.

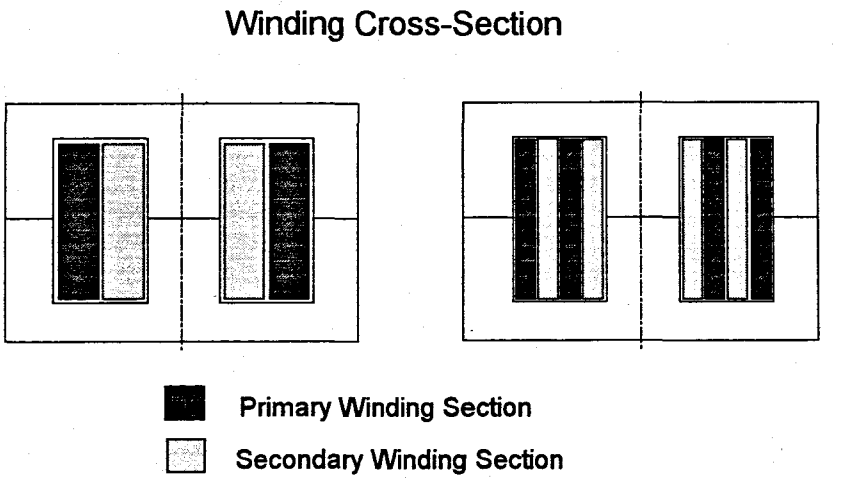

Figure. 4-6 Winding geometries considered for the design of the 1.5 kW monolithic transformer

Step 3: Selecting the optimum winding configuration

By using the software package mentioned earlier, the winding loss for each of the winding configurations illustrated in Figure. 4-6 was evaluated for a number of valid Litz wire compositions and for the appropriate single wire windings. The results of the analysis are tabulated in Table.4-3,

Description of winding conductors	Winding loss (two winding sections)	Winding loss (four winding sections)
solid wire (diameter = 1.8 mm)	**17 W**	**50 W**
Litz wire (5 strands with diameter = 0. 8 mm)	**10 W**	**27 W**
Litz wire (13 strands with diameter = 0.5 mm)	**7 W**	**13 W**

Table. 4-3 Results of analysis comparring various possible winding geometries for the 1.5 kW isolation transformer

From Table.4-3, it is seen that a winding geometry consisting of two winding sections of 32 turns each, will always exhibit lower losses, where the lowest losses are obtained for Litz wire windings made from 13 strands of copper wire, each 0.5 mm in diameter.

4.3.2.6. Manufacture

Standard techniques were employed in the manufacture of the monolithic transformer, and its typical assembly is illustrated in Figure.4-7.

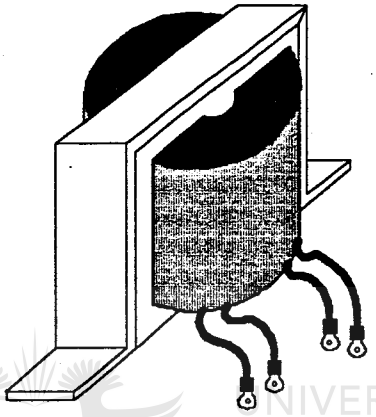

Figure. 4-7 Monolithic assembly

A description of the fully assembled 1.5 kW monolithic transformer is given as follows,

Magnetic core description:

Core geometry	-E-type core
Core size	-E65
Material grade	-grade 3C80 material

Winding description :

No. of winding sections	- 4
No. of turns	- 16 turns per winding section
Type of windings	- Litz wire windings with 13 strands of copper wire each 0.5 mm in diamter

4.3.3. The design of a 1.5 kW distributed transformer

The magnetic core design and winding design of the distributed transformer was determined from the design procedure discussed in chapter.3 and is given as follows;

4.3.3.1. Step 1-Core geometry and material grade specification

The twin E-core geometry, as manufactured by Phillips, is considered suitable for the elements of the proposed distributed transformer for the following reasons;

1. The core type is easily obtainable.

2. The elements can be assembled with ease, due to the square cross-section and simple shape of the core.

3. The core has the potential to realise a low profile structure, and has the potential to be mounted onto a PCB.

4. . The core has a relatively large ferrite area, which is beneficial for heat dissipation.

Grade 3C80 ferrite material was selected because it is recommended by Phillips, as suitable for use in power applications, particularly at the frequencies of operation in question.

4.3.3.2. Step 2-Core data base

Five different core sizes are made available in the E-core range and are listed in Table.4-4, together with pertinent information that will be required to make a selection of the optimum core size for the elements;

Core Size	Ac [mm^2]	A_{win} [mm^2]	B [T]	J [A / mm^2]
E20	**31**	**27**	**0.220**	**8.0**
E30	**60**	**80**	**0.210**	**7.5**
E42	**182**	**178**	**0.175**	**6.5**
E55	**354**	**250**	**0.160**	**6.0**
E65	**532**	**394**	**0.150**	**4.0**

Table. 4-4 Data base for E-core range

$\hat{B}$ ≡ The maximum permissable flux density excursion which does not lead to an increase in the core temperature of more than 10 °C, above a nominal room temperature of 25 °C. These values can be obtained from the measured data in Appendix.c.

J ≡ The maximum current density permitted in the windings of the transformer as a function of the core size. These values can be obtained from the graph in [3].

4.3.3.3. Step 3-Selection of optimum core size

The transformer must be designed to cope with a maximum volt-time integral of 4.3 mVs over its input when the input voltage to the converter reaches its peak value, and the switching frequency is at its minimum.

-a) The following results were obtained by making use of equations (3.39 - 3.42),

Core size	$F_1 = \frac{k_u A_{Win} J}{2 I_p}$	$F_2 = \frac{k_u A_{Win} J}{2 I_s}$	$\gamma = \frac{\left\|\int V_p dt\right\|_{max} \left\|\int V_s dt\right\|_{max}}{\left(2\hat{B}A_c\right)^2}$	$MN = \sqrt{\frac{\gamma}{F_1 F_2}}$
E20	**6.11**	**6.11**	**99 382.10**	**52**
E30	**16.97**	**16.97**	**29 116.28**	**8**
E42	**32.72**	**32.72**	**4556.78**	**2**
E55	**42.43**	**42.43**	**1 440.88**	**2**
E65	**44.58**	**44.58**	**725.90**	**1**

Table.4-5 Results of analysis for the selection of optimum core size for the 1.5 kW distributed isolation transformer

-b) The ferrite volume for each of the possible configurations tabulated in Table.4-5 is given as follows

Core size	No. of elements	Total ferrite volume [mm^3]
E20	**52**	**69 680**
E30	**8**	**32 000**
E42	**2**	**35 200**
E55	**2**	**87 400**
E65	**1**	**78 200**

Table. 4-6 Total ferrite volume for each of the possible distributed transformer configurations

From the analysis it is seen that the distributed transformer configuration which is suitable for use in the battery charger, will require eight E30 cores for the elements.

4.3.3.4. Step 4-Matrix dimensioning and winding design

Since the distributed transformer must make use of eight cores, it follows that there must be seven possible matrix configurations for its assembly. The first four possible configurations make use of elements which require only one E30 core in its assembly, and are listed as follows;

1. M : N = 1 : 8 i.e. one row, and eight columns

2. M : N = 2 : 4 i.e. two rows, and four columns

3. M : N = 4 : 2 i.e. four rows, and two columns

4. M : N = 8 : 1 i.e. eight rows, and one column

The remaining three possible configurations make use of elements which are assembled by stacking two E30 cores on top of each other, and are listed as follows;

1. M : N = 1 : 4 i.e. one row, and four columns

2. M : N = 2 : 2 i.e. two rows, and two columns

3. M : N = 4 : 1 i.e. four rows, and one column

It is desirable for the distributed transformer to have a structure as compact as possible, therefore, the 2:2 matrix configuration using two stacked E30 cores is selected for this application.

The 15A current harmonic at the input of the distributed transformer, is split into two equal parts due to the matrix configuration. The winding losses of each element can therefore be attributed to a 20 kHz current harmonic with an amplitude of 7.5A. Since each element in the distributed transformer is a two winding monolithic transformer, it is subject to the same considerations discussed for the winding design of the monolithic transformer in section.4.3.2.5.

An evaluation of the winding losses in each element, for the two winding geometries illustrated in Figure.4-6, produced the results tabulated in Table.4-7.

Description of winding conductors	Winding loss (two winding sections)	Winding loss (four winding sections)
Solid wire (diameter = 1mm)	**10 W**	**4.5 W**
Litz wire (two strands with diameter = 0.75 mm)	**6 W**	**5 W**

Table. 4-7 Results of analysis comparring various possible winding geometries for the 1.5 kW isolation transformer

From Table.4-7, it is seen that a winding geometry consisting of four winding sections with 18 turns per winding section, will always exhibit lower losses, where the lowest losses are obtained for windings using a single wire with a diameter of 1mm.

4.3.3.56. Manufacture

A manufacturing technique that can be used to mount the elements of the distributed transformer onto a PCB, while simultaneously favouring low profile characteristics, is illustrated in Figure.4-8.

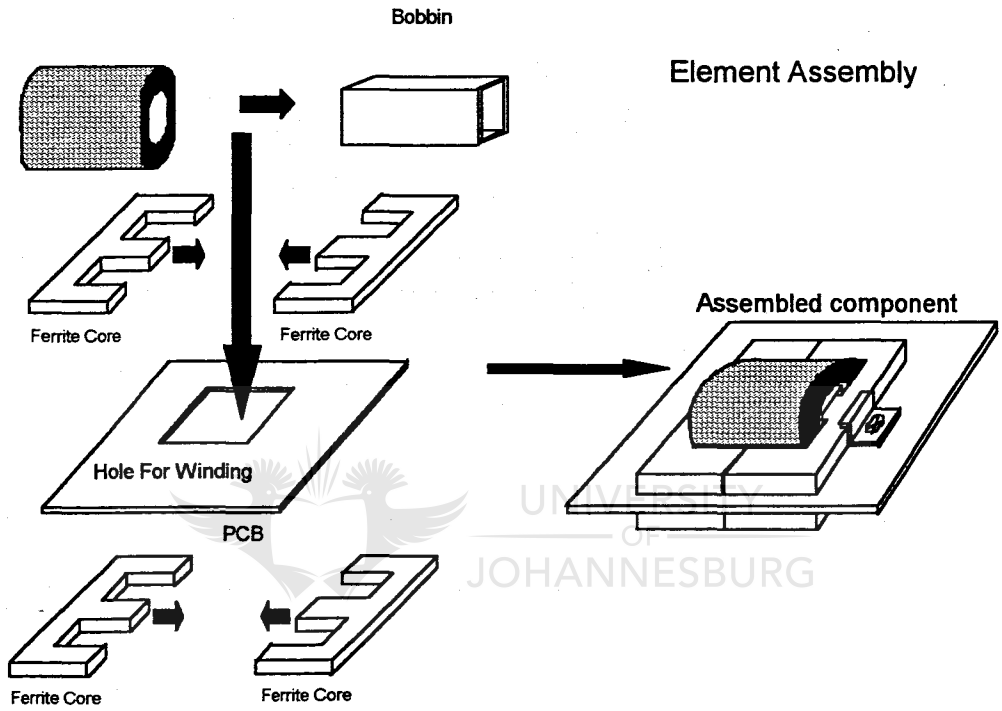

Figure. 4-8 A novel manufacturing technique for the elements in the distributed transformer

The coil illustrated in Figure.4-8, is obtained by winding a wire conductor, or wire bundle in the case of Litz wire, around an appropriately dimensioned bobbin. A hole is punched into the PCB to accommodate the coil, and once the bobbin is suspended in position the magnetic core may be slipped into place, clamped and fastened to the PCB.

An on board interconnection of the elements would result in a PCB mounted distributed transformer as illustrated in Figure.4-9.

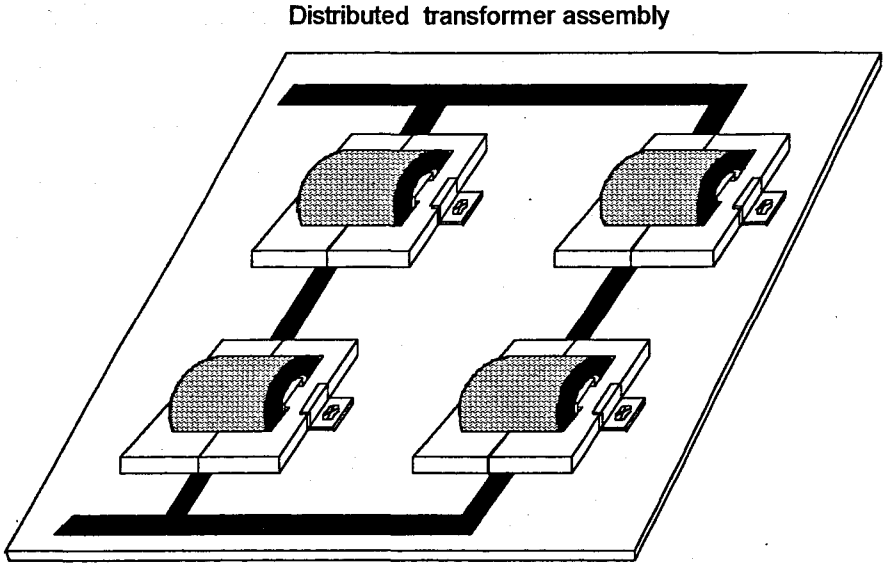

Figure. 4-9 The PCB mounted distributed transformer configuration

The manufacturing technique illustrated in Figure.4-9 was used for the distributed transformer, and a photograph is given in Figure.5-1 of chapter.5. A description of the fully assembled 1.5 kW distributed transformer is given as follows,

Magnetic core description:

No. of elements	-8
Core geometry	-E-type core
Core size	-E30
Material grade	-grade 3C80 material

Winding description :

No. of winding sections	- 4
No. of turns	- 18 turns per winding section
Type of windings	- Single round wire windings, 1 mm in diameter

4.4. CONCLUSION

A viable distributed transformer configuration was designed for use in the 1.5 kW battery charger , and a novel manufacturing technique which relies on current, well established methods was introduced. The manufacturing technique facilitates the stacked core assembly of the elements and ensures a low profile, PCB mountable assembly.

5. Case study - Experimental Results

5. CASE STUDY - EXPERIMENTAL RESULTS

5.1. INTRODUCTION

The transformer designs presented in the previous chapter, were assembled and their performance evaluated in the 1.5 kW battery charger. This chapter contains pertinent results required to make a critical evaluation with regards to the functionality of the distributed transformer, and also to serve as a basis for the practical verification of many of the predictions made with regards to its materials utilisation.

5.2. PRACTICAL REALISATION OF THE 1.5 KW MONOLITHIC AND DISTRIBUTED ISOLATION TRANSFORMERS

The monolithic and distributed transformers that were designed and built for use in the 1.5 kW battery charger, are illustrated in the photograph of Figure.5-1.

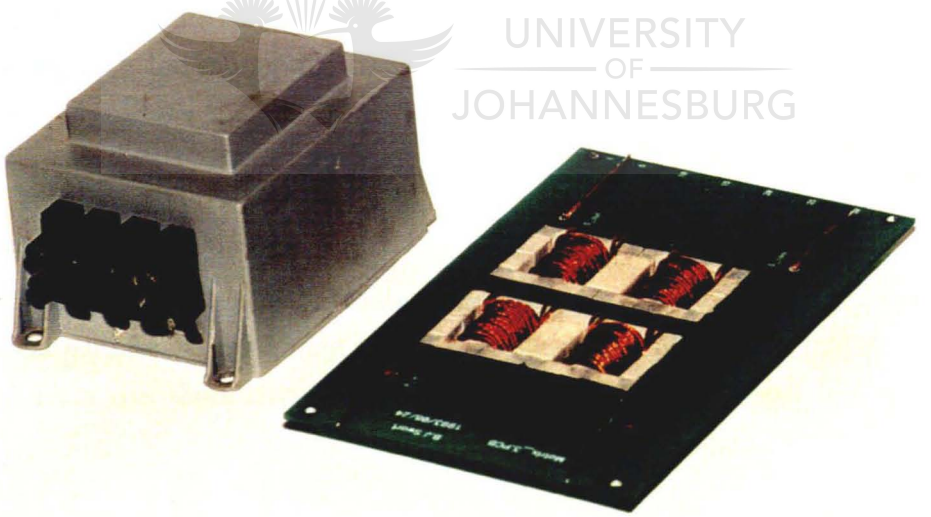

Figure. 5-1 Photograph of the barrel wound monolithic transformer (left) and the equivalent distributed transformer (right)

5.2.1. Physical characteristics

The key physical characteristics of the two transformers are summarised in Table.5-1.

	Monolithic transformer	Distributed transformer
Ferrite volume	**78 200 mm^3**	**32 000 mm^3**
Copper volume	**30 773 mm^3**	**20 793 mm^3**
Space volume consumption	**378 000 mm^3**	**95 550 mm^3**
Weight	**983.13 g**	**287.70 g**

Table. 5-1 Physical characteristics of the monolithic and distributed transformers

From Table.5-1, it is seen that the distributed transformer requires 60 % less ferrite, and 30 % less copper in its construction than the monolithic transformer. Furthermore, it is seen that the distributed transformer requires 60 % less space volume for heat dissipation and packaging than the monolithic transformer, and is seen to exhibit improved weight distribution.

5.2.2. Electrical characteristics

The electrical parameters pertaining to the winding design of the two transformers, were determined from the short circuit test over a wide frequency range, and are given as follows;

5.2.2.1. Short circuit impedance

The magnitude of the short circuit impedance for each transformer is illustrated graphically in Figure.5-2 as a function of frequency.

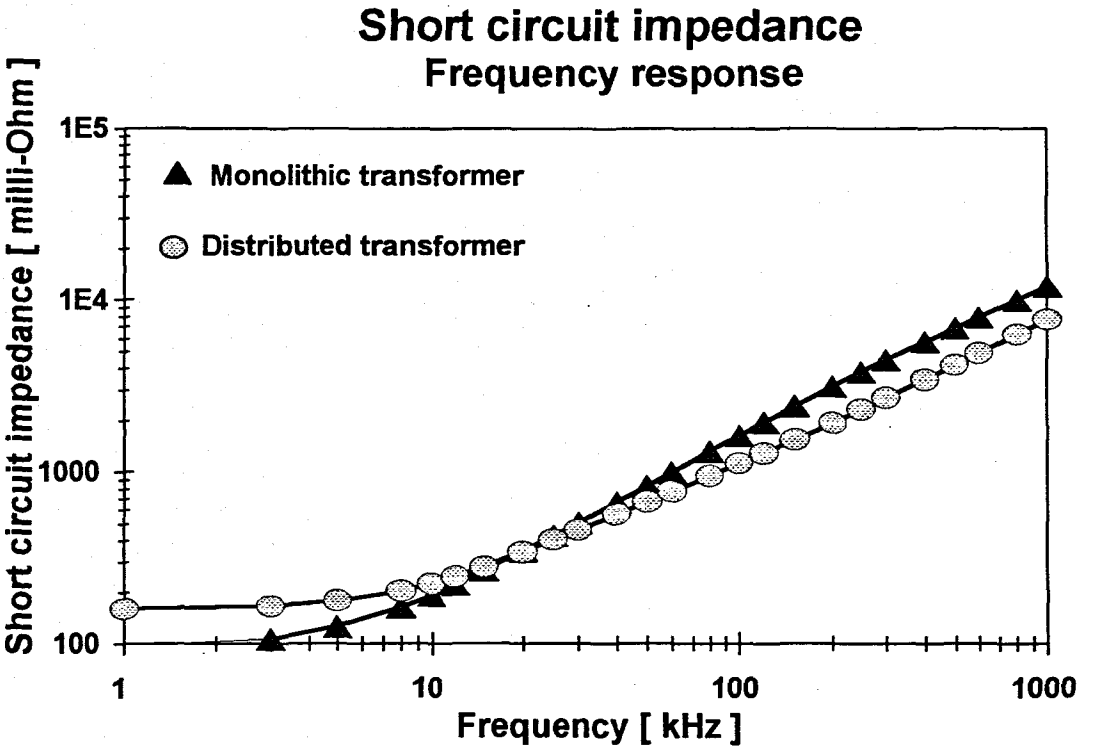

Figure. 5-2 Magnitude of short circuit impedance as a function of frequency

From Figure.5-2, it is seen that the short circuit impedance of the two transformers are within 10 % of each other, over the frequency range between 12 kHz and 30 kHz. Significant variations in the short circuit impedance of the two transformers are exhibited for all other frequencies, where the distributed transformer is seen to exhibit higher values than the monolithic transformer at frequencies less than 12 kHz, and lower values at frequencies higher than 30 kHz.

The phase of the short circuit impedance for each transformer is illustrated graphically in Figure.5-3 as a function of frequency.

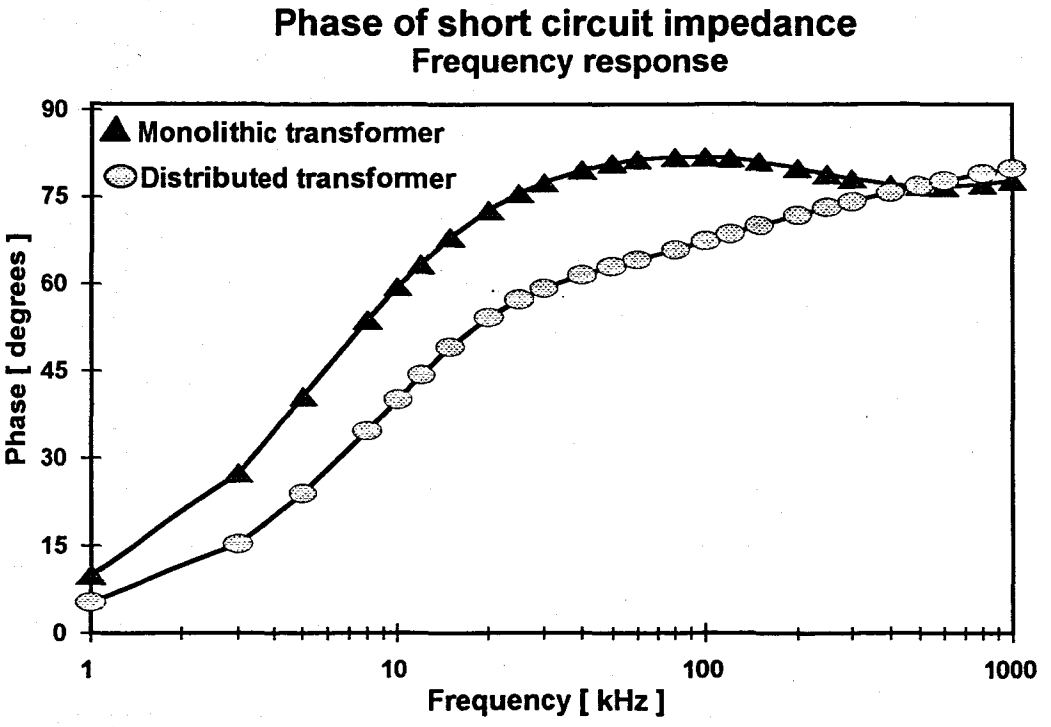

Figure. 5-3 Phase angle of short circuit impedance as a function of frequency

From Figure.5-3, it is seen that the phase angle of the short circuit impedance, is only comparable at frequencies above 200 kHz. At lower frequencies the short circuit impedance of the distributed transformer always exhibits smaller phase angles than that of the monolithic transformer.

The magnitude of the effective AC resistance for each transformer, which is the real value component of the short circuit impedance, is illustrated graphically in Figure.5-4 as a function of frequency.

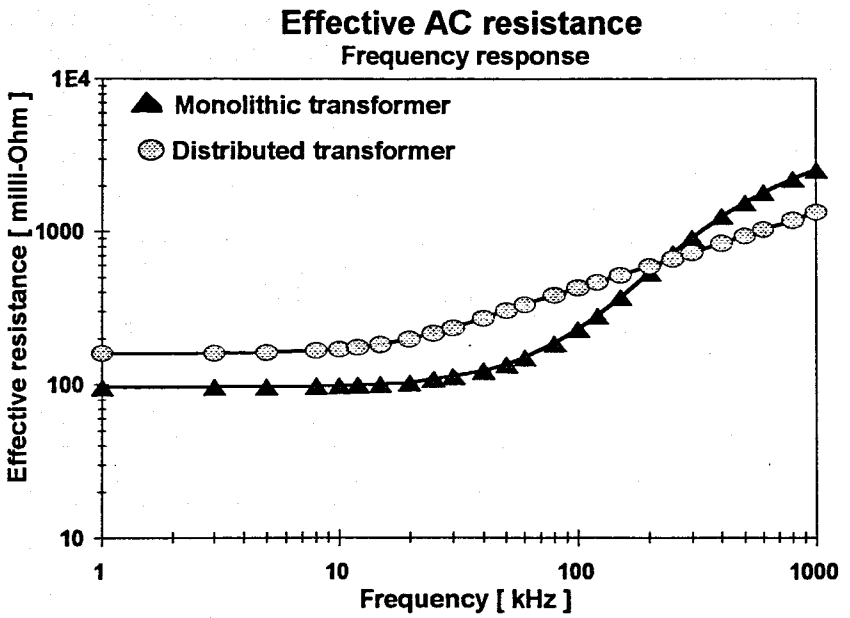

Figure. 5-4 Magnitude of effective AC resistance as a function of frequency

The distributed transformer is seen to exhibits higher values in AC resistance than the monolithic transformer at frequencies less than 250 kHz.

The consequent winding losses for each transformer at rated current, is illustrated graphically in Figure.5-5 as a function of frequency.

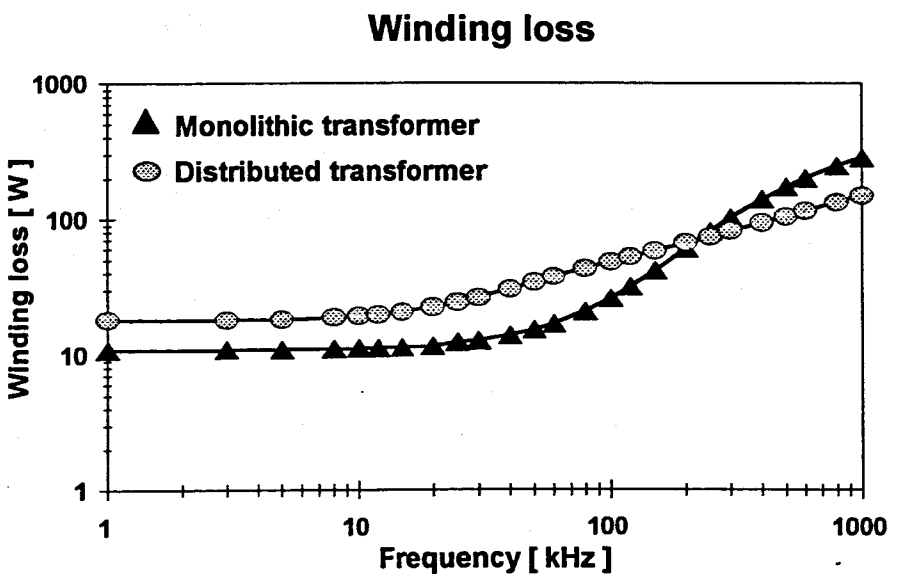

Figure. 5-5 Winding loss as a function of frequency

The magnitude of the leakage inductance for each transformer, which is responsible for the complex component of the short circuit impedance, is illustrated graphically in Figure.5-6 as a function of frequency.

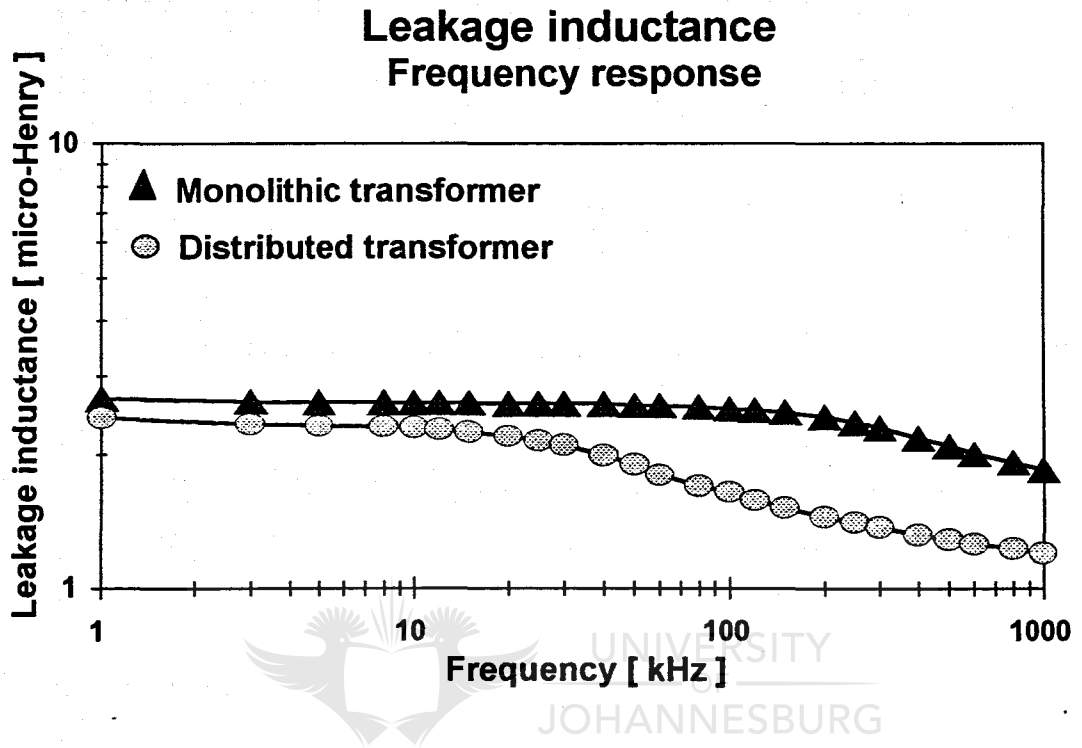

Figure. 5-6 Magnitude of leakage inductance as a function of frequency

The leakage inductance of the distributed transformer is always less than that of the monolithic transformer, particularly at frequencies higher than 20 kHz.

5.3. FUNCTIONALITY OF THE 1.5 KW MONOLITHIC AND DISTRIBUTED TRANSFORMERS

The electrical characteristics of the two transformers, pertaining to their operation within the battery charger, are tabulated in Table.5-2.

	Monolithic transformer	Distributed transformer
Magnetising inductance	**2.35 mH**	**1.88 mH**
Leakage inductance	**2.6 μH**	**2.2 μH**
Effective resistance	**103 mΩ**	**200 mΩ**
Winding loss	**11.5 W**	**22.5 W**
Core loss	**8 W**	**3.2 W**
Power density	**3.051 mW / mm^3**	**15.25 mW / mm^3**
Efficiency	**98.8 %**	**98.7 %**

Table. 5-2 Electrical characteristics of the monolithic and distributed transformers

From Table.5-2, it is seen that the distributed transformer has less core losses than that of the monolithic transformer but much higher winding losses. Consequently, the reduction in core loss, is counteracted by the increased winding losses, so that the efficiency of the two transformers are found to be comparable. Finally, the power density is found to be higher for the distributed transformer than for the monolithic transformer.

Both of the transformers were placed in the converter and its influence on converter operation investigated at a peak power transfer of 1.2 kW.

5.3.1. Source voltage and current

The 50 Hz mains supply is rectified, and used as an input to the converter in its unfiltered form, because of the converters ability to draw currents with a near unity power factor under such conditions. The source voltage and current is therefore an important consideration in the performance of the converter.

The measured voltage and current drawn from the mains utility grid was found to be the same for both transformer assemblies, and are illustrated in Figure.5-7 and Figure.5-8 for a peak power transfer of 1.2 kW.

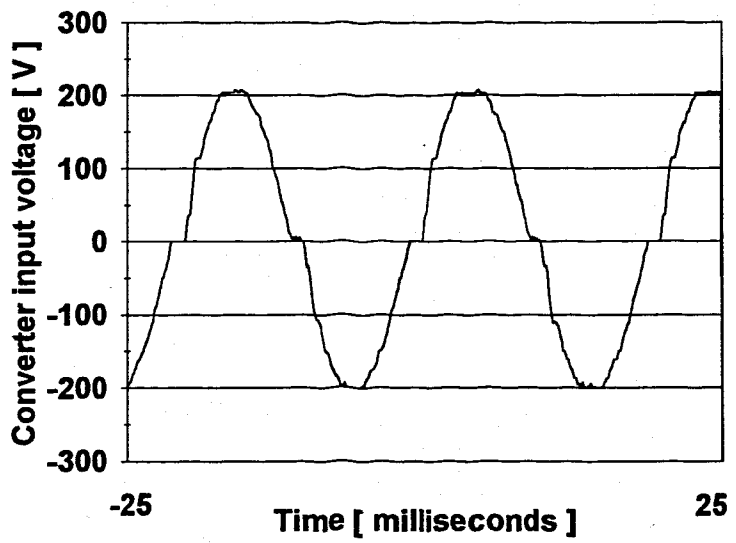

Figure. 5-7 Source voltage to converter at a peak power transfer of 1.2 kW

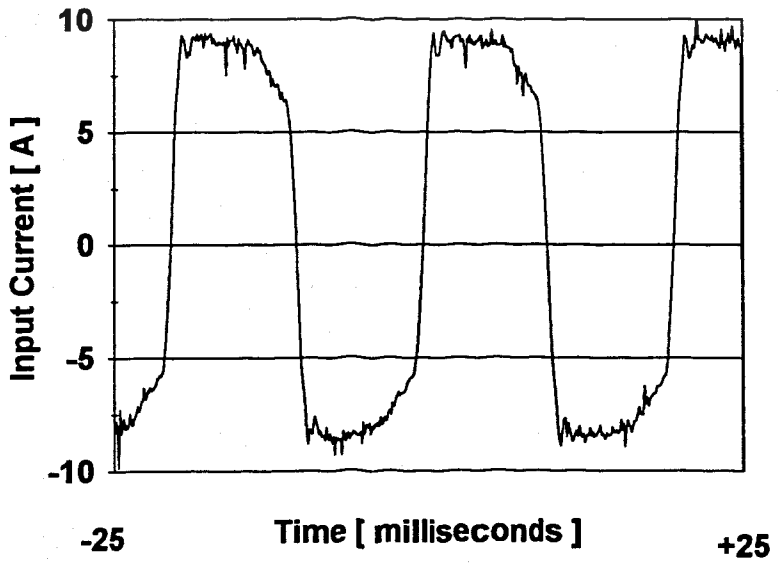

Figure. 5-8 Source current to converter at a peak power transfer of 1.2 kW

5.3.2. Transformer voltage and current

The distributed transformer was designed to cope with a maximum positive deviation in the volt-time integral of 4.3 mVs at peak power transfer. The voltage over the input of the transformer is therefore an important consideration in the performance of the converter.

The voltage and current measured at the inputs of the isolation transformer , was found to be the same for both transformer assemblies and are illustrated in Figure.5-9 and Figure.5-10, for a peak power transfer of 1.2 kW.

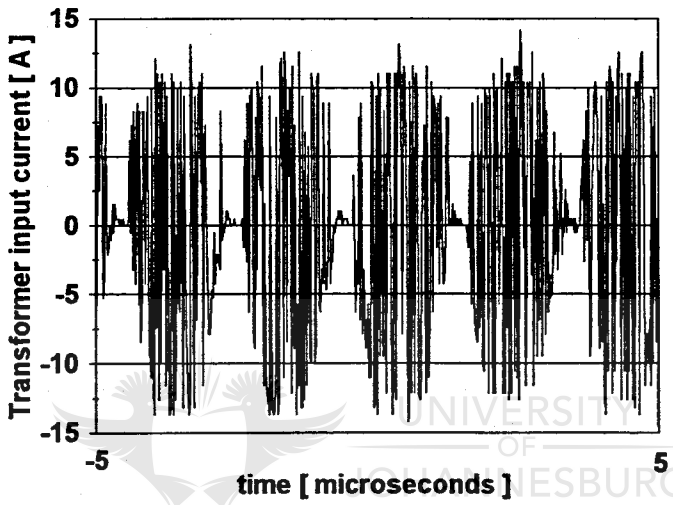

Figure. 5-9 Transformer input current at a peak power transfer of 1.2 kW

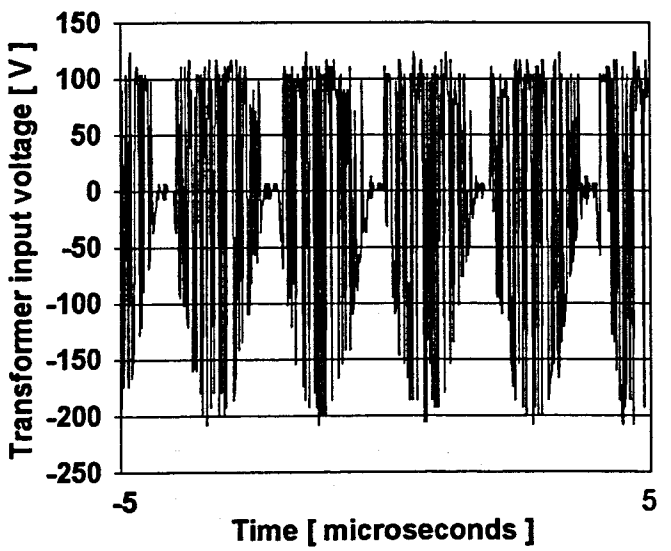

Figure. 5-10 Transformer input voltage at a peak power transfer of 1.2 kW

5.3.3. Converter Efficiency

The overall operation of the converter was evaluated for each of the transformers, and the efficiency measured up to a peak power transfer of 1.2 kW. The results of the measurements are illustrated in Figure.5.11.

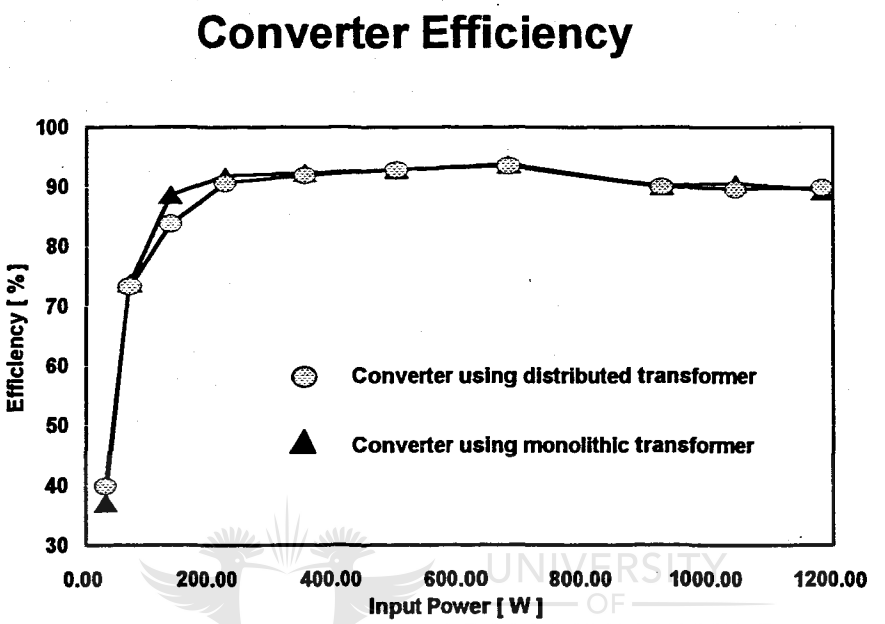

Figure. 5-11 Converter efficiency for monolithic and distributed transformers, up to a peak power transfer of 1.2 kW

From Figure.5-11, it is seen that the converter efficiency remains virtually unchanged for either of the transformer configurations.

5.4. CONCLUSION

From the measured results contained in Table.5-1, it is seen that the distributed transformer utilises materials more efficiently than the monolithic transformer, as expected. Furthermore, the results from Table.5-2 and Figure (5-7..5-11), show that the distributed transformer has no deleterious effect on the operation of the converter or its efficiency,

therefore, the distributed transformer can be used as a valid replacement for the monolithic transformer to realise galvanic isolation in the battery charger.

6. Conclusion

6. CONCLUSION

The success of any developmental work, must be evaluated by comparing the intent of the design with the outcome of its implementation. This chapter is dedicated to an evaluation of the distributed transformer, in terms of the requirements placed on its development in chapter.1, and discusses the conclusions which can be made with regards to its application in DC-DC converters.

6.1. Physical performance

The distributed transformer was found to exhibit the following advantageous characteristics, when compared with the conventional monolithic transformer,

(1) Less ferrite and copper material is required in its construction.

(2) Because less materials are used in its construction, it is smaller and lighter.

(3) It's total weight is evenly distributed over the elements in the configuration, and is, therefore, not prone to weight imbalances, if the elements are positioned properly.

The distributed transformer exhibits an improvement in materials utilisation while subjected to natural convection cooling, that has so far only been attained in conventional monolithic transformers subjected to forced cooling.

The distributed transformer, therefore, satisfies the first three physical requirements listed in section 1.3.2.

6.2. Electrical performance

The power loss in the magnetic material of the distributed transformer was found to be much smaller than that of the equivalent monolithic transformer, but exhibited an increase in its winding loss when tested in the battery charger. The power loss and efficiency of the distributed transformer was found to be comparable with that of the monolithic transformer.

Furthermore, the performance and efficiency of the converter remained unaltered for both transformer assemblies, therefore from an electrical viewpoint, the performance of the distributed transformer is identical to that of the conventional monolithic transformer assembly.

The distributed transformer, therefore, satisfies the fourth requirement listed in section.1.3.2.

6.3. Design

The design of the distributed transformer did not prove to be very difficult, since it is predominantly based on simple circuit theory and conventional transformer design. Once the operating conditions and optimum core size for a distributed transformer has been established, the engineer need only concentrate on the design of a single element, which is in essence nothing more than a conventional monolithic transformer. Consequently, the design of the distributed transformer is no more complex than the design of a conventional monolithic transformer.

The design of distributed transformers, offer an additional perk, because the total impedance parameters of the configuration can be tailored to meet certain requirements , by merely altering the dimensions of the matrix interconnection.

6.4. Ease of manufacture

At higher power levels, conventional magnetic components are too heavy to mount directly onto a PCB, but the lighter elements in a distributed transformer are suitable for just such a purpose. It is therefore, possible to mount distributed transformers onto a PCB together with remainder of the circuitry in a converter.

The elements of a distributed transformer do not necessarily have to be mounted onto a PCB, and in such cases can be assembled by making use of existing manufacturing techniques.

The distributed transformer, therefore, satisfies the fifth and final requirement listed in section 1.3.2

Monolithic transformers, however, only require a single set of windings, whereas distributed transformers, require a set of windings for each element in the configuration. The engineer must thereforee decide if the inclusion of additional windings in the manufacturing process of distributed transformers, can be justified by the gain in materials utilisation achieved by its use.

6.5. Summary

The distributed transformer assembly has been compared with conventional monolithic transformers and seems to exhibit improved physical characteristics unparalleled by conventional magnetic components, furthermore, it seems suitable for use in all DC-DC power converters. The distributed transformer can therefore, be considered as an invaluable first step to improving the industrialisation of DC-DC power converters.

Appendixes

A. Variability of current density in magnetic components - an analysis

APPENDIX.A. VARIABILITY OF CURRENT DENSITY IN MAGNETIC COMPONENTS - AN ANALYSIS

A.1. INTRODUCTION

This section is dedicated to the derivation of analytical expressions which can be used to describe the variability of current density in high frequency magnetic components, as a function of core size.

Consider the winding geometry of Figure.A-1,

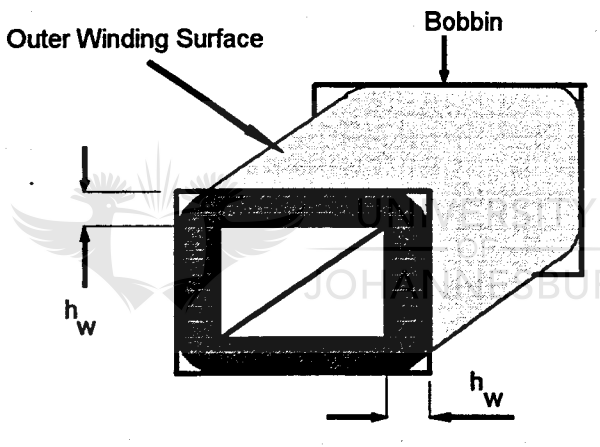

Figure. A-1 Schematic view of windings on bobbin

An exact mathematical description of the variation in current density with core size is complicated by high frequency loss mechanisms such as skin and proximity effects. These effects can be neglected, however, and a reasonable approximation obtained by assuming perfect litz wire windings . The current density in ideal litz wire windings is uniformly distributed over the cross-section of the winding conductors, the only opposition to current flow, therefore, is the DC resistance of the winding.

If the windings were to be cut down the middle and unrolled, it would form a single rectangular slab of conductive material as illustrated in Figure.A-2.

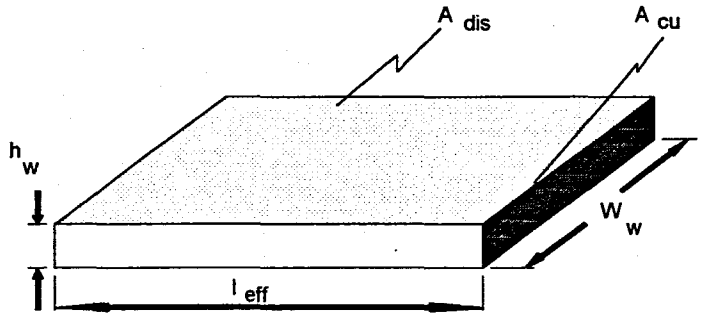

Figure. A-2 Schematic view of unrolled windings

The power loss in the windings is derived from Ohm's law and is given as follows

$$P_e = i_{rms}^2 R_{dc} \qquad \text{(A.1)}$$

The DC resistance of the windings is given as follows, with reference to Figure.A-2,

$$R_{dc} = \frac{l_{eff}}{\sigma A_{cu}} = \frac{l_{eff}}{\sigma W_w h_w} \qquad \text{(A.2)}$$

Substituting equation (A.2) into equation (A.1) results in the following expression for the winding losses,

$$P_e = J^2 W_w h_w \frac{l_{eff}}{\sigma} \qquad \text{(A.3)}$$

Furthermore, if it is assumed that the heat is dissipated predominantly from the upper surface indicated in Figure.A-2, due to natural convection, then the rate at which energy is dissipated as follows,

$$Q_{convection} = \bar{h} A_{dis} \Delta T = \bar{h} W_w h_w l_{eff} \Delta T \qquad \text{(A.4)}$$

Under steady state conditions thermal equilibrium is reached when the internally generated winding loss is equal to the rate at which heat energy is dissipated, i.e. equations (A.3) and (A.4) are equal,

$$J^2 W_w h_w \frac{l_{eff}}{\sigma} = \bar{h} W_w l_{eff} \Delta T \qquad \text{(A.5)}$$

Solving for J, and simplifying results in the following expression for current density,

$$J = \sqrt{\frac{\bar{h} \Delta T}{\sigma h_w}} \qquad \text{(A.6)}$$

The value of the convection heat transfer coefficient, can be evaluated for a horizontal plate with reference to [1,2]. Equation (A.6) for naturally cooled magnetic components is then given as follows,

$$J = \sqrt{\frac{1.03 \times 10^{-4}}{h_w}} \qquad \text{(A.7)}$$

The results obtained from equation (A.7), fall within 10 % of the data given in [3] for practical core sizes with an E-core geometry.

B. Temperature measurement of ferrite cores

APPENDIX.B. TEMPERATURE MEASUREMENT OF FERRITE CORES

B.1. INTRODUCTION

The power loss generated in the ferrite core of a magnetic component, under steady state conditions, is proportional to the frequency of excitation, f, and peak flux density, $\hat{B}$, as described by equation (2.1) and repeated as equation (B.1) for convenience,

$$P_{loss} = \eta f \left(\hat{B}\right)^{a} \qquad \text{(B.1)}$$

Thermal equilibrium is reached, when the total internally generated heat is equal to the heat lost at the surfaces of the core. This energy balance is described by the relationship in equation (B.2),

$$\textit{Rate of heat generation} = \textit{Rate of heat dissipation} \qquad \text{(B.2)}$$

When the heat energy generated in a magnetic core is lost to its surrounding environment by means of natural convection, equation (B.2) can be expressed as follows,

$$\begin{aligned} P_{loss} &= \bar{h}\, A_{core}\, \Delta T \\ &= \bar{h}\, A_{core} \left(T_s - T_A\right) \end{aligned} \qquad \text{(B.3)}$$

$\bar{h}$ ≡ Convective heat transfer coefficient
A_{core} ≡ Surface area of core
ΔT ≡ Temperature difference between core surface and environment
T_s ≡ Surface temperature of core
T_A ≡ Ambient temperature

If the thermally excited magnetic core is placed in an environment with a constant ambient temperature, then from equation (B.3) it is seen that an appropriate surface temperature will be established to ensure the transfer of the internally generated heat to the environment. The internally generated heat and consequently the surface temperature of the magnetic core, is a function of the frequency of excitation and peak flux density.

This section is dedicated to a description of the apparatus, its limitations, and the procedure which was followed to measure the relationship between surface temperature, surface area, size, frequency of excitation and peak flux density for a range of ferrite cores subjected to natural cooling.

B.2. THE MEASUREMENT SYSTEM

If the surface temperature of a **naturally cooled** ferrite core is to be accurately measured as a function of peak flux density and frequency of excitation, then the measurement system must include,

- a stable environment with a controllable ambient temperature.
- a variable frequency, variable voltage supply.

B.2.1. The physical construction of a stable environment with a controllable ambient temperature

It is imperative that the ferrite cores be measured in a closed, temperature controlled environment, and not in an open room or laboratory, for the following reasons,

- The ambient temperature in an open room fluctuates during the course of a day, and also from day to day, due to drafts, changes in weather, humidity, etc. Temperature measurements conducted in such an environment would fluctuate and the results obtained could never be repeated with any degree of accuracy.

- Air moving over the surface of the core due to drafts in an open room, would violate the conditions for natural convection cooling , and the measurement results obtained for such conditions would be invalid. Furthermore, it is very difficult to identify the many sources responsible for drafts in an open room and are therefore very difficult to stop or control.

The experimental system which was used to emulate a closed temperature controlled environment, is illustrated by the schematic in Figure.B-1.

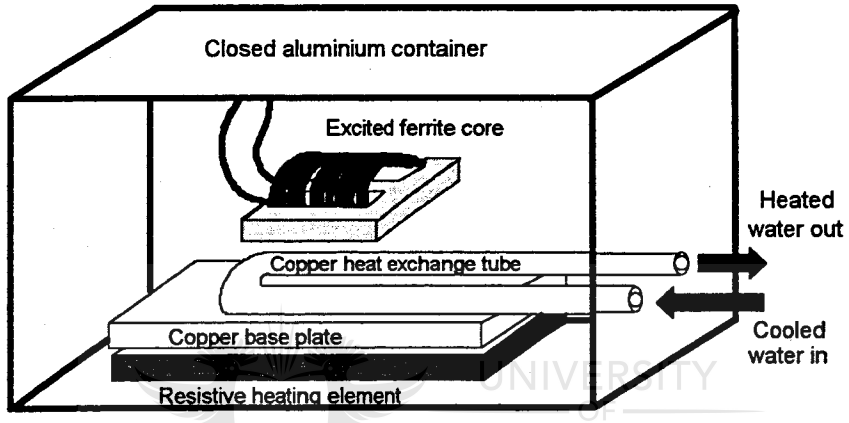

Figure. B-1 Schematic of the enclosed temperature controlled environment

The closed temperature controlled environment, illustrated in Figure.B-1, is made up of three basic constituents, namely (1) a closed container, (2) a heat exchanger, and (3) a resistive heat element.

(1) The closed container:

The closed container is made from aluminium plate, lined on the inside with asbestos material.

(2) The heat exchanger:

The heat exchanger consists of a copper tube embedded in a copper base plate. Chilled water is forced through the copper tube at a fixed rate when an external pump (not shown in Figure.B-1), is activated.

(3) The resistive heating element:

The resistive heating element consists of nichrome wire embedded in a metal base plate, which makes physical contact with the underside of the copper base plate of the heat exchanger. Current is passed through the nichrome wire when an external current source (not shown in Figure.B-1) is activated.

B.2.1.1. Steady state control of the ambient temperature

During the experiments, a thermally excited magnetic core will transfer heat energy to the container's interior at a rate governed by equation (B.1). The effect of this additional heat energy on the containers ambient temperature, is eliminated by activating the heat exchanger and heating element in a controlled sequence. The following two modes of operation can be identified in the system under steady state conditions,

Mode 1 Operation:

Mode 1 operation is initialised when the actual ambient temperature has increased beyond the required ambient temperature, T_A, by an amount, dT. At this point the heat exchanger is activated and the heating element is deactivated. The thermally excited ferrite core, is the only heat source in the container, and continues to transfer heat energy to its interior at a rate of Q_c .

The temperature of the copper base plate decreases as chilled water is pumped through the heat exchange tube at a constant flow rate. The base plate then stabilises at a temperature of $T_a < T_A$, and heat energy is transferred from the containers interior to the base plate, at a rate given by equation (B.4),

$$Q_a = h_a A_a (T_A - T_a) \qquad \text{(B.4)}$$

Q_a ≡ Rate at which energy is absorbed from the containers interior due to natural convection.

h_a ≡ Convective heat transfer coefficient for the copper base plate configuration.

A_a ≡ Upper surface area of the copper base plate.

The heat energy absorbed by the copper base plate is removed and transported to the container's exterior by forced convection, at a rate given by equation (B.5),

$$Q_f = \dot{m}_{water} C_p (T_{out} - T_{in}) \qquad \text{(B.5)}$$

Q_f ≡ Rate at which energy is removed from the base plate due to forced convection (flow of chilled water in heat exchange tubes)

$\dot{m}_{water}$ ≡ Mass flow rate of water

C_p ≡ Specific heat capacity of water

T_{in} ≡ Temperature of the at the inlet of the heat exchange tube

T_{out} ≡ Temperature of water at the outlet of the heat exchange tube

The surface temperature of the copper base plate, is seen to stabilise at the temperature T_a, when $Q_a = Q_f$. In the actual system, the heat exchanger is purposely dimensioned so that $Q_a > Q_c$, consequently the ambient temperature of the container is seen to decrease.

Mode 2 operation:

Mode 2 operation is initialised when the actual ambient temperature, has decreased beyond the required temperature, T_A , by an amount dT. At this point the heating element is activated and the heat exchanger is deactivated. The activated heating element transfers additional energy to the container's interior, at rate given by equation (B.6).

$$Q_R = i_{rms}{}^2 R \qquad \text{(B.6)}$$

Q_R ≡ Rate at which heat energy is transferred to the containers interior.
i ≡ Effective value of current flowing in the nichrome wire.
R ≡ Resistance of nichrome wire.

Since no heat sinks are present in the system, the ambient temperature is seen to increase.

The steady state variation in the ambient temperature of the container during any measurement process, is seen to exhibit the characteristics illustrated in Figure.B-2.

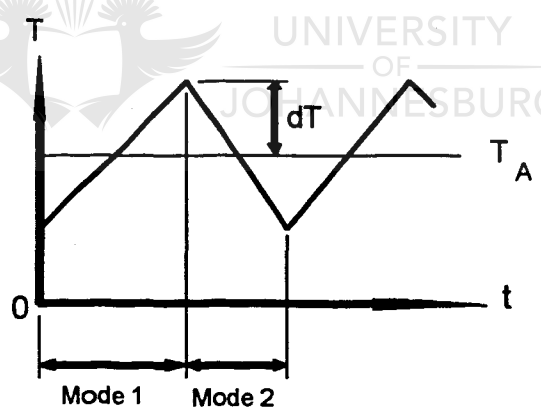

Figure. A-2 Variation in ambient temperature during steady state operation of measurement system

A total dT of 0.3 °C was measured for a required T_A of 25 °C, in the practical system, for a 40 °C increase in core temperature over a period of one hour.

B.2.1.2. Limitations of the temperature controlled environment

The ambient temperature of the container can be controlled, as described in the previous section, if it is executed within the bounds of the energy balance described in equation (B.7),

Heat energy added to container = Heat energy removed from container (B.7)

The appropriate energy balance for the temperature controlled environment is therefore given as follows,

$$Q_c + Q_R = Q_a \tag{B.8}$$

The heating element is inactive during mode 1 operation of the temperature controlled environment, thereforee Q_R in equation (B.8) can be made equal to zero. The energy balance that must be maintained during mode 1 operation of the temperature controlled environment, is therefore given as follows,

$$Q_c \leq Q_a \tag{B.9}$$

It is seen from equation (B.9), that the maximum power loss permitted in any ferrite core, must not exceed the maximum power that can be absorbed by the heat exchanger.

This limitation can be alleviated, and the range of the system improved as follows

1. From equation (B.5), it is seen that Q_a, can be increased if,

   - the mass flow of the water through the heat exchange tube is increased.
   - the temperature of the water at the inlet of the heat exchange tube is decreased.
   - the water through the heat exchange tube is replaced by a fluid with a higher specific heat capacity.

2. From equation (B.4), it is seen that Q_a, can be increased if the surface area of the copper base plate can be increased.

B.2.2. The physical construction of a variable frequency variable voltage supply

It must be possible, during the measurement procedure, to control the peak flux density excursion within a ferrite core. This can be easily accomplished if the core is used in the construction of an inductor, because the frequency of excitation and the magnitude of the peak flux density, is related to the core dimensions and voltage over its winding in the following manner,

$$V = k N \hat{B} f A_C \qquad \text{(B.10)}$$

V ≡ rms voltage applied to inductor windings
k ≡ form factor for applied voltage, (k = 4 for square wave, k=4.44 for a sinusoid)
N ≡ Number of turns in the winding
B ≡ Peak flux density excursion in the ferrite core
f ≡ Frequency of applied voltage
A_c ≡ cross-sectional area perpendicular to flow of flux

It is seen from equation (B.10) that the peak flux density in the core for a given frequency, can be changed by changing the magnitude of the applied voltage, hence the necessity for a variable frequency, variable voltage supply.

The experimental set-up makes use of the half bridge circuit topology, illustrated in Figure.B-3.

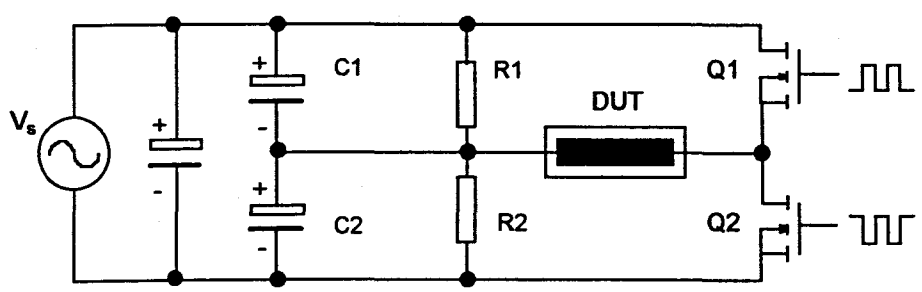

Figure.B-3 Half bridge circuit topology

B.3. MEASUREMENT PROCEDURE

The following procedure was followed to measure the surface temperature of each core in the selected range.

1. The core is fitted with a single winding and placed into the temperature controlled environment in such a manner so as to ensure no physical contact between the magnetic core and any other body, effectively cancelling conductive heat transfer.

2. The ambient temperature within the temperature controlled environment, is raised to a given value, and allowed to stabilise.

3. The winding is energised in accordance with equation (B.10), so that the core is excited at a given frequency and peak flux density excursion. The system is left to stabilise before the temperature distributions are measured on the open surface areas of the core.

4. Step 3 is repeated for a number of peak flux densities over a frequency range of interest.

B.4. MEASUREMENT RESULTS

Typical results, showing the relationship between rise in surface temperature, flux density and frequency, are given for five E-type cores of grade 3C80 ferrite material in Figures (C-1..C-10) of Appendix.C.

C. Results of temperature measurements

APPENDIX.C. RESULTS OF TEMPERATURE MEASUREMENTS

The measured results, showing the relationship between rise in surface temperature, flux density and frequency, are given for five E-type cores of grade 3C80 ferrite material.

B [T]	ΔT at 10 kHz [°C]	ΔT at 20 kHz [°C]	ΔT at 30 kHz [°C]	ΔT at 40 kHz [°C]	ΔT at 50 kHz [°C]
0.15	**2.6**	**3.2**	**3.8**	**5.1**	**8.3**
0.175	**3.2**	**4.5**	**6.3**	**7.9**	**10.3**
0.2	**3.8**	**5.8**	**7.9**	**10.7**	**12.6**
0.225	**4.4**	**6.8**	**9.7**	**12.8**	**14.6**
0.25	**5.1**	**8.2**	**11.1**	**14.5**	**16.8**

Table.C-1 Temperature rise in E20 core, measured at an ambient temperature of 25 °C

The results tabulated in Table.C-1 for the E20 core, are illustrated graphically in Figure.C-1.

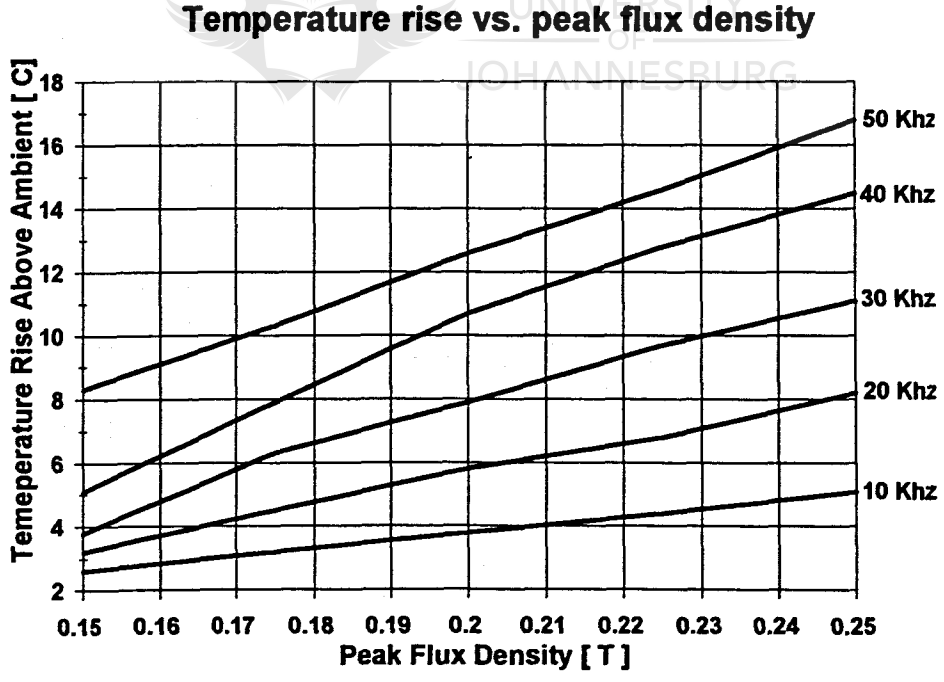

Figure.C-1 Temperature rise in E20 core as a function of frequency and flux density

B [T]	ΔT at 10 kHz [°C]	ΔT at 20 kHz [°C]	ΔT at 30 kHz [°C]	ΔT at 40 kHz [°C]	ΔT at 50 kHz [°C]
0.15	**3.01**	**4.00**	**4.2**	**5.8**	**9.0**
0.175	**3.7**	**5.5**	**7.3**	**8.9**	**11.6**
0.2	**4.4**	**6.7**	**9.3**	**11.7**	**15**
0.225	**5.3**	**8.2**	**11.5**	**15.6**	**19.7**
0.25	**6.1**	**10.4**	**14.1**	**19.5**	**24.9**

Table.C-2 Temperature rise in E30 core, measured at an ambient temperature of 25 °C

The results tabulated in Table.C-2 for the E30 core, are illustrated graphically in Figure.C-2.

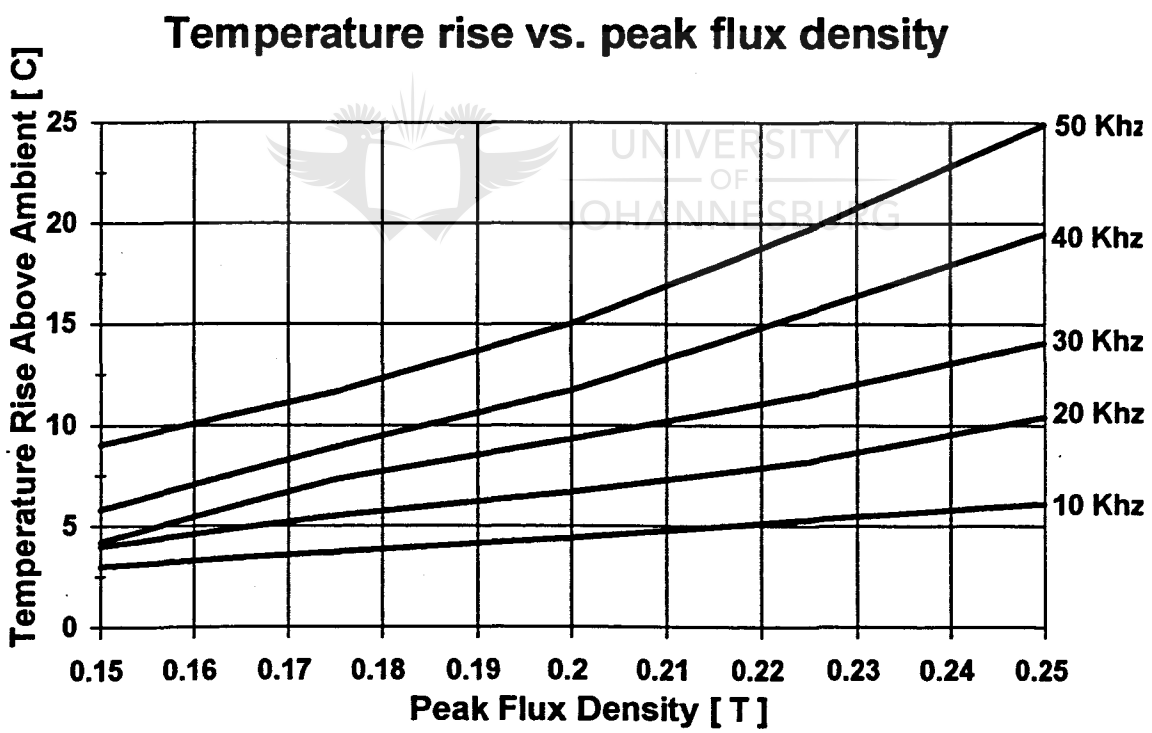

Figure.C-2 Temperature rise in E30 core as a function of frequency and flux density

B [T]	ΔT at 10 kHz [°C]	ΔT at 20 kHz [°C]	ΔT at 30 kHz [°C]	ΔT at 40 kHz [°C]	ΔT at 50 kHz [°C]
0.15	**3.6**	**4.6**	**5.6**	**6.7**	**11.3**
0.175	**4.3**	**7.2**	**10.0**	**12.0**	**16.9**
0.2	**5.7**	**10.2**	**14.8**	**17.0**	**24.8**
0.225	**7.2**	**13.9**	**20.2**	**26.5**	**33.8**
0.25	**9.7**	**17.4**	**25.1**	**35.1**	**42.7**

Table.C-3 Temperature rise in E42 core, measured at an ambient temperature of 25 °C

The results tabulated in Table.C-3 for the E42 core, are illustrated graphically in Figure.C-3.

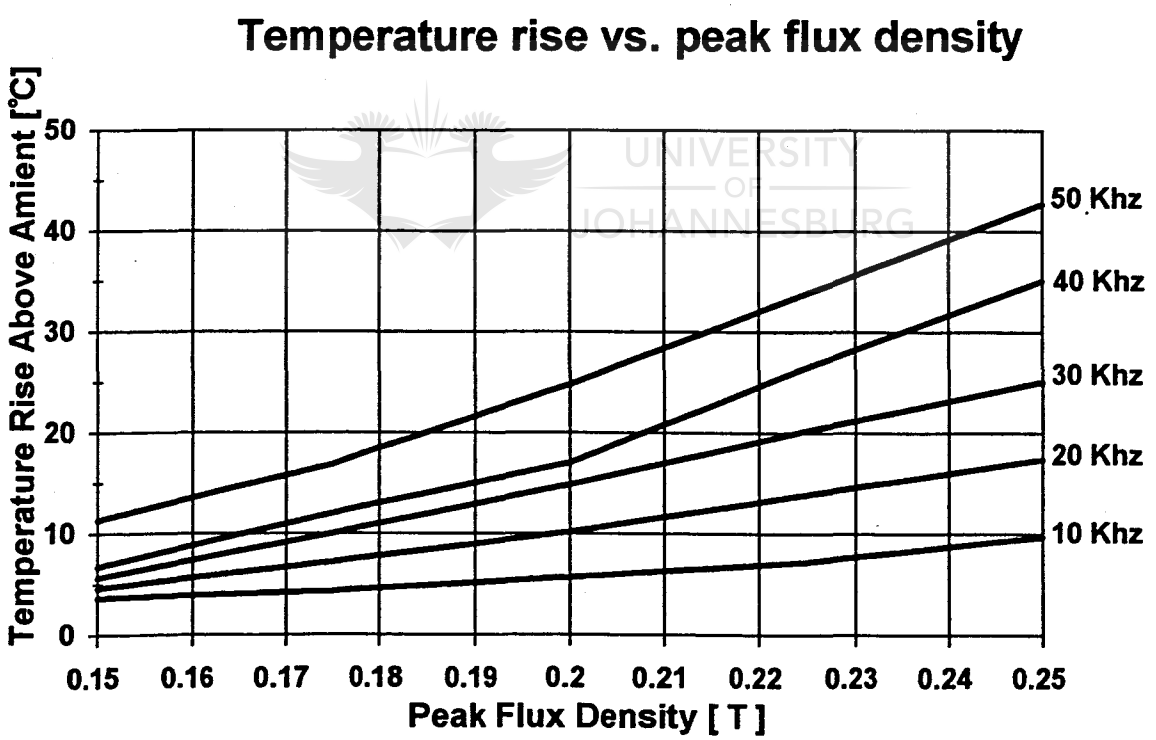

Figure.C-3 Temperature rise in E42 core as a function of frequency and flux density

B [T]	ΔT at 10 kHz [°C]	ΔT at 20 kHz [°C]	ΔT at 30 kHz [°C]	ΔT at 40 kHz [°C]	ΔT at 50 kHz [°C]
0.15	**5.1**	**5.9**	**7.3**	**11.6**	**12.8**
0.175	**6.2**	**9.3**	**13.2**	**18.3**	**20.9**
0.2	**7.9**	**13.6**	**20.0**	**28.6**	**31.6**
0.225	**10.3**	**18.0**	**26.4**	**38.0**	**41.5**
0.25	**13.4**	**23.0**	**32.8**	**50.5**	**53.0**

Table.C-4 Temperature rise in E55 core, measured at an ambient temperature of 25 °C

The results tabulated in Table.C-4 for the E55 core, are illustrated graphically in Figure.C-4.

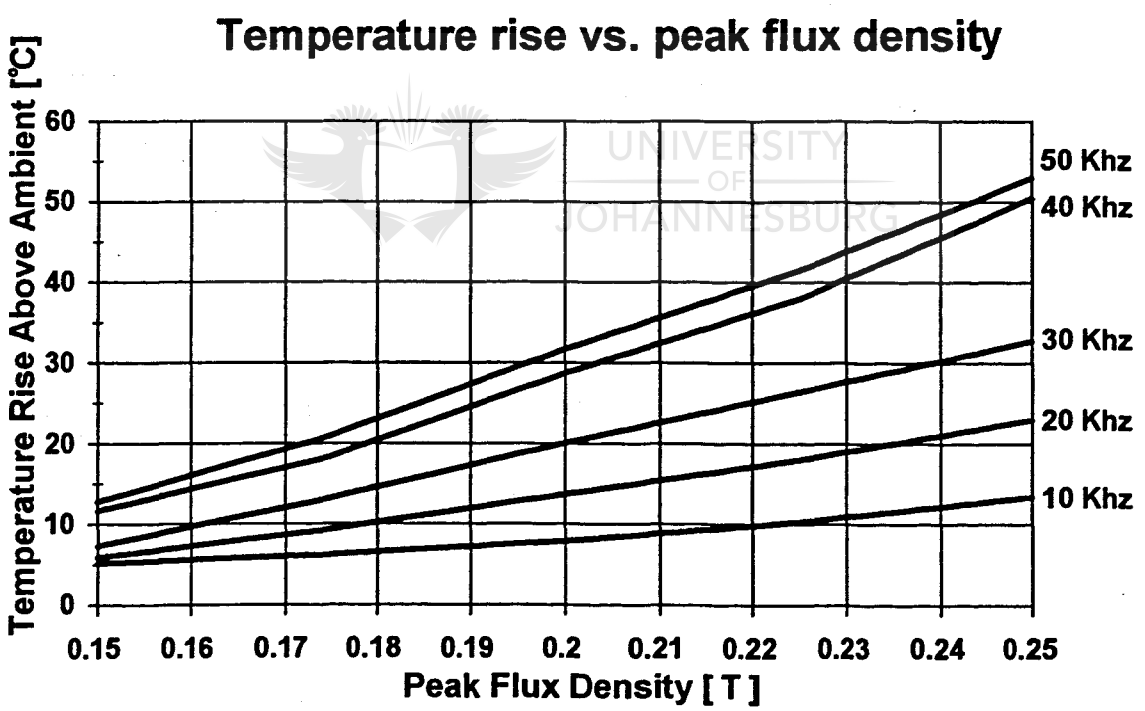

Figure.C-4 Temperature rise in E55 core as a function of frequency and flux density

B [T]	ΔT at 10 kHz [°C]	ΔT at 20 kHz [°C]	ΔT at 30 kHz [°C]	ΔT at 40 kHz [°C]	ΔT at 50 kHz [°C]
0.15	**7.2**	**8.8**	**10.9**	-	-
0.175	**8.3**	**11.8**	**16.3**	-	-
0.2	**10.0**	**15.7**	**22.5**	-	-
0.225	**12.0**	**20.1**	**29.0**	-	-
0.25	**15.0**	**25.0**	**37.2**	-	-

Table.C-5 Temperature rise in E65 core †, measured at an ambient temperature of 25 °C

The results tabulated in Table.C-5 for the E65 core, are illustrated graphically in Figure.C-5.

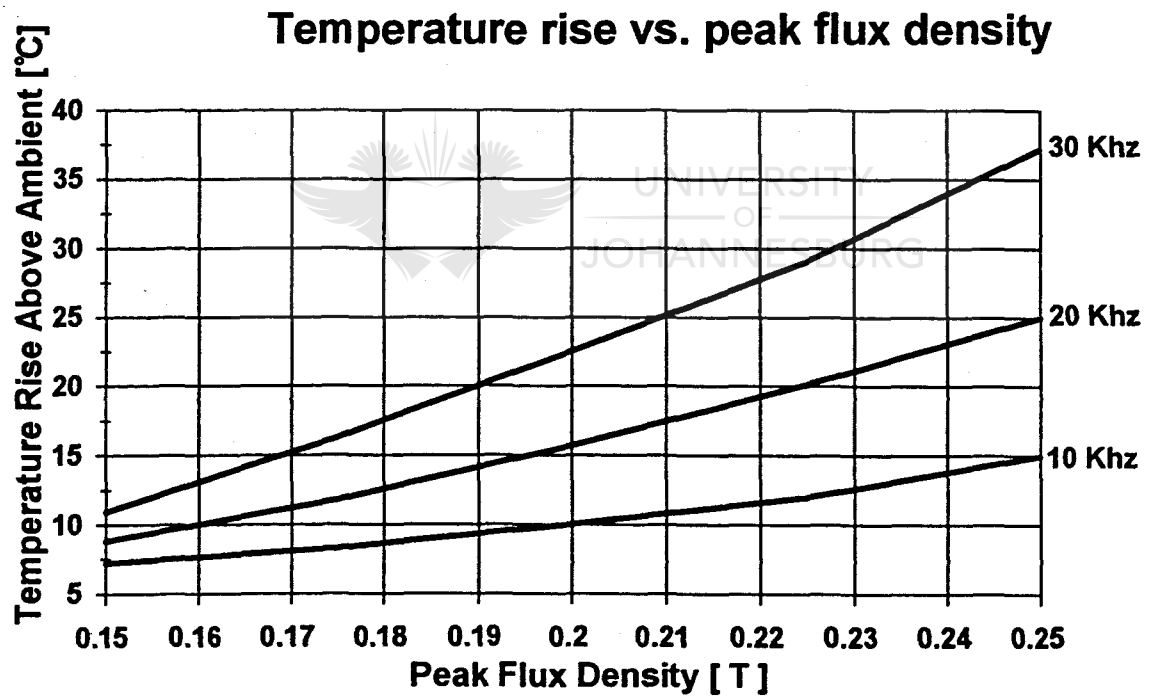

Figure.C-5 Temperature rise in E65 core as a function of frequency and flux density

†Results not available for frequencies above 30 kHz, due to limitations of measurement system.

The graphic comparison between the core sizes are given in Figures (C-6 .. C-10).

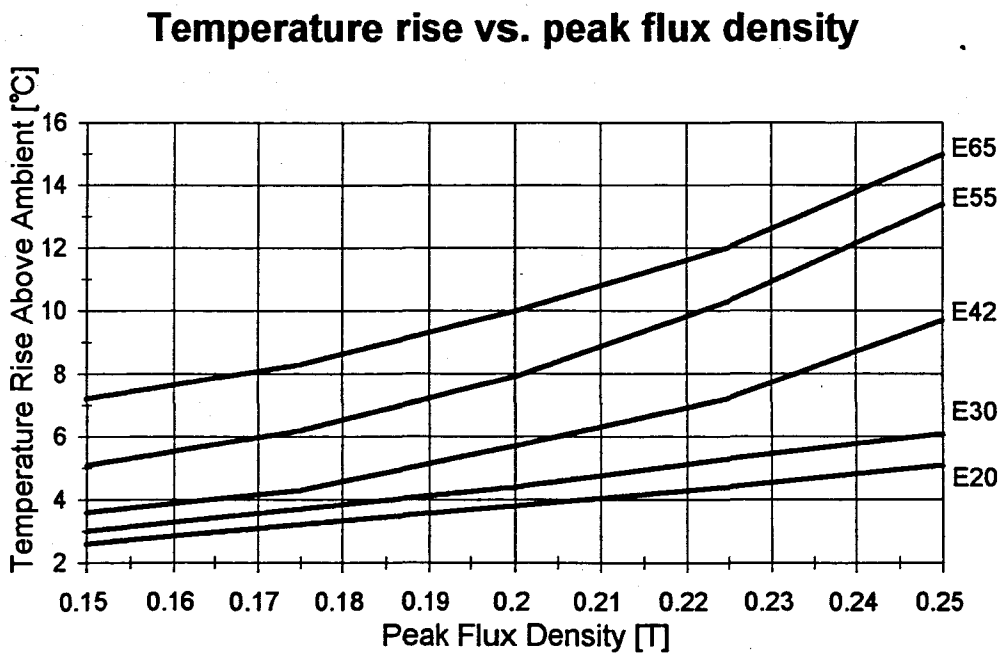

Figure. C-6 Surface temperature comparisons for various size E-cores at 10 kHz

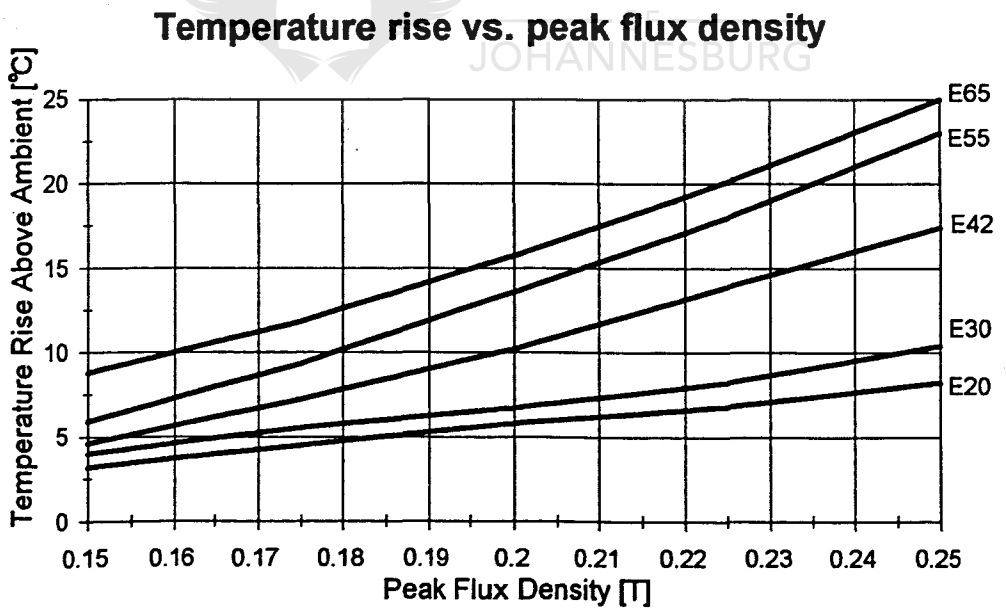

Figure. C-7 Surface temperature comparisons for various size E-cores at 20 kHz

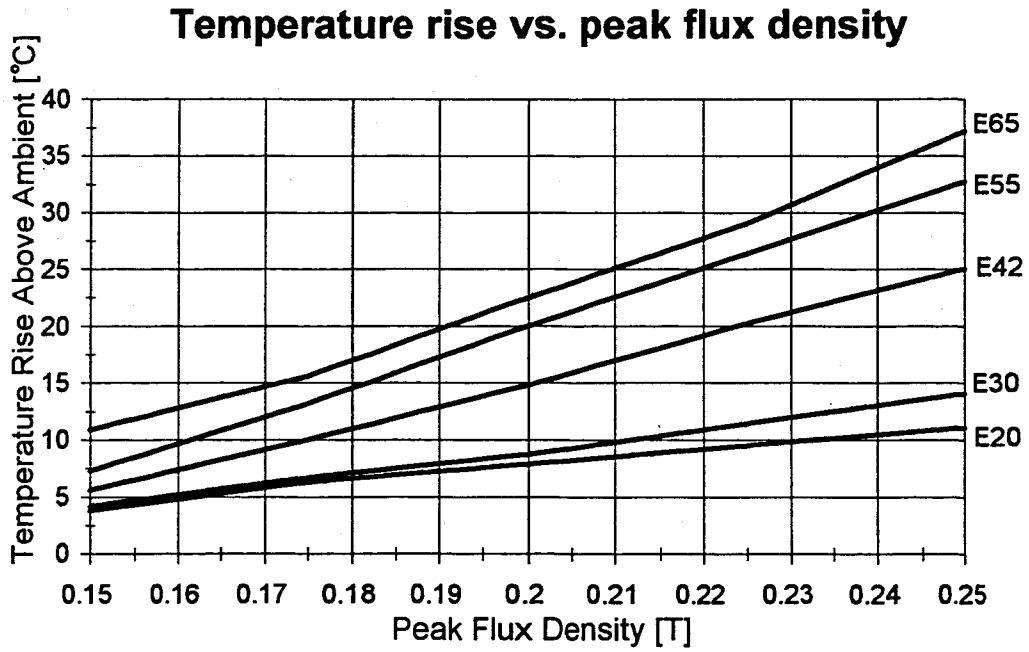

Figure. C-8 Surface temperature comparisons for various size E-cores at 30 kHz

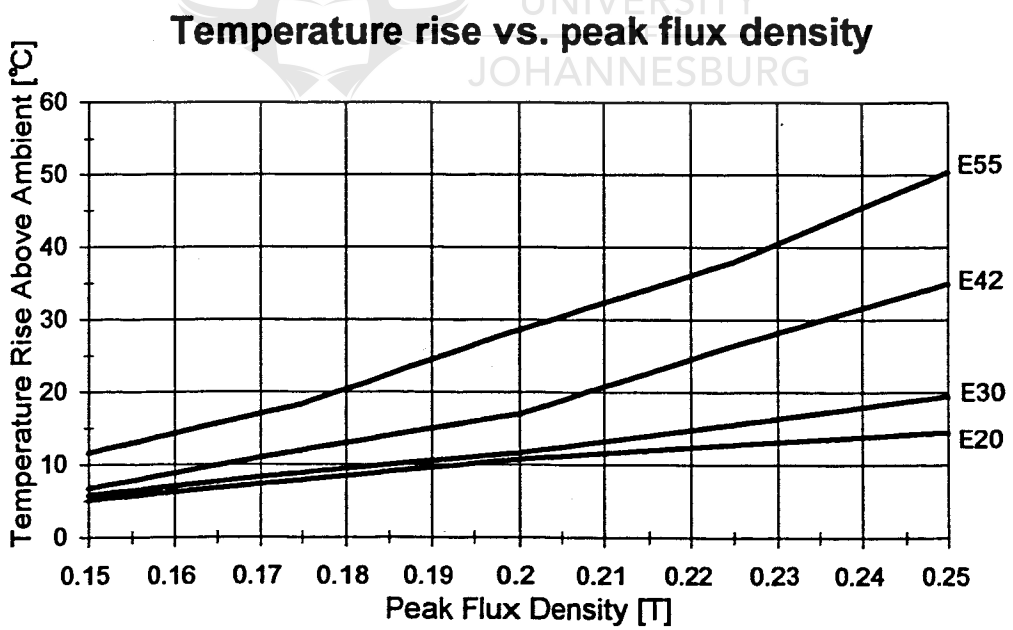

Figure. C-9 Surface temperature comparisons for various size E-cores at 40 kHz

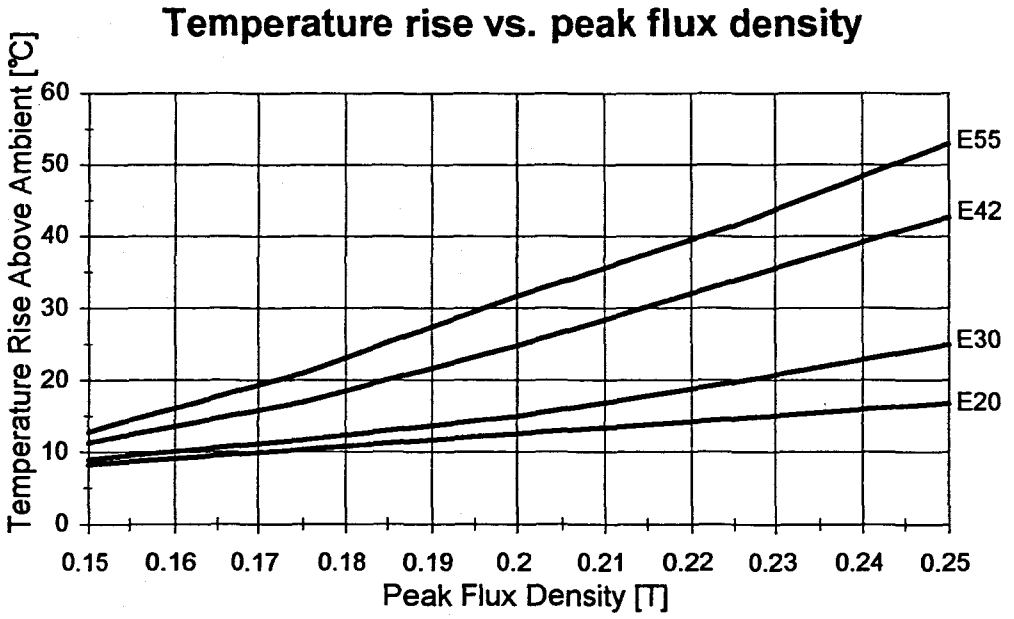

Figure. C-10 Surface temperature comparisons for various size E-cores at 50 kHz

D. Operation of the Cuk DC-DC converter

APPENDIX.D. OPERATION OF THE CUK DC-DC CONVERTER

D.1. THE CUK CONVERTER

The Cuk converter is the newest addition to the basic family of single switch DC - DC converters, and was designed by Slobodan Cuk in 1980. As a result of painstaking analysis described in detail in [1], the basic Cuk converter topology illustrated in Figure.D-1 was developed from the buck-boost switching topology.

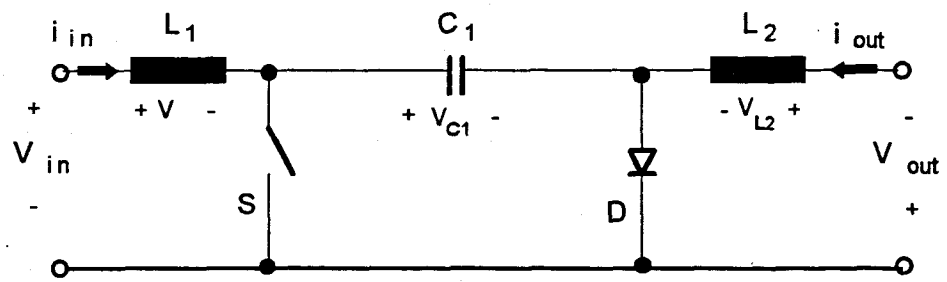

Figure. D-1 The basic Cuk converter

The increasing need for galvanic isolation between the input and output of converters, lead to the development of the basic isolated Cuk converter illustrated in Figure.D-2.

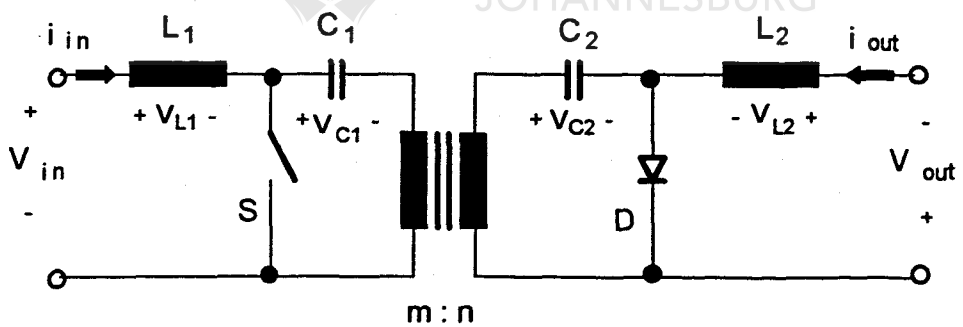

Figure. D-2 The isolated Cuk DC-DC converter

A regulated and inverted DC voltage is obtained at the output of the converter for a given positive DC voltage input, where the input could be a filtered DC voltage, or an unfiltered, full wave rectified DC voltage. The output is particularly suited for battery charger applications as in the case under investigation.

D.2. OPERATION OF THE ISOLATED CUK CONVERTER WITH A FILTERED INPUT VOLTAGE

Very often, the 50 Hz mains supply is rectified and filtered to provide a constant non-varying voltage at the input of the Cuk converter. The Cuk converter, transforms the constant input voltage and current into a regulated output voltage and current by making use of the switchmode principle [2], i.e. the output voltage and current of the converter is determined by controlling the repetitive switching action of the switch.

D.2.1.Steady state operation of the Cuk converter

Due to the repetitive closing and opening of the switch at a switching frequency of f_s , the following two basic modes of operation can be identified during the steady state operation of the isolated Cuk converter[†],

Mode 1 operation :

Mode 1 operation, as illustrated in figure.D-3, is initialised by forcing the switch, S, into conduction while the diode, D, is simultaneously forced into a state of non-conduction.

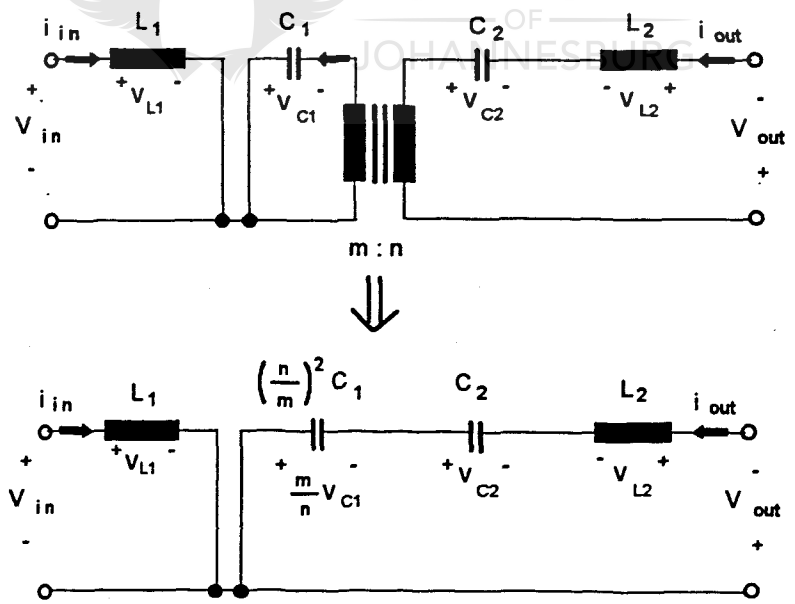

Figure. D-3 Mode 1 operation of the isolated Cuk DC-DC converter

[†] Other modes of operation do exist but are not required for a fundamental understanding of the operation of a Cuk converter.

When the switch, S, is forced into conduction, the choke, L_1 , is coupled directly over the voltage source, i.e. the voltage over L_1 , is equal to the input voltage as described by equation (D.1);

$$v_{L1} = V_{in} \qquad \text{(D.1)}$$

The input current is seen to increase linearly as energy is supplied to L_1 by the voltage source.

Furthermore, the capacitor, C_1 , is coupled directly across the primary windings of the transformer so that its voltage, V_{C1} , is reflected to the secondary side of the circuit by transformer action. The diode, D, is reverse biased by the reflected capacitor voltage, $\frac{n}{m}V_{C1}$, in series with the capacitor voltage, V_{C2} . Consequently, the voltage over L_2 is given as follows;

$$v_{L2} = \left(\frac{n}{m}V_{C1} + V_{C2}\right) - V_{out} \qquad \text{(D.2)}$$

The output current is therefore seen to increase linearly as the energy stored in capacitors, C_1 and C_2 , is released to the load, via the series interconnected choke, L_2.

Mode 2 operation:

Mode 2 operation, as illustrated in Figure.D-4, is initialised by forcing the switch, S, into a non-conducting state while the diode, D, is simultaneously forced into conduction;

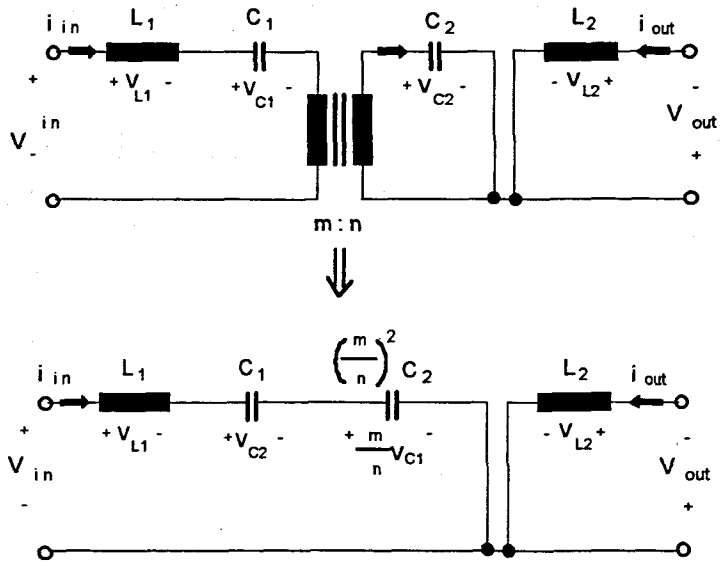

Figure. D-4 Mode 2 operation of the isolated Cuk DC-DC converter

When the switch is forced into a non-conducting state, the input choke, L_1, and the capacitor, C_1, are coupled across the voltage source via the primary windings of the transformer. Consequently, the voltage over L_1 is given as follows;

$$v_{L1} = V_{in} - \left(V_{C1} + \frac{m}{n} V_{C2}\right) \qquad \text{(D.3)}$$

The input current decreases linearly as energy from the choke, L_1, is transferred to the capacitor, C_1, together with energy from the voltage source.

The current flowing in the primary windings of the transformer is reflected to the secondary side of the circuit by transformer action. The reflected current flows through the diode, D, and additional energy is transferred to the capacitor, C_2. The choke, L_2, is coupled across the load because the output current finds a closed conduction path through the forward biased diode, D, i.e. the voltage over L_2, is equal to the output voltage as described in equation (D.4);

$$v_{L2} = -V_{out} \qquad \text{(D.4)}$$

The output current decreases linearly as energy is transferred from the choke, L_2, to the load.

D.2.2. Steady state operating conditions for the input and output chokes

The voltages and currents described by equations (D.1 - D.4), are repeated for each period of the switching frequency, f_s, where each period can be divided into two time intervals as follows;

$$T = \frac{1}{f_s} = t_{on} + t_{off} \qquad \text{(D.5)}$$

where : t_{on} ≡ time interval during which the switch conducts
t_{off} ≡ time interval during which the switch does not conduct

Equation (D.5) can be defined in terms of the switch duty ratio, D, as follows;

$$T = \frac{1}{f_s} = DT + (1-D)T \qquad \text{(D.6)}$$

where : DT ≡ t_{on}
(1-D)T ≡ t_{off}

The steady state voltages and currents for the two chokes, L_1 and L_2, are illustrated in Figure. D-5.

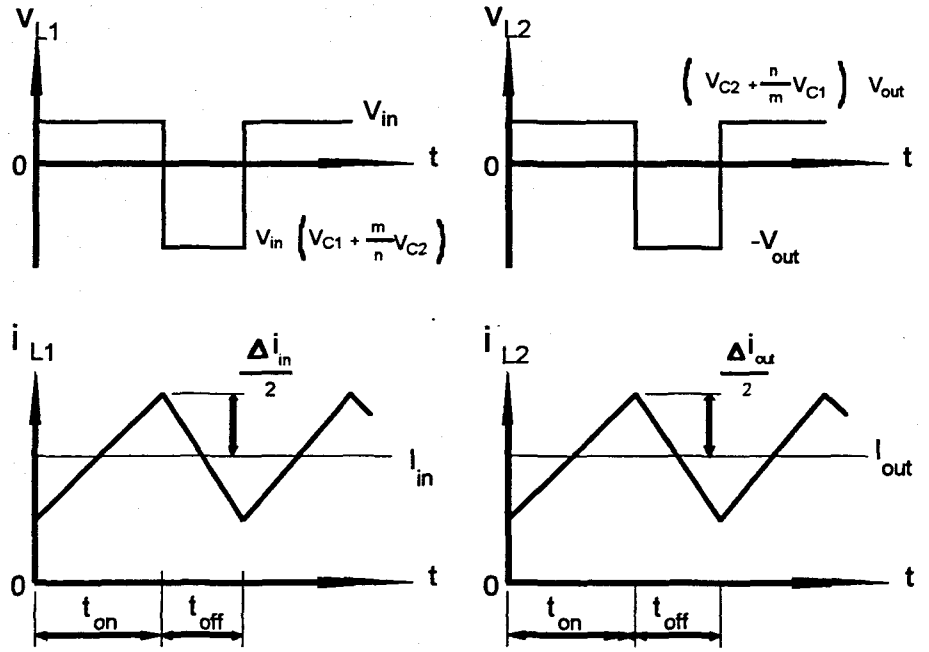

Figure. D-5 Currents and voltage for L_1 and L_2 at a switching frequency f_s

D.2.3. Input current ripple

From Figure.D-5, it is seen that a significant current ripple is superimposed over the DC input current of the converter. The magnitude of this ripple current is determined by the input choke, L_1 , as described by the following differential equation.;

$$v_{L1} = L_1 \frac{di_{in}}{dt} \qquad \text{(D.7)}$$

With reference to Figure.D-5, equation (D.7) can be simplified and an expression for the ripple current can be obtained as follows;

$$\Delta i_{in} = \frac{v_{in} DT}{L_1} \qquad \text{(D.8-a)}$$

or

$$\Delta i_{in} = \frac{V_{out}(1-D)T}{L_1} \qquad \text{(D.8-b)}$$

Combining equations (D.8-a) and (D.8-b) with equation (D.6) leads to an expression for the input ripple current in terms of the switching frequency;

$$L_1 \Delta i_{in} = \frac{v_{in} V_{out}}{f_s (v_{in} + V_{out})} \qquad \text{(D.9)}$$

Since the input and output voltages of the converter is constant, and the inductance of the choke is constant, it follows from equations (D.8) and (D.9) that the magnitude of the peak to peak current ripple remains fixed for a given switching frequency.

D.2.4. Output current ripple

From Figure.D-5, it is seen that a significant current ripple is superimposed over the DC output current of the converter. The magnitude of this ripple current is determined by the output choke, L_2, as described by the following differential equation.;

$$v_{L2} = L_2 \frac{di_{out}}{dt} \qquad \text{(D.10)}$$

With reference to Figure.D-5, equation (D.10) can be simplified and an expression for the peak to peak ripple current can be obtained as follows;

$$\Delta i_{out} = \frac{V_{out}(1-D)T}{L_2} \qquad \text{(D.11-a)}$$

or

$$\Delta i_{out} = \frac{v_{in} DT}{L_2} \qquad \text{(D.11-b)}$$

Combining equations (D.11-a) and (D.11-b) with equation (D.6) leads to an expression for the output ripple current in terms of the switching frequency;

$$L_2 \Delta i_{out} = \frac{V_{out}\ v_{in}}{f_s\left(V_{out} + v_{in}\right)} \qquad (D.12)$$

Since the input and output voltages of the converter is constant, and the inductance of the choke is constant, it follows from equations (D.11) and (D.12) that the magnitude of the peak to peak current ripple remains fixed for a given switching frequency.

D.2.5. Steady state operating conditions for the energy transfer capacitors

The average voltage of each choke is zero over one switching period, because of the inherent symmetry in their waveforms [2].

Consequently, the voltage over capacitor C_1 during steady state operation is given as follows;

$$v_{C1} = v_{in} \qquad (D.13)$$

and the voltage over capacitor C_2, as follows,

$$v_{C2} = V_{out} \qquad (D.14)$$

The voltage over each capacitor is seen to remain constant eventhough they store and transfer energy from the input of the converter to its output.

D.2.6. Steady state operating conditions for the isolation transformer

During mode 1 operation, the capacitor is coupled over the primary windings of the transformer as the switch is forced into conduction. The voltage impressed over the primary windings is therefore given as follows;

$$v_p = v_{C1} = -v_{in} \qquad (D.15)$$

During mode 2 operation, the capacitor C_2 is coupled over the secondary windings of the transformer as the diode is forced into conduction. The voltage impressed over the primary windings is therefore given as follows;

$$v_{prim} = \frac{m}{n} v_{C2} = \frac{m}{n} V_{out} \qquad \text{(D.16)}$$

The voltage impressed over the primary windings of the transformer during steady state operation is illustrated in Figure.D-6.

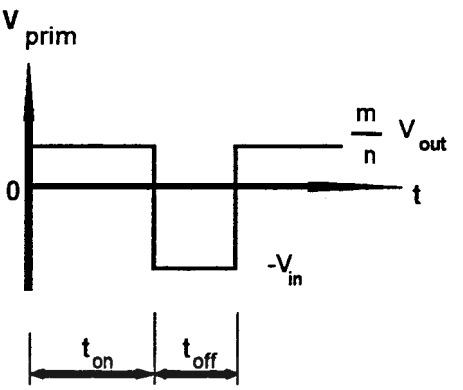

Figure. D-6 Voltage over primary windings of isolation transformer

The maximum positive deviation in the volt-time integral over the primary windings of the isolation transformer, can be determined from Figure.D-6 and equation (D.8-b), as follows;

$$\left| \int v_{prim}\, dt \right|_{max} = \frac{m}{n} V_{out} (1-D)T = \frac{m}{n} L_1 \Delta i_{in} \qquad \text{(D.17)}$$

The following result is obtained by substituting equation (D.12) into equation (D.17);

$$\left| \int v_{prim}\, dt \right|_{max} = \left(\frac{m}{n}\right) \frac{v_{in} V_{out}}{f_s (v_{in} + V_{out})} \qquad \text{(D.18)}$$

Once the input and output voltages of a given application are known together with inductance of the input choke, the isolation transformer can be designed for the maximum volt-time integral as given by equation (D.18).

During mode.1 operation, the the primary winding of the transformer is decoupled from the source and the linearly increasing output current is reflected by transformer action to its input. The current flowing in the primary windings of the isolation transformer is therefore given as follows;

$$i_{prim} = -\frac{n}{m} i_{out} \qquad \text{(D.19)}$$

During mode.2 operation, the secondary windings of the transformer is decoupled from the load. The linearly decreasing input current, therefore, flows through the primary windings of the isolation transformer as described in equation (D.20);

$$i_{prim} = i_{in} \qquad \text{(D.20)}$$

The current flowing in the primary winding of the isolation transformer during steady state operation, is illustrated in Figure.D-7.

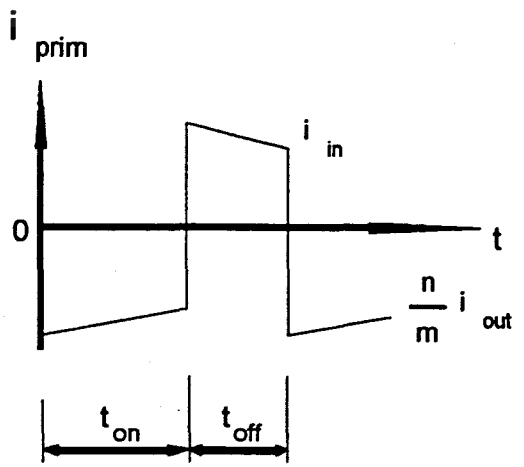

Fig.D-7 Primary current of isolation transformer

D.2.7. Voltage and current transfer functions

The output voltage can be made smaller or larger in magnitude, than the input voltage, by respectively decreasing or increasing the duty ratio of the switch. The output voltage of the Cuk converter is also regulated by the same means, i.e. the switch duty ratio is changed in response to changing load conditions. The exact relationship between switch duty ratio, input voltage and output voltage is determined as follows;

The voltage waveform of L_1 is repeated for every period during steady state operation of the converter. Integrating the voltage of L_1 over one period must produce the zero result given in equation (D.21), because of its symmetry [1,2].

$$\int_0^T V_{L1}\,dt = 0 \qquad \text{(D.21)}$$

With reference to figure.D-5, equation (D.21) can be expressed as follows;

$$\int_0^T V_{L1}\,dt = \int_0^{DT} (V_{in})\,dt + \int_{DT}^T V_{out}\,dt - \int_{DT}^T \left(V_{C1} + \frac{m}{n}V_{C2}\right)dt = 0 \qquad \text{(D.22)}$$

which can be simplified to provide the following result;

$$\Rightarrow \qquad \left(\frac{n}{m}V_{C1} + V_{C2}\right) = \frac{V_{out}}{D} \qquad \text{(D.23)}$$

The voltage waveform of L_2 is repeated for every period during steady state operation of the converter. Integrating the voltage of L_2 over one period must produce the zero result given in equation (D.24), because of its symmetry [1,2].

$$\int_0^T V_{L2}\,dt = 0 \qquad \text{(D.24)}$$

with reference to figure.D-5, equation (D.24) can be expressed as follows;

$$\int_0^T V_{L2}\,dt = \int_0^{DT}\left(\frac{n}{m}V_{c1}+V_{C2}\right)dt - \int_0^{DT} V_{out}\,dt - \int_{DT}^{T} V_{out}\,dt = 0 \qquad \text{(D.25)}$$

Equation (D.25) can be simplified to provide the following result;

$$\Rightarrow \qquad \left(\frac{m}{n}V_{C2}+V_{C1}\right) = \frac{V_{in}}{(1-D)} \qquad \text{(D.26)}$$

Since equations (D.23) and (D.26) are equal, the following expression can be obtained for the voltage transfer function of an isolated Cuk converter;

$$V_{out} = \frac{D}{(1-D)}V_{in} \qquad \text{(D.27)}$$

The output current also changes in response to a change in the duty ratio of the switch because, the input power must be equal to the output power of the converter, if all losses are neglected, i.e.

$$V_{in}\,i_{in} = V_{out}\,i_{in} \qquad \text{(D.28)}$$

Substituting equation (D.27) into equation (D.28), results in the following expression for the current transfer function of an isolated Cuk converter;

$$i_{in} = \frac{(1-D)}{D}i_{in} \qquad \text{(D.29)}$$

List of Symbols

List of symbols

Symbol	Description	Unit
a	Steinmetz constant	
A_C	Effective cross-sectional area of core	mm^3
A_{win}	Window area of core	mm^3
A_{cu}	Cross-sectional area of copper windings	mm^3
$A_{conduction}$	Surface are available for heat dissipation by conduction	mm^2
$A_{convection}$	Surface area available for heat dissipation by convection	mm^2
$A_{radiation}$	Surface area available for heat dissipation by radiation	mm^2
$\hat{B}$	Peak flux density	T
B_s	Saturation flux density	T
d	Length of extreme core dimensions to sides of space volume boundry	mm
D	Duty ratio	
ΔT	Temperature difference	°C
dT	Small variation in temperature	°C
e	Emissivity	
f	Frequency	Hz
f_s	Switching frequency	Hz
f_m	Supply frequency	Hz
$\overline{h}$	Convection heat transfer coefficient	
h_c	Height of magnetic core	mm
h_w	Winding height	mm
H_s	Saturation magnetic field intensity	
I_p	Primary current of transformer	A
I_{rms}	Effective value of current in windings	A
$[I_p]_{ij}$	Effective primary current in the windings of element ij	A
i_{in}	Input current to Cuk converter	A
$\hat{I}_{in}$	Peak input current to Cuk converter	A

Symbol	Description	Unit
Δi_{in}	Input current ripple of Cuk converter	A
i_{out}	Output current of Cuk converter	A
Δi_{out}	Output current ripple of Cuk converter	A
i_{L1}	Current in input choke of the Cuk converter	A
i_{L2}	Current in output choke of the Cuk converter	A
J	Current density	A/mm^2
k	Conduction heat transfer coeeficient	$W/m^2.°C$
k_u	Packing factor	
l	Magnetic core length	mm
L	Inductance	H
L_1	Inductance of the input choke of the Cuk converter	H
L_2	Inductance of the output choke of the Cuk converter	H
L_M	Magnetising inductance of a distributed transformer	H
$[L_M]_{ij}$	Magnetising inductance of element ij	H
L_σ	Leakage inductance of a distributed transformer	H
$[L_\sigma]_{ij}$	Leakage inductance of element ij	H
m	Number of primary turns in an element	
M	Row dimension of a distributed transformer	
(MLT)	Mean length of turn	mm
n	Number of secondary turns in an element	
N	Column dimension of a distributed transformer	
P_e	Eddy current losses	W
P_h	Hysteresis losses	W
$Q_{conduction}$	Heat transfer rate by conduction	W

Symbol	Description	Unit
$Q_{convection}$	Heat transfer rate by convection	W
$Q_{radiation}$	Heat transfer rate by radiation	W
R_{dc}	DC resistance of windings	Ω
R_c	Core loss resistance of a distributed transformer	Ω
$[R_c]_{ij}$	Core loss ressitance of element ij	Ω
R_{eff}	Effective AC resistance of element ij	Ω
$[R_{eff}]_{ij}$	Effective resistance of element ij	Ω
S	kVA Rating of a transformer	kVA
σ	Conductivity of conductive material	
σ_R	Stefan-Boltzman constant	
T	Period of switching frequency	s
T_s	Surface temperature	°C
T_∞	Environment temperature	°C
μ_{ave}	Average permeability of core	
V_p	Primary voltage of a distributed transformer	V
$[V_p]_{ij}$	Primary voltage of element ij	V
V_s	Secondary voltage of a distributed transformer	V
$[V_s]_{ij}$	Secondary voltage of element ij	V
v_{in}	Input voltage of a Cuk converter	V
v_{out}	Output voltage of a Cuk converter	V
W_w	Winding width	m

References

References

Chapter.1.

[1] B. K. Bose, "Modern Power Electronics - Evolution, Technology, and Applications", IEEE Press, Piscataway, New Jersey, pp. 3 - 73, (1991).

[2] S. Cuk, R. D. Middlebrook, "Advances in switched mode power conversion - Modelling, Analysis, and Measurement", TESLAco, Pasadena, California, pp. 11 - 15, (1981).

[3] G. J. de J. Cronje, E. W. Neuland, W. M. J. Hugo, M. J. Van Reenen, "Introduction to Business Management, second edition", Southern Book Publishers (Pty) Ltd. , pp.17, (1991).

[4] B,Breen, "Multi-Layer Inductor for High Frequency Applications", Conf. Rec. , Electronic Components and Technology Conference, pp.551 - 554, (1991).

[5] H. Matsuki, N. Fujii, K. Shirakawa, J. Toriu, K. Murakami, "Magnetic-Multi-Turn Planar Coil Inductor", IEEE Trans. on Magn. , Vol.27, No.6, pp. 5438 - 5440, November (1991).

[6] K. Shirakawa, H. Kurata, J.toriu, H. Matsuki, K. Murakami, "A New Planr Inductor With Magnetic Closed Circuit", IEEE Trans. on Magn. , Vol.27, No.6, pp.5432 - 5434, November (1991).

[7] E. J. Osegueda, K. D. T. Ngo, "Analysis and Design of Perforated-Plate Matrix Transformers", Conf. Rec. PESC, Vol. 2,pp.1393 - 1400, June (1992).

[8] E. C. Snelling, "Soft Ferrites, Properties and Applications", Iliffe Books Ltd. , London, pp.297 - 326, pp.337 - 358, (1969).

[9] K. Billings, "Switchmode Power Supply Handbook", McGraw-Hill Publishing Company, New York, pp. 3.65 - 3.114, (1989).

References

Chapter.1. (continued)

[10] J. A. Ferreira, W. G. Odendaal, W. A. Cronje, "Scant Modelling: A new Method for Optimising Functionality and Form of Transformers", IEEE Industry Applications Society 29th Annual Meeting, Denver, Colorado, pp. 1218 - 1224, October (1994).

[11] T. M. Undeland, J. Lode, R. Nilssen, W. P. Robbins, N. Mohan, "A Simple Non-iterative Procedure for Designing Naturally Cooled High Frequency Inductors and Transformers Based Upon Limitation of the Maximum Device Temperature", IEEE Industry Applications Society 29th Annual Meeting, Denver, Colorado, pp. 1253 - 1260, October (1994).

Chapter.2.

[1] A. W. Kelley, F. P. Symonds, "Plastic-Iron-Powder Distributed-Air-Gap Magnetic Material", IEEE PESC Conf. Rec., Vol. 1, pp. 25 - 34, (1990).

[2] E. Herbert, K. K. Sum, "Design and Applications of Matrix Transformers and Inductors", A Seminar presented at the fourth International High Frequency Power Conversion Conference, Naples, Florida, May 15 - 18, (1989).

[3] D. J. Nelson, J. P. Jessee, "A Coupled Thermal Magnetic Model for High Frequency Transformers: Part I - Model formulation and Material Properties", IEEE Transactions on Components Hybrids, and Manufacturing Technology, Vol. 15, No. 5, October (1992).

[4] K. Billings, "Switchmode Power Supply Handbook", McGraw-Hill Publishing Company, New York, pp. 3.65 - 3.114, (1989).

[5] E. C. Snelling, "Soft Ferrites, Properties and Applications", Iliffe Books Ltd., London, pp.297 - 326, pp.337 - 358, (1969).

References

Chapter.2. (continued)

[6] C. G. Koops, "On the Dispersion of resistivity and dielectric constant of some semi-conductors at at audio frequencies," Phys. Rev. , Vol. 83, pp. 121 - 125, (1951).

[7] R. F, Soohoo, "Theory and Applications of Ferrites", Englewood Cliffs, NJ: Prentice-Hall, (1960).

[8] McLyman, Colonel Wm. T, "Transformer and Inductor Design Handbook", Marcel Dekker, New York, (1978).

[9] N. Mohan, T. M. Undeland, W. P. Robbins, "Power Electronics: Converters, Applications and Design", John Wiley & Sons, pp. 639 - 649, (1989).

[10] A. M. Urling, V. A. Niemela, G. R. Skutt, T. G. Wilson, "Characterising High Frequency Effects In Transformer Windings - A Guide to Several Significant Articles", 4th Annual IEEE Applied Power Electronics Conference, Baltimore, Maryland, pp. 373 - 385, March 13 - 17, (1989).

[11] J. P. Holman, "Heat Transfer, Sixth Edition", McGraw-Hill Book Company, Singapore, (1987).

[12] D. R. Pitts, L.E. Sissom, "Heat Transfer, Schaums Outline Series", McGraw-Hill Book Company, New York, (1987).

Chapter.3.

[1] R. J. Smith, "Circuits, Devices and Systems", 4th Edition, John Wiley & Sons, pp. 594 - 608, (1983)

[2] Van A. Niemela, G. R. Skutt, A. M. Urling, Y. Chang, T. G. Wilson, H. A. Owen Jr, R. C. Wong, "Calculating the Short-Circuit Impedance of a Multiwinding Transformer from its Geometry", IEEE 20th Annual Power Electronic Specialist Conference, pp. 607 - 617, (1989).

References

Chapter.3. (continued)

[3] E. C. Snelling, "Soft Ferrites, Properties and Applications", Iliffe Books Ltd. , London, pp.297 - 326, pp.337 - 358, (1969).

[4] Philips Components, "Soft Ferrites, Data Handbook", Book MA01, (1993).

[5] K. Billings, "Switchmode Power Supply Handbook", McGraw-Hill Publishing Company, New York, pp. 3.65 - 3.114, (1989).

[6] McLyman, Colonel Wm. T, "Transformer and Inductor Design Handbook",Marcel Dekker, New York, (1978).

[7] N. Mohan, T. M. Undeland, W. P. Robbins,"Power Electronics: Converters, Applications and Design", John Wiley & Sons, pp. 639 - 649, (1989).

[8] A. M. Urling, V. A. Niemela, G. R. Skutt, T. G. Wilson, "Characterising High Frequency Effects In Transformer Windings - A Guide to Several Significant Articles", 4th Annual IEEE Applied Power Electronics Conference, Baltimore, Maryland, pp. 373 - 385, March 13 - 17, (1989).

[9] E. Herbert, K. K. Sum, "Design and Applications of Matrix Transformers and Inductors", A Seminar presented at the fourth International High Frequency Power Conversion Conference, Naples, Florida, May 15 - 18, (1989).

[10] E. J. Osegueda, K. D. T. Ngo, "Analysis and Design of Perforated-Plate Matrix Transformers", Conf. Rec. PESC, Vol. 2,pp.1393 - 1400, June (1992).

[11] S. Kirli, K. D. T. Ngo,"Inductance Modelling for a Mode-2 Perforated-plate Matrix Inductor/Transformer", IEEE 24th Annual Power Electronics Specialist Conference, pp. 1130 - 1138, Seattle, Washington, June,(1993).

References

Chapter.4.

[1] R.A. Langley, J. D. van Wyk, J. J. Schoeman, " A High Technology Battery Charging System for Railway Signalling Applications", Proceedings of the Third European Conference on Power Electronics and Applications, (EP-89),Aachen, BRD, pp. 1433 - 1437, October, (1989).

[2] Philips Components, "Soft Ferrites, Data Handbook", Book MA01, (1993).

[3] N. Mohan, T. M. Undeland, W. P. Robbins,"Power Electronics: Converters, Applications and Design", John Wiley & Sons, pp. 639 - 649, (1989).

[4] J. A. Ferreira,"Electromagnetic modelling of Power Converters", Kluwer Academic Publishers, Boston, (1989).

Appendix.A.

[1] J. P. Holman, "Heat Transfer, Sixth Edition", McGraw-Hill Book Company, Singapore, (1987).

[2] D. R. Pitts, L.E. Sissom, "Heat Transfer, Schaums Outline Series", McGraw-Hill Book Company, New York, (1987).

[3] N. Mohan, T. M. Undeland, W. P. Robbins,"Power Electronics: Converters, Applications and Design", John Wiley & Sons, pp. 639 - 649, (1989).

Appendix.D.

[1] S. Cuk, R. D. Middlebrook, "Advances in switched mode power conversion - Modelling, Analysis, and Measurement", TESLAco, Pasadena, California, (1981).

[2] N. Mohan, T. M. Undeland, W. P. Robbins,"Power Electronics: Converters, Applications and Design", John Wiley & Sons, pp. 25 - 101, (1989).